1999

Self-excited oscillations of a horizontal cylinder adjacent to a free-surface

Nattapong Saelim
Lehigh University

Saelim, Nattapong

Self-excited Oscillations of a Horizontal Cylinder Adjacent to a Free-Surface

January 2000

SELF-EXCITED OSCILLATIONS OF A HORIZONTAL CYLINDER ADJACENT TO A FREE-SURFACE

by

Nattapong Saelim

A Thesis

Presented to the Graduate and Research Committee

of Lehigh University

in Candidacy for the Degree of

Master of Science

in

Department of Mechanical Engineering and Mechanics

Lehigh University

December 1999

This thesis is accepted and approved in partial fulfillment of the requirements for the Master of Science.

12/14/99

Date

Thesis Advisor

Chairperson of Department

ACKNOWLEDGMENTS

The author would like to express his gratitude to the many people who have been very supportive of this research. First of all, I would like to thank Dr. Donald. O. Rockwell for providing me the opportunity and guidance throughout this project. Many thanks to Mr. Hermann Baader for his kindly help with preparing the experimental components. I would also like to thank Dr. J.-C. Lin, Mr. Keith Downes, Mr. Hussain Akili, Mr. Muammer Ozgoren, and other colleagues in the fluid lab for their technical advice and discussions. Many thanks to my friend, Mr. Theeraphong Wongratanaphisan, for his suggestion and encouragement. I would like to thank to my family who have always been there for me; to my farther who is now looking at me from above for his inspiration and strength. Special thanks to grandma who always provides me with a warm hug.

Thanks all of you with my whole heart.

TABLE OF CONTENTS

LIST OF FIGURES

ABSTRACT

A horizontal, elastically-mounted cylinder is located beneath a free-surface, and the nature of self-excited transverse vibrations of the cylinder are examined as a function of nominal depth of submergence beneath the free-surface. The cylinder has an extremely low value of mass-damping ratio, attained by use of a leaf spring arrangement. The oscillation amplitude and frequency are characterized as a function of reduced velocity and depth of submergence.

When the cylinder is well submerged beneath the free-surface, the variation of oscillation amplitude with reduced velocity is in accord with recent findings. When the cylinder is located sufficiently close to the free-surface, a number of distinctive, new features are evident. The amplitude of the oscillating cylinder actively exhibits a dual amplitude response, whereby not only the upstroke motion has a smaller amplitude than the downstroke motion, but the downstroke modulates between relatively large and small values. Moreover, for locations of the cylinder close to the free-surface, very large regions of hysteresis occur in the variation of oscillation amplitude as a function of reduced velocity.

These features of the amplitude response are linked to unusual variations of the oscillation frequency as a function of reduced velocity. For larger values of nominal submergence of the cylinder, the frequency of large amplitude, locked-on vibrations is located above the natural frequency and below the inherent vortex shedding frequency of the cylinder. When the depth of submergence is very small, the cylinder vibrates at a frequency much higher than the natural frequency and takes on values close to the vortex-shedding frequency.

1. INTRODUCTION

1.1 Background

Of all self-excited flow instabilities, vortex shedding from bluff bodies has been the focus of the largest number of investigations in this century. Vortex shedding can induce vibrations of elastically-mounted cylinders, which are of a great practical importance, since failure of the bluff body structure can occur. These vibrations occur in both water and air, and for flexible and rigid (elastically-mounted) cylinders, which can have a wide variety of cross-sectional shapes. Experiments, theoretical models, and numerical simulations have been extensively pursued. Among others, Sarpkaya (1979), Bearman (1984), and Parkinson (1989) provide extensive reviews of vortex-induced vibration. Blevins (1990), Naudascher and Rockwell (1994) and Blake (1986) describe loading of cylinders and associated vibrations, which can be due not only to classical vortex shedding, but also to flutter-type instabilities, as well as buffet-induced loading.

Representative investigation focusing on the physics of vortex formation in the near-wake has been addressed by Griffin and Ramberg (1974), Zdravkovich (1982, 1996), Williamson and Roshko (1988), Unal and Rockwell (1988a,b), and Ongoren and Rockwell (1988a,b). These studies represent but a few of those that have provided physical insight into the near-wake structure.

The fundamental mechanism giving rise to vortex formation, and thereby the origin of vortex-induced vibration, has been interpreted in a simple, physical way by Naudascher and Rockwell (1994). The presence of a bluff body induces a difference between a high velocity free-stream and a low (even negative) velocity in the base region. This type of mean velocity distribution promotes what has become known as a global

instability. Basically, the important feature of this global instability is that it grows in place and can lead to highly organized, persistent oscillations of the near-wake. The concept of a global instability has received much attention in recent years, and recent investigations are summarized by Huerre and Monkewitz (1990) and Oertel (1990).

The concept of a global instability is a linear description of the near-wake. When the wake starts to exhibit large amplitude oscillations, the flow pattern becomes particularly complex. The interaction between the separating shear layers formed from either side of the cylinder eventually leads to a pattern of alternating vortices. These vortices grow, as they are fed by circulation from the shear layers separating from the cylinder. In fact, when the vortices are sufficiently developed, they can draw the opposing shear layers across the near-wake region. Eventually, however, this supply of circulation, or vorticity, from the cylinder is terminated and the vortices are shed and convected downstream.

The investigation of vortex-induced vibration has been in two basic classes: self-excited vibration of an elastically-mounted cylinder; or externally-imposed, forced oscillation of the cylinder. The detailed review of these types of experiments is beyond the scope of the present work. It should be noted, however, as pointed out by Sarpkaya (1979), that forced vibrations cannot account for hysteresis effects, which are basically history-type effects. Moreover, forced excitations provide a fixed amount of energy input per cycle, which actually may exceed that required to induce self-excited vibrations of the corresponding, elastically-mounted body.

The focus of this investigation is on vibrations of an elastically-mounted cylinder. The next section gives a brief summary of recent, related investigations.

1.2 Previously Related Investigations: Self-Excited Elastic Vibrations of a Fully-Submerged Cylinder

Summaries of recent investigations of self-excited vibrations of elastically-mounted cylinders are given by Vandiver (1993), Khalak and Williamson (1996), Sarpkaya (1996, 1997).

Particularly relevant to the present considerations are the works on vortex-induced vibration of an elastically-mounted ridge and cylinder, as addressed by Feng (1968), Brika and Laneville (1993), and Khalak and Williamson (1996). In the following, the central features of these investigations are addressed briefly. The experiments of Feng (1968) and Brika and Laneville (1993) were performed in air. They note the appearance of two branches, i.e., upper and lower branches of the synchronized motion of the cylinder and the vortex shedding. On the other hand, the experiments of Khalak and Williamson (1996) were performed in water. The cylinder was oriented vertically, such that one end pierced the free-surface, and the other end was subjected to a controlled end condition in the form of a type of end plate. Use of an airbearing allowed attainment of a very low damping and, when compared to previous experiments, their system possessed a mass-damping ratio of order 10^{-2}, which is an order of magnitude lower than previous values. As a result, the range of locked-on response of the cylinder motion was about two folds larger than that of Feng (1968) and Brika and Laneville (1993), for which the values of mass-damping ratios $m^*\zeta$ were 0.36 and 0.41 respectively. The above results are consistent with that of Meier-Windhorst (1939). The effect of mass-damping parameter ($Sc \equiv 2m\zeta/\rho D^2$) on transverse vibration of a circular cylinder in water was investigated by Meier-Windhorst (1939). By increasing the damping ratio ζ, Meier-

Windhorst found the reductions in maximum amplitude and width of the synchronization range. Griffin and Koopmann (1977) and Sarpkaya (1978) mention the primary influence of the mass-damping parameter or the response parameter (which is proportional to $m^*\zeta$) on the maximum relative amplitude of cross-flow vibrations achieved for a given cross-sectional shape at resonance near $V_r = 1/S$. In addition, Khalak and Williamson (1996), also observed the effect of parallel and oblique vortex shedding on the force coefficients.

In a subsequent investigation, Khalak and Williamson (1997) reported additional results. In this work, it is pointed out that the variation of the dimensionless frequency f^*, defined as the oscillation frequency of the cylinder normalized by the natural frequency of the cylinder, showed a non-classical form. That is, in the region of synchronization or lock-on, the oscillation frequency is larger than the natural frequency, while remaining below the vortex shedding frequency of the corresponding stationary cylinder.

These experimental observations are, of course, linked to theoretical concepts. In the two sections that follow, these concepts are briefly outlined.

1.3 Governing Equation for a Flexibly-Mounted Bluff Body

Bearman (1984) presented the equation of motion for a two-dimensional bluff body elastically supported and submerged in a free-stream. The equation of motion is expressed as

$$m\ddot{y} + \zeta\dot{y} + ky = F(t) \tag{1}$$

where F(t) is the transient fluid force acting on the body. In term of a force coefficient $c_y = 2F(t)/\rho U^2 D$ which accounts for the y component of the total instantaneous fluid force and the embodies fluid inertia and damping forces. In addition, by replacing the term ζ by

$4\pi\delta_s m f_n$, where δ_s is the fraction of critical damping, we come up with another from of the equation (1)

$$m\ddot{y} + 4\pi f_n \delta_s m\dot{y} + 4\pi^2 f_n^2 my = \frac{1}{2}\rho c_y U^2 D \tag{2}$$

An important point mentioned by Bearman is not to separate the fluid force into components in order to understand the mechanism of the fluid loads caused by the vortex shedding. Equation (2) is also considered to be a general equation expressing the response in the transverse or stream-wise directions caused by galloping, turbulence or vortex shedding.

For the case of interest here, the response y is considered to be in the transverse direction and the coefficient c_y is the transverse force coefficient regarding the vortex shedding from the bluff body. In the synchronization range of the steady state, vortex-induced vibration of large amplitude, the oscillation frequency and the vortex shedding frequency are the same (f_v) and generally it is close to the natural frequency of the system f_n. By accounting for the phase angle ϕ, both y and c_y can be expressed in a sinusoidal form, as follows:

$$y = A\sin(2\pi f_v t) \tag{3}$$

$$c_y = C_y \sin(2\pi f_v t + \phi) \tag{4}$$

where ϕ is the phase angle which the fluid excitation leads the body response. Substituting y and c_y in equation (2), and equating the coefficients of the sine and cosine terms, one can achieve the following relationships.

$$\frac{f_n}{f_v} = \left(1 - \frac{C_y}{4\pi^2}\cos\phi\left(\frac{\rho D^2}{2m}\right)\left(\frac{U}{f_n D}\right)^2\left(\frac{y}{D}\right)^{-1}\right)^{-\frac{1}{2}} \tag{5}$$

$$\frac{A}{D} = \frac{C_y}{8\pi^2}\sin\phi\left(\frac{\rho D^2}{2m\delta_s}\right)\left(\frac{U}{f_n D}\right)^2\left(\frac{f_n}{f_v}\right) \tag{6}$$

Parkinson (1974) and Bearman (1984) note the effect of the mass ratio term. In experiments in water, $\rho D^2/2m$ may be normally of order one and the body frequency can deviate from its natural frequency, whereas for oscillation in air, the same term is of order 10^{-3} and the difference between the frequency of oscillation and the natural frequency should be very small.

Apparently, from the last two expressions, the response amplitude depends upon the part of C_y that is in phase with the bluff body velocity. In the other words, the phase angle ϕ plays an important role.

1.4 Flow-Induced Transverse Forces

Among others, Griffin (1978, 1980), Sarpkaya (1977), Griffin and Koopmann (1977) developed the modeling expressions to describe the vibrations due to a vortex-induced force acting transversely on an elastically mounted, rigid cylinder at resonance. Since the expressions proposed by Griffin (1978) and Griffin and Koopmann (1977) have the identical form as those of Sarpkaya (1977), the symbols and the terminology used in the first two sources are adopted here. For cross flow vibration at resonance, the governing equation takes form,

$$\ddot{y} + 2\zeta\dot{y} + y = \mu\left(\frac{\omega}{\omega_n}\right)^2\left(\tilde{C}_L - \tilde{C}_R\right) \tag{7}$$

where $\tau = \omega t$, the mass ratio $\mu = \rho D^2/8\pi^2 S^2 m$ (which differ from the mass ratio used as one of the parameters in the present experiment), $y = \bar{y}/D$, ζ is the structural damping factor, and $\tilde{C}_L$ and $\tilde{C}_R$ are the fluid lift and reaction force coefficients, respectively. Herein, the fluid lift and reaction force coefficients can be written as,

$$\tilde{C}_L = \frac{\bar{F}_L}{\frac{1}{2}\rho U^2 D} = C_L \sin(\alpha\tau + \phi) \tag{8}$$

$$\tilde{C}_R = \frac{\bar{F}_R}{\frac{1}{2}\rho U^2 D} = C_R \sin(\alpha\tau + \psi) \tag{9}$$

where ϕ and ψ are the phase angles between the lift and the displacement, and between the reaction and the acceleration, respectively. The relation between ϕ and ψ can be written as,

$$\tan\phi = -\frac{1}{\tan\psi} \tag{10}$$

Afterwards, the displacement $y = Y \sin(\alpha\tau)$ is introduced into the equation of motion and according to the cos $(\alpha\tau)$ and sin $(\alpha\tau)$ terms, the fluid and structural forces can be individually considered, such that

cos $(\alpha\tau)$:
$$2\alpha\zeta Y = \mu\left(\frac{\omega}{\omega_n}\right)^2 [C_L \sin\phi - C_R \sin\psi] \tag{11}$$

sin $(\alpha\tau)$:
$$-\alpha^2 Y + Y = \mu\left(\frac{\omega}{\omega_n}\right)^2 [C_L \cos\phi - C_R \cos\psi] \tag{12}$$

Subsequently, decomposing the total force separates the structural forces from the fluid forces, and so the fluid forces can be determined individually. The structural forces

have representative terms in the form of the structural inertia ($-\alpha^2 Y$), the structural stiffness (Y), and the structural damping ($2\alpha\zeta Y$). The representative fluid force terms are fluid inertia ($MC_L \cos\phi$), the fluid added mass ($-MC_R \cos\psi$), the fluid excitation ($MC_L \sin\phi$), and the fluid damping ($-MC_R \sin\psi$) where $M = \mu(\omega/\omega_n)^2$.

By squaring and adding equation (11) and (12), the relation between the total fluid force and the displacement Y is derived,

$$\left(\left(1-\alpha^2\right)^2 + 4\alpha^2\zeta^2\right)Y^2 = \mu^2\left(\frac{\omega}{\omega_n}\right)^4\left(C_L^2 + C_R^2\right) \tag{13}$$

More importantly, Griffin (1980) also addressed the dependency of the maximum effective amplitude on a response or damping parameter which is proportional to the mass-damping. From the data amassed both in air and in water indicate that the maximum displacement A/D is approximately 1 to 1.5. Sarpkaya (1978, 1979) obtained an expression for the relative amplitude: $A/D = 0.32/[0.06 + S_G^2]^{1/2}$ as discussed by Sarpkaya (1997). Khalak and Williamson (1996) have considered the issue of the amplitude limit at low reduced damping.

1.5 Linear Theory for Low Mass Ratio Cylinder System

From the particular viewpoint of low mass-damping ratio of the present investigation, the linear theory describing vortex-induced oscillations developed by Khalak and Williamson (1996) is relevant. It is discussed in this section. Excited by the fluid fluctuating force, the response of a second order linear system is according to

$$m\ddot{y} + c\dot{y} + ky = \bar{F}_v \cdot \bar{e}_y + \bar{F}_{inv} \cdot \bar{e}_y \tag{14}$$

Herein, the total force is separated into two components i.e. the viscous force ($\vec{F}_v$) and the inviscid force ($\vec{F}_{inv}$). The latter is expressed in term of the inviscid added mass m_a. The instantaneous transverse force coefficient c_y is introduced to define the viscous force:

$$\vec{F}_v \cdot \vec{e}_y = \frac{1}{2} c_y \rho U^2 DL \tag{15}$$

$$\vec{F}_{inv} \cdot \vec{e}_y = -m_a \ddot{y} \tag{16}$$

The displaced fluid mass m_d for a circular cylinder is defined as,

$$m_d = \frac{1}{4} \pi \rho D^2 L \tag{17}$$

Furthermore, in order to non-dimensionalize the governing equation the following dimensionless parameters are defined,

$$f_n = \frac{1}{2\pi} \sqrt{\frac{k}{m + m_a}} \tag{18}$$

$$\zeta_a = \frac{c}{2\sqrt{k(m + m_a)}} \tag{19}$$

$$m^* = \frac{m}{m_d} \tag{20}$$

$$C_a = \frac{m_a}{m_d} \tag{21}$$

$$Y = \frac{y}{D} \tag{22}$$

$$U^* = \frac{U}{f_n D} \tag{23}$$

After introducing the above parameters and substituting into equation (14), and using equations (15), (16), and (17), we come up with

$$\left(m^* + C_a\right)\left(\frac{1}{f_n^2}\ddot{Y} + \frac{4\pi\zeta_a}{f_n}\dot{Y} + 4\pi^2 Y\right) = \frac{2}{\pi}U^{*2}c_y \tag{24}$$

(Note: The terms $T_n\ddot{Y}$ and $4\pi\zeta_a\dot{Y}$ in the equation $\left(m^* + C_a\right)\left(T_n\ddot{Y} + 4\pi\zeta_a\dot{Y} + 4\pi^2 Y\right) = 2U^{*2}c_y/\pi$ in Khalak and Williamson (1996) are apparently in error; but the correct terms are $\ddot{Y}/f_n^2$ and $4\pi\zeta_a/f_n$, respectively as shown in equation (24) and herein f_n is used instead of T_n).

As mentioned earlier, the amplitude and the fluctuating force coefficient can be described approximately in a sinusoidal form (Bearman 1984) as in the equation (1) and (2). After substituting y and c_y and equating cosine and sine terms, we have

$$A\left(m^* + C_a\right)\left(1 - \left(\frac{f_v}{f_n}\right)^2\right) = \frac{1}{2\pi^3}U^{*2}C_y\cos\phi \tag{25}$$

$$A\left(m^* + C_a\right)\left(2\zeta_a\left(\frac{f_v}{f_n}\right)\right) = \frac{1}{2\pi^3}U^{*2}C_y\sin\phi \tag{26}$$

In the lock-in range, f_v / f_n can be estimated as unity. Herein, since the effect of the added mass is already taken care of, the value of this ratio is unity (Khalak and Williamson 1996). By solving for the amplitude A, we arrive at

$$A = \frac{1}{4\pi^3}\frac{U^{*2}C_y\cos\phi}{\left(m^* + C_a\right)}\left(1 \pm \left(1 + \zeta_a^{-2}\tan^2\phi\right)^{\frac{1}{2}}\right) \tag{27}$$

Regarding the lightly damped system in the synchronization range, because of the small value ζ_a, and the fact that ϕ is close to $\pi/2$, the term $\zeta_a^{-2}\tan^2\phi$ is much larger than unity. Thus,

$$A = \frac{1}{4\pi^3}\frac{U^{*2}C_y\cos\phi}{(m^*+C_a)}\left(1\pm\frac{|\tan\phi|}{\zeta_a}\right) \tag{28}$$

Similarly, $|\tan\phi|/\zeta_a >> 1$ by the same reasons, we obtain

$$A = \frac{1}{4\pi^3}\frac{U^{*2}C_y\sin\phi}{(m^*+C_a)\zeta_a}\,. \tag{29}$$

This linear theory accounts for the effect of the added mass in a system of low m^* by using $(m^*+C_a)\zeta_a$ instead of $m^*\zeta$; there is a contradiction between the theory and the experimental result in the lower branch of resonance. A critical evaluation of this linear theory is given by Sarpkaya (1997).

1.6 Previously Related Investigations: Effect of Free-Surface

Although vortex-induced vibration of an elastically-mounted cylinder has received considerable attention for the case where the cylinder is well-submerged beneath a free-surface, the consequence of an adjacent free-surface has remained unclarified. It is worthwhile to first consider the case of oscillations of a cylinder or sphere in absence of a steady flow velocity. In this case, it is straightforward to describe the effect of the free-surface on the non-dimensional added-mass and -damping, as described by Naudascher and Rockwell (1994). As a result of previous investigations, they point out that the major parameters are the geometry of the body and nearby structures (if any), a viscous parameter, which has a Reynolds-number-like form $\omega D^2/\nu$ and a Froude-number-like

parameter ωD/c, the relative amplitude and direction of the oscillation and the nominal position of the body relative to the free-surface. In general, the added mass can change quite dramatically if a body is located either adjacent to a solid boundary or a free-surface. Patton (1965) provides information on the added-mass coefficient force sphere near an undisturbed free-surface and an cylinder adjacent to a wall in absence of viscous effects. Regarding the case of the sphere, the added-mass will change by more than a factor of two when the cylinder is located close to the free-surface. With increasing submergence beneath the free-surface, the limiting value of unity is attained, i.e., the completely-submerged condition is reached. A similar effect is observed regarding the added-mass of the circular cylinder adjacent to a wall (after Chen and Chung 1976). Again, the added mass can be increased by nearly a factor of two when the cylinder is brought very close to the surface.

In the presence of a steady flow, the effect on the added-mass cannot be determined analytically; nevertheless, the foregoing results do provide a basis for considering the more complex case. It should be pointed out, at this juncture, that in the event that an equivalent added mass can be determined, the mass-damping ratio will be influenced accordingly. The appropriate equation is:

$$\left(m^* + C_a\right)\zeta_a = \frac{c}{2m_d}\sqrt{\frac{m+m_a}{k}} \tag{30}$$

Loading on a cylinder undergoing motion adjacent to, and penetrating, a free-surface is described in the experimental investigation of Zhu et al. (1999). They studied the flow patterns and loading on the cylinder due to combined translatory and sinusoidal motion of the cylinder in the vicinity of a free-surface by employing a cinema technique

of high-image-density particle image velocimetry and simultaneous force measurements. The proximity of the free-surface to the upper surface of the cylinder advances the process of vortex shedding from the upper surface relative to that for the case of the completely-submerged cylinder. When the cylinder pierces the free-surface, both the lift and drag force coefficients exhibit a deep trough as the cylinder reaches its maximum vertical displacement. They reported large and negative values of lift coefficient that are dominated by a change in the buoyancy force.

Miyata et al. (1990) have addressed the case of a cylinder translating with uniform speed beneath a free-surface, without undergoing simulated transverse motion. Their investigation included both experimental and numerical considerations. At the shallow submerged condition, the difference of flow velocity in the vicinity of the top and bottom surfaces of the cylinder causes a symmetric vortex formation. As a consequence, this results in a lower drag coefficient and a higher frequency of vortex shedding. An interesting finding is that the force coefficient in the vertical direction (positive downward) gradually decreases when the cylinder is placed further from the free-surface and, at sufficiently deep submergence, it takes on a nearly constant value for any further increases in submergence.

Another class of related investigations is the case of nominally steady flow at sufficiently high Froude number past a stationary cylinder. Sheridan et al. (1997) observed the flow structure in the near-wake of the circular cylinder located at various depths of submergence. The intent of their investigation was to characterize the possible states of the wake as the depth between the free-surface in the cylinder was varied, without piercing the free-surface. Generally speaking, they observed that small changes

of depth of submergence could cause radical changes of the near-wake patterns. At sufficiently small submergence, a jet-like flow exists between the free-surface and the upper surface of the cylinder. When the depth of submergence is altered, it is possible to witness detachment of the jet from the cylinder surface. In fact, at certain critical values of submergence, the jet proceeds immediately beneath the free-surface, inducing a quasi-standing wave pattern. They point out that the possible stage of the wake can, in certain cases, exist only in a metastable form. That is, the flow pattern could gradually transform, in a self-sustaining fashion, between two states. The typical frequency of this type of transformation is, however, one or two magnitudes lower than the Kármán frequency of vortex formation from the completely submerged cylinder.

1.7 Objectives

It is evident from the foregoing that, at present, no investigation exists for the case of an elastically-mounted horizontal cylinder beneath the free-surface and the possibility of self-excited vibrations of the cylinder system. The overall objective of this research is to address this configuration, and determine the effect of depth of submergence on the possible states of oscillation of the cylinder. The dimensionless amplitude and frequency of the cylinder oscillation will be characterized for the case of a cylinder having a very low value of mass-damping ratio.

2. EXPERIMENTAL SYSTEM AND TECHNIQUES

A cylinder having a very low value of mass-damping ratio $m^*\zeta$ was mounted within a special test section insert, which, in turn, was placed within a main test section of a large-scale, free-surface water channel. These components of the experimental system, as well as the experimental techniques and procedures, are described in the following.

2.1 Description of Experimental System

All experiments were performed in a free-surface water channel having a main test section 914 mm wide, 610 mm deep, and 4572 mm long. This test section was preceded by a 2:1 contraction. At the inlet of the contraction, a honeycomb-screen system was deployed, in order to maintain the free-stream turbulence intensity < 0.1%. For the entire range of experiments, the water level was maintained at a depth of 546 mm. The free-stream velocity was varied over the range 25.4 mm/sec $\leq U \leq$ 152.4 mm/sec. This range of flow velocity represented a range of Reynolds number based on cylinder diameter of $321 \leq Re_D \leq 1927$.

A test section insert was deployed within the main test section of the water channel. This insert ensured that end wall boundary layer effects were minimal, and provided for adjustable elastic mounting of the cylinder system. This insert was 308 mm wide, 476 mm high, and 546 mm long. The vertical side (faults) walls were 6.4 mm thick, and made of optically transparent Plexiglas. Figures 2-2 to 2-4 exhibit the side, plan and end views of the test section insert, with the cylinder. The circular cylinder was solid, made of aluminum and had a diameter D = 12.7 mm and a length L = 305 mm,

thereby providing an aspect ratio L/D = 24. In order to preclude corrosion, the cylinder was polished, then painted flat black. Care was taken to ensure that small and consistent end gaps were maintained between the end of the cylinder and the vertical false wall for all experiments. These gaps were 0.125·D. On the near-wall, the surface is continuous, while on the far wall, a slot was machined to allow the cylinder to vibrate in the vertical direction; they extended this slot, which was 17.5 mm wide by 22.2 mm high, which was minimized in order to prevent significant distortion of the vortex shedding in this region.

The cylinder is held in position by a leaf spring made of brass. The length of the spring from the end of the cylinder to the mounting in the vertical wall is 195.6 mm. The cross-section of the spring is 12.7 mm wide by 0.79 mm thick. Static deflection tests reveal that the spring stiffness was 14.6 mm when mounted to attain a horizontal orientation of the cylinder beneath the free-surface in presence of buoyancy effects; the corresponding angle of this spring at the vertical false wall was, in this case, 55.3°. This arrangement was used for all experiments. The spring linearity was examined for the extreme deflection of 1.75·D considered in the present experiments. This was accomplished by applying a sequence of increasing weights in a suspended container from the cylinder. A further important consideration is the symmetry of the cylinder response about its equilibrium position in absence of free-surface effects. Various amplitude perturbations were applied to the cylinder, both in still air and in water, and the cylinder exhibited a symmetrical response below and above its equilibrium position.

The damping factor and natural frequency of the system were determined in both air and water by examining the free decay of the cylinder to an initial perturbation. In air, the damping ratio is $\zeta = 0.0006$ and the natural frequency $f_n = 0.876$ Hz. The value of

mass ratio m^* is defined as the mass of the displaced water to the mass of the cylinder system is $m^* = 2.7$. As a result of this consequence, the value of the mass-damping ratio is $m^*\zeta = 0.0017$. These values compare with those of Khalak and Williamson (1996), $m^* = 2.4$ and $m^*\zeta = 0.013$. Representative, earlier investigations of Feng (1968) and Brika and Laneville (1993) employed values of $m^*\zeta = 0.36$ and 0.41. It should be noted that the experimental configurations of all of these previous investigations are distinctly different from the present. Khalak and Williamson (1996) employed a vertical cylinder penetrating the free-surface, which was supported by an air-bearing arrangement. The experiments of both Feng (1968) and Brika and Laneville (1993) were both performed in air, the former involving a rigid circular cylinder and the latter a long flexible cylinder.

2.2 Experimental Techniques

A video recording system was employed to determine the history of the time-dependent fluctuations of the tip of the cylinder. The framing rate of the video system was thirty frames per second. This corresponds to the range of periods of the cylinder motion observed in this study, $0.547 \leq T_c \leq 1.786$ sec. This video technique was employed for all preliminary experiments for determining the damping and natural frequency of the cylinder, linearity of the spring and symmetry of the cylinder oscillation about its equilibrium position.

The distance between the cylinder and the free-surface was varied by moving the entire test section insert, which was supported by a large-scale traverse table. In turn, this traverse table was connected to a stepping motor arrangement. The flow speed U was varied by a high-resolution motor controller. The channel was calibrated using a sequence of PIV images at various motor settings, then checked using a floating marker

technique. The importance of sufficiently small velocity increments is underscored by the work of Brika and Laneville (1993), who noted that the nature of possible discontinuities of the amplitude response curve appeared to be different, depending upon the incremental velocity. In the present investigation, the smallest value of velocity increments corresponded to 1.27 mm/sec. In order to ensure that the cylinder oscillation attained its steady-state value, a five-minute delay was employed after attainment of a given value of velocity U, until video recording of the cylinder oscillation. This delay corresponds, for the longest period T_c of the cylinder oscillation to approximately 168 T_c.

A value of submergence h_o = 0 mm corresponds to intersection of the upper surface of the cylinder with the free-surface in absence of flow. For the present experiments, the dimensionless depths of submergence h^* at various values of h_o are indicated in Table 1.

h_o	$h^* = h_o/D$
0	0
1.59	0.125
3.18	0.25
4.76	0.375
6.35	0.5
9.53	0.75
12.7	1.0
19.1	1.5
25.4	2.0
38.1	3.0

Table 1: Experimental conditions.

The value of submergence h_o = 38.1 mm ($h^* = h_o/D \doteq 3$) was taken as equivalent to a fully-submerged cylinder, based upon the static loading experiments of Miyata et al. (1990), who towed a cylinder at steady velocity through quiescent water. For this case, as addressed subsequently herein, the dynamic response of the self-excited cylinder oscillation is compared with that of Khalak and Williamson (1996).

3. EXPERIMENTAL RESULTS AND DISCUSSION

3.1 Hydroelastic Response of Fully-Submerged Cylinder

Prior to establishing the effect of an adjacent free-surface on the self-excited oscillation characteristics of the cylinder, it is insightful to examine the response of the present cylinder system at a location sufficiently far beneath the free-surface, such that it is considered to be a fully-submerged cylinder. The experimental results of Miyata, Shikazono and Kanai (1990) examined the case of a steadily-towed cylinder beneath a free-surface. The results show that, for the case of $h^* = h_o/D = 3$, the steady lift on the cylinder corresponded to the limiting, fully-submerged case. This value of dimensionless submergence is therefore considered in comparison with previous investigations.

As discussed in Section 1.2, the relevant investigations of oscillating cylinders are those of Khalak and Williamson (1996), as well as earlier investigations of Feng (1968) and Brika and Laneville (1993). Even though the damping factors of all of these experiments are very low, the combined mass-damping ratios $m^*\zeta$ of the latter two studies are relatively high. Since both Feng (1968) and Brika and Laneville (1993) conducted their experiments in air, their values of mass ratio m^* were relatively high, and the corresponding values of $m^*\zeta$ are 0.36 and 0.41 respectively, as pointed out by Khalak and Williamson (1996). In contrast, the value of mass-damping ratio $m^*\zeta$ in the study of Khalak and Williamson (1996) is about thirty times smaller than the value of Feng (1968). As a consequence, the maximum amplitude of oscillation of the investigation of Khalak and Williamson (1996) is about twice that of Feng (1968). Most interesting,

however, is the fact that the synchronization range of Khalak and Williamson (1996) extends over a range of frequencies about four times larger than the frequency range of Feng (1968). Furthermore, the appearance of two branches of synchronization, i.e., lower and upper branches, is one of the key features of all three of the foregoing studies. In the investigation of Khalak and Williamson (1996), however, the lower branch is relatively flatter and longer compared to that of Feng (1968) and Brika and Laneville (1993). The most directly relevant investigation, considering the values of mass ratio m^* and mass damping ratio $m^*\zeta$ for comparison with the present study is the work of Khalak and Williamson (1996).

Figure 3-1 shows the comparison between the work of Khalak and Williamson (1996), corresponding to a mass ratio $m^* = 2.4$ and a mass damping ratio $m^*\zeta = 0.013$ with the present investigation, for which $m^* = 2.7$ and $m^*\zeta = 0.0017$. Despite the fact that the value of $m^*\zeta$ in the present investigation is about one order of magnitude smaller than that of Khalak and Williamson (1996), the values of maximum amplitude in both investigations are nearly equal. This suggests that an asymptotic value of mass-damping has been attained. A distinction between the present results and those of Khalak and Williamson (1996) is the fact that the maximum amplitude of the present data occurs at $V_r = 4.8$, whereas in the work of Khalak and Williamson (1996), it occurs at $V_r = 5$. In the initial region, corresponding to the onset of self-excited excitation, the agreement of both sets of data is very remarkable.

Moreover, both investigations exhibit lower and upper branches of synchronization, whereas a relatively large discontinuity, corresponding to an abrupt decrease in amplitude is observed in the data of Khalak and Williamson (1996). A

smaller discontinuity, which occurs at lower value of V_r is evident for the present data. For the present data, this abrupt drop in amplitude occurs at a value of V_r of about 5, whereas in the work of Khalak and Williamson, it occurs at about $V_r = 6$.

The issue arises as to whether hysteresis is significant in these types of response curves shown in Figure 3-1. In the article of Khalak and Williamson (1996), the hysteresis phenomenon was not addressed. For the present experiment, the effect of hysteresis is shown in Figure 3-2. For increasing values of flow velocity, the amplitude of vibrations deeply climbs due to increase in higher values until a value of $V_r = 4.7$ is reached. Then, the amplitude A/D abruptly drops. Further increases in reduced velocity V_r yield continuous decreases in A/D until, at a value of $V_r = 10$, the value of oscillation amplitude A/D is approximately equal to zero. This contrasts with the data of Khalak and Williamson (1996), shown in Figure 3-1, where the oscillation amplitude persists at a value of A/D = 0.1 for higher values of V_r.

After the increasing values of V_r reach the value in excess of $V_r = 10$, for which the cylinder no longer vibrated, the free-stream velocity was then gradually decreased. Generally speaking, the values of A/D took on the same values as for the case of increasing velocity. At a reduced velocity of approximately $V_r = 5$, however, instead of jumping back to the higher amplitude, the values of A/D proceed along the lower path indicated by the symbols in Figure 3-2. Over this range of V_r, the value of A/D had a nearly constant value of A/D = 0.8.. Then, at a value of $V_r = 3.7$, the data followed the same trend as for increasing flow velocity. It is therefore clear that the response curve of the present experiment exhibits a well-defined hysteresis loop, which is indicated by the small arrows in Figure 3-2. A major point of this investigation is to determine the effect

of an adjacent free-surface on this type of hysteresis loop, as well as the possible occurrence of other types of hysteresis.

3.2 Hydroelastic Response of Cylinder Located Extremely Close to Free-Surface

When the cylinder is located very close to the free-surface, in fact in the limiting case touches the free-surface for $h^* = h_0/D = 0$, the response of the cylinder h/D is dramatically altered. Figures 3-3 through 3-12 show the response curve corresponding to three values of submergence $h^* = 0$, 0.125 and 0.25. The range of lock-on for each of these cases is generally the same, except that it starts and ends at different values of reduced velocity V_r for each value of dimensionless submergence $h^* = 0$. In addition, two remarkable phenomena occur at these depths of submergence, i.e., a dual-amplitude response of the cylinder vibration and a remarkably large hysteresis loop, both of which are associated with a variation of the static position of the cylinder beneath the free-surface.

Dual Response Amplitude

In Figures 3-3, 3-7 and 3-11, it is clear that at a given value of reduced velocity V_r, two distinguishable response amplitudes occur. The values of each of these response amplitudes, as well as their average, are indicated on each of these figures. The ranges of reduced velocity for which these dual responses occur are as follows: for $h^* = 0$, $5.71 \leq V_r \leq 9.59$; for $h^* = 0.125$, $5.94 \leq V_r \leq 9.36$; and for $h^* = 0.25$, $6.28 \leq V_r \leq 7.65$. Notably, the deeper the submergence, the narrower the range of dual-amplitude response.

For the case $h^* = 0$, the cylinder oscillation starts at $V_r = 5.48$. The amplitude of vibration then ascends rapidly with increases in V_r until, at a value of $V_r = 5.71$, two

different amplitudes, A/D = 0.151 and A/D = 0.493 occur. At V_r = 5.82, the dual amplitudes come closer again, and at higher values of V_r, the difference between these amplitudes gradually increases. Over the range of V_r = 7.8 to 9.36, the difference varies between 0.26 and 0.43 A/D. In fact, the maximum difference occurs at the value of V_r = 8.11, where the larger relative amplitude A/D = 0.91 and the lower is 0.48. Eventually, at V_r = 9.70, the dual amplitude is submerged to a single value of A/D = 0.753. It is interesting to observe that the branch of the curve of Figure 3-3 corresponding to the lower amplitude attains its maximum-negative value at a lower value of V_r than the upper, larger-amplitude branch attains its maximum value.

After the dual amplitudes have merged to a single value at V_r = 9.7, the values of A/D continue to increase, then show a sharp decrease, followed by an abrupt drop to A/D = 0 at V_r = 12.56. This abrupt drop at high V_r suggests that, in analogy with a small-amplitude abrupt drop of Figure 3-2, the possible occurrence of hysteresis. This aspect will be addressed subsequently.

For a larger value of submergence, corresponding to lower h^* = 0.125, indicated in Figure 3-7, response curves are very similar in shape and trend to those of h^* = 0, shown in Figure 3-3. The maximum amplitude A/D of the higher-dual amplitude curve is achieved at V_r = 8.9 and, after the dual-response curves merge to a single value, the peak amplitude of the averaged response is at V_r = 10.16.

For still larger values of submergence, represented by h^* = 0.25, the range of values of V_r for which dual amplitudes occur is much smaller than in the foregoing cases. As indicated in Figure 3-11, dual-amplitude response extends only over the range $6.28 \leq V_r \leq 7.65$. The maximum value of A/D, corresponding to the higher dual-amplitude

curve is A/D = 0.815, whereas for the averaged curve, the maximum value is A/D = 0.78. It is clear that the maximum attainable amplitude at this larger value of $h^* = 0.25$ is significantly smaller than that observed for the previous cases of $h^* = 0$ and 0.125.

The occurrence of the dual-amplitude response observed in the foregoing cases is most likely related to a process of free-surface penetration, when the cylinder vibrates very close to the free-surface. Figures 3-21 to 3-22 show the occurrence of free-surface penetration, i.e., positive h_u over a certain range of the reduced velocity for each depth of submergence. Of course, when penetration occurs, the displaced fluid mass, and thereby the buoyancy force, decrease. Even though the motion of the cylinder is not perfectly two-dimensional, the fraction of the volume of the cylinder that pierces the free-surface is larger for lower values of h^* when the magnitude of penetration h_u is maintained constant. Generally speaking, it is recognized, as noted earlier in Section 1.6, that the presence of the free-surface affects the added mass and damping terms; a more complete analysis is called for.

Certain of these observations related to surface piercing are addressed in the experiment of Zhu et al. (1998). In that experiment, a circular cylinder was subjected to simultaneous translation and vertical acceleration in proximity to a free-surface. Large negative values of lift coefficient C_L were dominated by the change in the buoyancy force when the cylinder pierced the free-surface. This large negative value of C_L may be analogous to occurrence of C_L in the present experiment. That is, it is possible that the larger amplitude branch of the higher-dual-amplitude curve is related to this effect. The issue then arises as to why the lower branch of the dual-amplitude curve occurs. Perhaps

the vortex shedding process from the cylinder is altered during a portion of the cylinder cycle. It is evident that flow visualization is now required to resolve this issue.

Another interesting issue is, as already discussed in Section 1.6, the fact that the free-surface tends to decrease the added mass and increase the damping. From equation (30) it is clear that the amplitude of vibration is inversely proportional to the square root of the added mass. However, the oscillation amplitude is also proportional to the displaced fluid mass, so when there is free-surface piercing, the effect due to the change of added mass is probably offset by that of the displaced fluid mass.

Static Position of Cylinder

From a physical standpoint, it is clear that a finite gap between the upper surface of the cylinder and the free-surface is necessary to allow vortex formation from the upper surface of the cylinder, leading to alternate vortex shedding from both sides of the cylinder associated with the self-excited vibration. One expects, at these very small values of submergence h^* that the onset of cylinder vibration will occur at a higher velocity when the cylinder is located closer to the free-surface. Indeed, this seems to be the case. For values of $h^* = 0$, 0.125 and 0.25, the cylinder begins to vibrate at values of reduced velocity $V_r = 5.48$, 4.91 and 3.31 respectively. Values of the static displacement of the cylinder h_s/D are illustrated for the case $h^* = 0$ in Figure 3-21. With increasing value of V_r, the magnitude of h_s/D increases until it attains the value of $h_s/D = 0.65$, at which self-excited oscillations occur. Similarly, for values of $h^* = 0.125$ and 0.25, shown in Figure 3-22 and 3-23, the static position of the cylinder prior to the onset of vibration is respectively $h_s/D = 0.198$ and 0.250 respectively.

Furthermore, the static position of the cylinder at the upper end of each lock-on range, shown in Figures 3-21 through 3-23, is relevant to the previous investigation of Miyata et al. (1990), corresponding to steady translation of the cylinder beneath the free-surface. Their results indicate that the force coefficient, in the vertical direction (positive downward) is at a maximum value of 0.8 for the shallowest depth of submergence, equivalent to the present case of $h^* = 0$. The magnitude of the force coefficient F_z then gradually decreases to about 0.1 at values of $h^* = 0.5$. In accordance with these trends of the force coefficients of Miyata et al. (1990), a larger relative deflection of the cylinder from its original position can be expected when it occurs closer to the free-surface. For the case $h^* = 0$, represented in Figure 3-21, a relatively large value of the static position $h_s/D = 0.733$ occurs at the end of the synchronization range, corresponding to $V_r = 12.9$. For $h^* = 0.125$ and 0.25, represented in Figures 3-22 and 3-23, the relative deflections at the end of the lock-on region are $h_s/D = 0.619$ and 0.182 respectively.

Hysteresis Effect

For the cases where the cylinder is located very close to the free-surface, corresponding to the case of $h^* = 0$, 0.125 and 0.25, as addressed in the foregoing, a key feature is the occurrence of substantial hysteresis. This type of hysteresis appears to be distinguished from that described in Section 3.1 for the case of the fully-submerged cylinder.

As indicated in Figures 3-4 to 3-6, for the case $h^* = 0$, when the flow velocity was decreased from $V_r = 12.79$, corresponding to the value at which the cylinder stopped vibrating, the cylinder oscillates at relatively small amplitudes, $A/D < 0.1$, relative to the large amplitude at the same value of reduced velocity when the value of reduced velocity

V_r is increased. As the value of reduced velocity V_r is decreased further, the relatively low amplitude vibrations persist until, at a value of $V_r = 9.93$. The amplitude A/D rapidly jumps to a value of A/D = 0.76. For further decreases in V_r, the amplitude values of A/D proceed along the same path as when the flow velocity is increased.

A generally similar trend is evident for a value of $h^* = 0.125$. It is indicated in Figures 3-8 to 3-10. The hysteresis loop extends over the range of reduced velocity from $V_r = 12$ to $V_r = 9.4$.

It is particularly interesting to note that, for both cases, $h^* = 0$ and 0.125. The end of the hysteresis loop is nearly coincident with the point at which the higher and lower values of dual amplitude response merge to a single value of response. Afterwards, as the flow velocity is further decreased, the dual amplitude reappears in the same range of reduced velocity for which it occurs for the case of increasing reduced velocity V_r, compare Figures 3-4 and 3-5 and 3-8 and 3-9.

For the largest value of submergence $h^* = 0.25$ considered in this category, the hysteresis effect seems to extend over a larger range of reduced velocity, i.e., from V_r = 10.16 to 5.48. As a matter of fact, this is the largest hysteresis loop of all cases investigated. Figure 3-12 shows that the vibration amplitude remains relatively small until the reduced velocity V_r is decreased to a value of $V_r = 5.37$, at which the amplitude A/D abruptly increases to A/D = 0.615. The lower end of the hysteresis loop, which occurs at $V_r = 5.48$ is, however, for this particular case, outside of the dual-amplitude response region.

3.3 Hydroelastic Response of Cylinder Located Moderately Close to Free-Surface

Whereas the previous section addressed cases of a cylinder very close to the free-surface, this section considers the response of the cylinder at locations moderately close to the free-surface. As will be discussed, the response characteristics of the cylinder in this category show distinctive features relative to those discussed in Section 3.2. The depths of submergence of interest in this section include $h^* = 0.375$, 0.5, 0.75 and 1.0. The corresponding response curves are shown in Figures 3-13 to 3-16. These amplitude response A/D curves are actually derived from curves representing the extreme values of cylinder deflection measured with respect to the free-surface, as shown in Figures 3-24 to 3-27. In essence, these extreme values of displacement, or deflection, are designated as h_u and h_ℓ, as defined in the schematics of Figures 3-24 to 3-27. In addition, the static displacement, or deflection, of the cylinder h_s is also indicated. As is evident from examination of Figures 3-13 to 3-16, as well as Figures 3-24 to 3-27, the cylinder response in this category does not exhibit a so-called dual-amplitude response, in contrast to the cases of a cylinder located very close to the free-surface addressed in Section 3.2.

Consider, first of all, the case $h^* = 0.375$, represented by Figures 3-13 and 3-24, which show, respectively, the response curve and the extreme deflections of the cylinder. Although Figure 3-24 shows a small amount of free-surface penetration, it represents a significantly lower value of volume of the cylinder that pierces the free-surface, relative to the cases discussed in Figure 3.2. As a consequence, this condition may not be strong enough to induce a dual amplitude response.

Figure 3-13, corresponding $h^* = 0.375$, shows a response curve generally similar to that of $h^* = 0.25$ addressed in Section 3.2. That is, two dominant peaks can be

recognized, but in the case shown in Figure 3-13, the first peak A/D = 0.817 (at V_r = 5.48) is significantly larger than the second peak A/D = 0.699 (at V_r = 8.11).

Also shown in Figure 3-13 is the extent of the hysteresis loop. This loop has the same general extent as the loops discussed previously for h^* = 0 and 0.125, but is about one-half the extent of the loop at h^* = 0.25. This distinction occurs in spite of the fact that the overall range of synchronization of the cylinder oscillation shown in Figure 3-13 extends only from V_r = 3.31 to 8.33, which is a narrower band than observed for h^* = 0, 0.125 and 0.25 addressed in Section 3.2.

For a deeper submergence of the cylinder, corresponding to h^* = 0.5, shown in Figure 3-14, the range of V_r for which lock-on occurs is substantially contracted and, moreover, the extent of the hysteresis loop dramatically shrinks. A similar observation holds for the value of submergence h^* = 0.75 and 1.0, represented by Figures 3-15 and 3-16, except that at these two depths the hysteresis effect does not exist.

A further point regarding the response is illustrated in Figures 3-26 and 3-27. When the cylinder is located deeper beneath the free-surface, the displacement curves h_u and h_ℓ exhibit an increasingly similar shape.

3.4 Hydroelastic Response of Nearly Fully-Submerged Cylinder

For deeper values of response than discussed in Sections 3.2 and 3.3, the response of the cylinder tends towards that of a fully-submerged cylinder, addressed in Section 3.1. Figures 3-17 and 3-18 show the response amplitude A/D for the case of h^* = 1.5 and 2 respectively. In comparison with the cases discussed in Section 3.3, the range of lock-on occurring at these depths of submergence is larger and, moreover, is nearly as larger as that occurring for the fully-submerged case.

For the case $h^* = 1.5$, shown in Figure 3-17, the lock-on or synchronization extends over the range of reduced velocity V_r from 2.85 to 9.02. Immediately after the onset of oscillation, the response amplitude climbs very rapidly and approaches its maximum value A/D = 0.946 at $V_r = 4.34$. Subsequently, the amplitude drops, then shows only mild decrease for increasing values of reduced velocity V_r. At, for example, $V_r = 4.79$, the normalized amplitude A/D = 0.811. Starting at $V_r = 7.08$, the response amplitude decreases very rapidly until the cylinder ceases vibration at $V_r = 9.02$.

Also shown in Figure 3-17 is the case where the flow velocity V_r was decreased. These data are nearly coincident with date corresponding to increase in flow velocity and, therefore, no hysteresis occurs.

For the case $h^* = 2$, shown in Figure 3-18, the response curve is nearly identical to that at $h^* = 1.5$, except that the range of lock-on is slightly larger and the discontinuity between $V_r = 4.57$ and 4.68 is more apparent. No hysteresis occurs in this case.

The shapes of the deflection curves h_u and h_ℓ corresponding to $h^* = 1.5$ and 2.0 are exhibited in Figures 3-28 and 3-29. These curves are nearly identical, which means that the upstroke and downstroke portions of the oscillation cycle, relative to the equilibrium position of the cylinder, are essentially symmetrical. This observation indicates that the mounting arrangement of the cylinder does not contribute any bias to the amplitude response.

3.5 Frequency of Vibration

An important feature of lock-on response of an elastically-mounted, fully-submerged cylinder is oscillation of the cylinder at a frequency corresponding to the natural frequency of the elastically-mounted cylinder. The issue arises as to whether

presence of the free-surface has a significant influence on the generic plot of f/f_n versus V_r for the case of the fully-submerged cylinder. Figures 3-31 through 3-40 illustrate this type of frequency plot for varying degrees of cylinder submergence h^*.

Consider, first of all, the case of the fully-submerged cylinder shown in Figure 3-40. Denote frequency ration f^* as the ratio of the oscillation frequency of the cylinder to the natural cylinder frequency of the cylinder system, i.e., $f^* = f/f_n$. The solid, inclined line shown in Figure 3-40 is based on a Strouhal number S = 0.2. At lower values of V_r, values of f^* are nearly parallel to the S = 0.2 characteristic. Then, at $f^* = 1.0$, and towards a constant, even though V_r varies, and, finally, at highest values of V_r show a gradual increase. From the study of Meier-Windhorst (1939), the results indicate the variation in vibration frequency f between 80% and 120% of the natural frequency f_n (measured in still water). This is rather typical for the experiments in water, as opposed to experiments in air, for which f is close to f_n over the entire range of oscillation. Khalak and Williamson (1997) also reported this type of non-classical variation of f^*, whereby the value of f^* lies above the natural frequency in, but below the inherent vortex shedding line. They also further mention that this sort of occurrence is found in experiments of Govardham and Williamson (1997).

These results can be interpreted in comparison with those of Feng (1968), for which the mass ratio m^* is relatively large, as discussed in Sections 2.1 and 3.1. In his results, it is evident that the oscillation frequency is at an essentially constant value, but slightly lower than the natural frequency line. In other words, his experiments did not show the non-classical behavior. These observations suggest that attainment of a very

low mass-damping ratio of order 10^{-2} plays an important role on the vibrational response, in particular the frequency f^* response; simply considering low damping is not adequate.

When the effect of the free-surface is considered, the complexity of the f^* versus V_r plots increases substantially. Consider, for instance, the case $h^* = 0$, shown in Figure 3-31. The cylinder starts vibrating at a relatively high velocity $V_r = 5.71$, compared to the more deeply submerged cases. It is clear from the plot of Figure 3.31 that the dimensionless frequency f^* is higher than both the inherent vortex shedding frequency and the natural frequency of elastic system. The frequency f^* gradually increases and approaches the inherent shedding frequency at about $V_r = 6.85$. For further increases in V_r, it tends towards a plateau value, that is, exhibits only mild increases. Then, over the highest range of V_r, it is essentially parallel to the line representing the inherent vortex shedding frequency. It must be emphasized, however, that when the cylinder is located close to the free-surface, the inherent shedding frequency from the corresponding stationary cylinder is expected to differ substantially from the value corresponding to a fully-submerged cylinder. In fact, if the cylinder is held in a stationary position just beneath the free-surface, it is questionable that periodic vortex formation will occur. It is intended to address this aspect in conjunction with PIV measurements. The result may show that oscillations of the cylinder are necessary in order to detect a periodic vortex formation. Of course, this hypothesis contrasts with the case of a fully-submerged cylinder, for which cyclic vortex formation occurs when the cylinder is held stationary. Another distinctive feature of the plot of Figure 3-31 is that "lock-on" does not really appear to occur in the usual sense. That is, the data do not exhibit a relatively constant value of f^* for variations of V_r. The question then arises as to why the response of the

cylinder, shown in terms of A/D versus V_r in Figure 3-1 has a form that is generally similar to the locked-on response of the fully-submerged cylinder. This aspect also requires further investigation.

For the values of h^* represented in Figures 3-32 through 3-39, the frequency response f^* versus V_r generally show a transformation towards the case of the fully-submerged cylinder. Peculiarities are evident, for example, in Figures 3-34 and 3-35, for which the data at the lowest values of V_r seem to be nearly parallel to the natural frequency line. Moreover, not until a value of h^* represented in Figure 3-36, does the onset of a lock-on response appear to be evident.

4. CONCLUSIONS

This investigation has addressed the elastic response of a horizontal cylinder beneath a free-surface. In doing so, a cylinder system having an extremely low value of mass-damping ratio, $m^*\zeta = 0.0017$, was designed and implemented. The dimensionless amplitude of the vibrational response of the cylinder was characterized using a video recording technique and, in addition, the dimensionless frequency was also determined. Both the amplitude and frequency are found to be the strong functions of reduced velocity, and the effect of an adjacent free-surface has, in some cases, a profound effect on the vibration characteristics of the cylinder.

For the case where the cylinder is submerged well beneath the free-surface, its response characteristics agree well with recent, independent investigations. In fact, the dimensionless amplitude as a function of reduced velocity exhibits remarkable agreement with a previously-investigated configuration of a vertical cylinder that pierces the free-surface. Both lower and upper branches of the response are detectable, although the jump between the branches is not as pronounced as for the case of the vertical cylinder. Most likely, this is due to a combination of end effects and the fact that, in the present case, the cylinder was cantilevered, as opposed to vibrating in a one-dimensional mode. Nevertheless, this agreement with the previously studied reference case provides a suitable basis for comparing the effect of an adjacent free-surface. A further aspect of agreement with the previously studied case of a vertical cylinder is a variation of dimensionless frequency with reduced velocity. It is found that in the region of lock-on, or synchronized, response of the cylinder, it is possible to generate the value of

dimensionless frequency lying above the natural frequency of the cylinder system and below the inherent vortex shedding frequency from the corresponding stationary cylinder. With close agreement between the present case of a horizontal, well-submerged cylinder and a vertical surface piercing cylinder, the distinctive features of the cylinder oscillation in close proximity to the free-surface can be characterized with confidence.

The range of reduced velocity over which lock-on or synchronization occurs is a strong function of proximity to the free-surface. For certain values of submergence, it is possible to attain ranges of synchronization that are either larger or smaller than the reference case of the fully-submerged cylinder. This range of synchronization occurs in accord with a dual amplitude response, for the case where the nominal position of the cylinder is immediately beneath the free-surface. In this case, the response of the cylinder is asymmetric about its equilibrium position. That is, the magnitude of the upstroke is smaller than the magnitude of the downstroke. Most importantly, however, is the fact that the downstroke exhibits two amplitudes, i.e., a dual amplitude response. The time trace of amplitude response shows alternating small and large values of magnitude of the downstroke displacement of the cylinder. Since this dual amplitude response occurs only during free-surface penetration, it is most likely linked to a change in buoyancy force during penetration of the free-surface.

Another important observation is the occurrence of dramatic hysteresis of the cylinder amplitude response, which extends over a relatively wide range of reduced velocity. This type of hysteresis is distinctly different from that occurring for the case of the fully submerged cylinder, i.e., hysteresis between the upper and lower branches of response. For the case where the cylinder is located sufficiently close to the free-surface,

values of dimensionless amplitude of the cylinder oscillation extend to relatively high values of reduced velocity when the velocity is increased; on the other hand, when the velocity is decreased, these large amplitudes first occur at much lower values of reduced velocity. In these cases, the size of the hysteresis loops is surprisingly large. When the nominal submergence between the free-surface is sufficiently large, this type of hysteresis disappears.

Regarding the dimensionless frequency of oscillation, well-defined regions of locked-on response can be observed for sufficiently deep submergence beneath the free-surface. That is, the oscillation frequency of the cylinder remains nearly parallel to the constant value of natural frequency of the elastically-mounted cylinder as reduced velocity is increased. In contrast, for sufficiently small values of submergence beneath the free-surface, no such locked-on region is detectable. Yet, the amplitudes of oscillation in these cases are relatively large. The physical explanation of this effect requires further consideration.

It is evident from the foregoing that a number of new findings have been obtained and shown to be consistent with variations in nominal depth of submergence. Further efforts are required, however, in order to determine the relationship between the vortex structure from the oscillating cylinder and the new types of amplitude and frequency response described in the foregoing.

REFERENCES

Blevins, R.D., 1990. Flow-Induced Vibration. Krieger Publishing Company.

Blake, W.K., 1986. Mechanics of Flow-Induced Sound and Vibration–Vol. 1: General Concepts and Elementary Sources. Academic Press, Inc.

Bearman, P.W., 1984. "Vortex Shedding from Oscillating Bluff Bodies," *Annual Review of Fluid Mechanics*, Vol. 16, pp. 195-222.

Brika, D., and Laneville, A., 1993. "Vortex-Induced Vibrations of a Long Flexible Circular Cylinder," *Journal of Fluid Mechanics.* Vol. 250, pp. 481-508.

Chen, S.S. and Chung, H., 1976. "Design Guide for Calculating Hydrodynamic Mass," ANL-CT-76-45, Argonne National Laboratory, Argonne, Illinois.

Feng, C.C., 1968. "The Measurement of Vortex-Induced Effects in Flow Past Stationary and Oscillating Circular and D-Section Cylinders," *MASc Thesis, University of British Columbia.*

Govardhan, R., and Williamson, C.H.K., 1997. "Vortex Induced Motions of a Tethered Sphere," *Journal of Wind Engineering and Industrial Aerodynamics (in press).*

Griffin, O.M., 1978. "Vortex-Excited Unsteady Forces on Resonantly Vibrating Bluff Structures," Naval Research Laboratory, Memorandum Report 3820. Washington, Aug.

Griffin, O.M., 1980. "Vertex-Excited Cross-Flow Vibrations of a Single Cylinder Tube," *Journal of Pressure Vessel Technology,* Vol. 102, pp. 158-166.

Griffin, O.M., and Kooper, G.H., 1977. "The Vortex-Excited Lift and Reaction Forces on Resonantly Vibrating Cylinders," *Journal of Sound and Vibration,* Vol. 54, pp. 435-448.

Griffin, O.M., and Ramberg, S.E., 1974. "The Vortex Street Wakes of Vibrating Cylinders," *Journal of Fluid Mechanics* Vol. 66, pp. 553-576.

Huerre, P., and Monkewitz, P.A., 1990. "Local and Global Instabilities in Spatially Developing Flows," *Annual Review of Fluid Mechanics,* Vol. 22, pp. 473-537.

Khalak, A. and Williamson, C.H.K., 1996. "Dynamics of a Hydroelastic Cylinder with Very Low Mass and Damping," *Journal of Fluids and Structures,* Vol.10, pp.455-472.

Khalak, A. and Williamson, C.H.K., 1997. "Fluid Forces and Dynamics of a Hydroelastic Structure with Very Low Mass and Damping," *Journal of Fluids and Structures*, Vol. 11, pp. 973-982.

Meier-Windhorst, A., 1939. "Flatterschwingungen von Zylindern in Gleichmassigen Flussigkeitsstrom," *Mitteilungen Hydraul. Inst. Techn. Hochschule, Munchen.* Vol. 9, pp. 3-9.

Miyata, H., Shikazono, N. and Kanai, M., 1990. "Forces on a Circular Cylinder Advancing Steadily beneath the Free Surface," *Journal of Ocean Engineering,* Vol. 17, pp. 81-104.

Naudascher, E. and Rockwell, D., 1994. Flow-Induced Vibrations–An Engineering Guide. A.A.Balkema.

Oertel, H. Jr., 1990. "Wakes Behind Blunt Bodies," *Annual Review of Fluid Mechanics,* Vol. 22, pp. 539-564.

Ongoren, A. and Rockwell, D., 1988a. "Flow Structure from an Oscillating Cylinder. Part 1–Mechanisms of Phase Shift and Recovery in the Near Wake," *Journal of Fluid Mechanics.* Vol. 191, pp. 197-223.

Ongoren, A. and Rockwell, D., 1988b. "Flow Structure from an Oscillating Cylinder. Part 2–Mode Competition in the Near Wake," *Journal of Fluid Mechanics.* Vol. 191, pp. 225-245.

Parkinson, G.V., 1989. "Phenomena and Modelling of Flow-Induced Vibrations of Bluff Bodies," *Progress in Aerospace Sciences.* Vol. 26, pp. 169-224.

Parkinson, G.V., 1974. "Mathematical Models of Flow-Induced Vibrations of Bluff Bodies," Flow Induced Structural Vibrations. (ed. E. Naudascher), pp. 81-127, Springer.

Patton, K.T., 1965. "Tables of Hydrodynamic Mass Factors for Translational Motion," Winter Annual Meeting ASME, Chicago, Illinois, Paper 65-WA/UNT-2.

Sarpkaya, T., 1977. "Transverse Oscillations of a Circular Cylinder in Uniform Flow," Naval Postgraduate School, Monterey, Report NPS-69SL77071-R, Dec.

Sarpkaya, T., 1978. "Fluid Forces on Oscillation Cylinders," *ASCE Journal of Waterways, Ports, Coastal Ocean Division,* Vol. 104, pp. 275-290.

Sarpkaya, T., 1979. "Vortex-Induced Oscillations–A Selective Review," *Journal of Applied Mechanics.* Vol. 46, pp. 241-258.

Sarpkaya, T., 1996. "Vorticity, Free Surface, and Surfactants," *Annual Review of Fluid Mechanics,* Vol. 28, pp. 83-128.

Sarpkaya, T. 1997. "Discussion on Khalak and Williamson (1996)," *Journal of Fluids and Structures*, Vol. 11, pp. 549-552.

Shabana, A.A., 1991. Theory of Vibration: An Introduction. Vol. 1, Springer-Verlag New York, Inc.

Sheridan, J., Lin, J.-C., and Rockwell, D., 1997. "Flow Past a Cylinder Close to a Free Surface," *Journal of Fluid Mechanics.* Vol. 330, pp. 1-30.

Staubli, T., 1983. "Calculation of the Vibration of an Elastically Mounted Cylinder Using Experimental Data from Forced Oscillation," *The Journal of Fluids Engineering,* Vol. 105, pp. 225-229.

Szepessy, S., Bearman, P.W., 1992. "Aspect Ratio and End Plate Effects on Vortex Shedding from a Circular Cylinder" *The Journal of fluid Mechanics,* Vol. 234, pp. 191-217.

Unal, M.F., and Rockwell, D. 1988a. "On Vortex Formation from a Cylinder. Part 1. The Initial Instability," *Journal of Fluid Mechanics,* Vol. 190, pp. 491-512.

Unal, M.F., and Rockwell, D. 1988b. "On Vortex Formation from a Cylinder. Part 2. Control by Splitter Plate Interference," *Journal of Fluid Mechanics,* Vol. 190, pp. 513-529.

Vandiver, J. K. 1993. "Dimensionless Parameters Important to the Prediction of Vortex-Induced Vibration of Long, Flexible Cylinders in Ocean Currents," *Journal of Fluids and Structures*, Vol. 7, pp. 423-455.

Williamson, C.H.K., and Roshko, A., 1988. "Vortex Formation in the Wake of an Oscillating Cylinder," *Journal of Fluids and Structures,* Vol. 2, pp. 355-381.

Williamson, C.H.K., 1996. "Vortex Dynamics in the Cylinder Wake" *Annual Review of Fluid Mechanics,* Vol.28, pp. 477-539.

Zhu, Q., Lin, J.-C., Unal, M.F., and Rockwell, D., 1998. "Motion of a Cylinder Adjacent to a Free-Surface: Flow Patterns and Loading," submitted to *Experiments in Fluids* (May 18, 1998).

Zdravkovich, M.M., 1982. "Modification of Vortex Shedding in the Synchronization Range," *Journal of Fluid Mechanics,* Vol. 104, pp. 513-517.

Zdravkovich, M.M., 1996. "Different Modes of Vortex Shedding–An Overview," *Journal of Fluids and Structures,* Vol. 10, pp. 427-437.

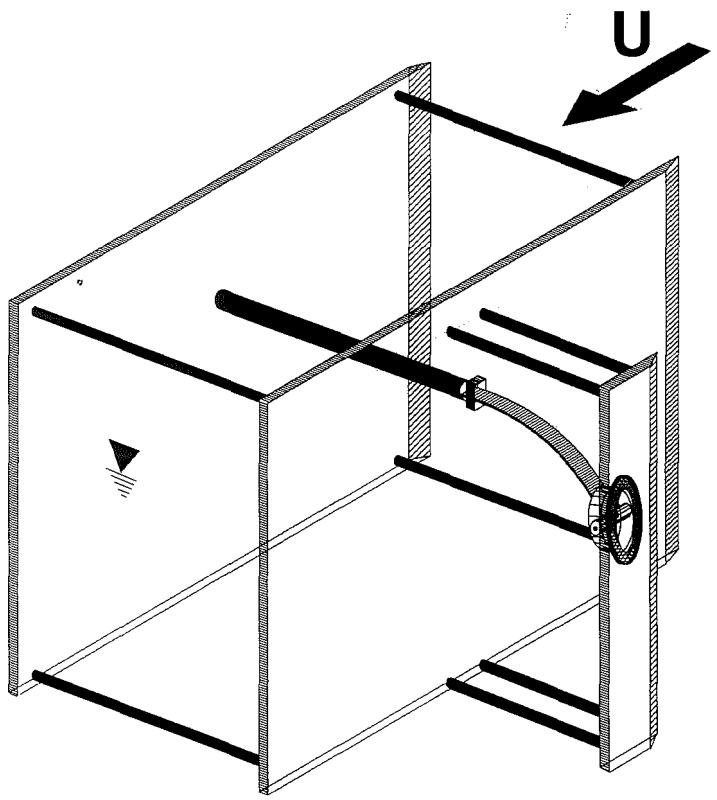

Figure 2-1: Perspective view of the test section of experimental system.

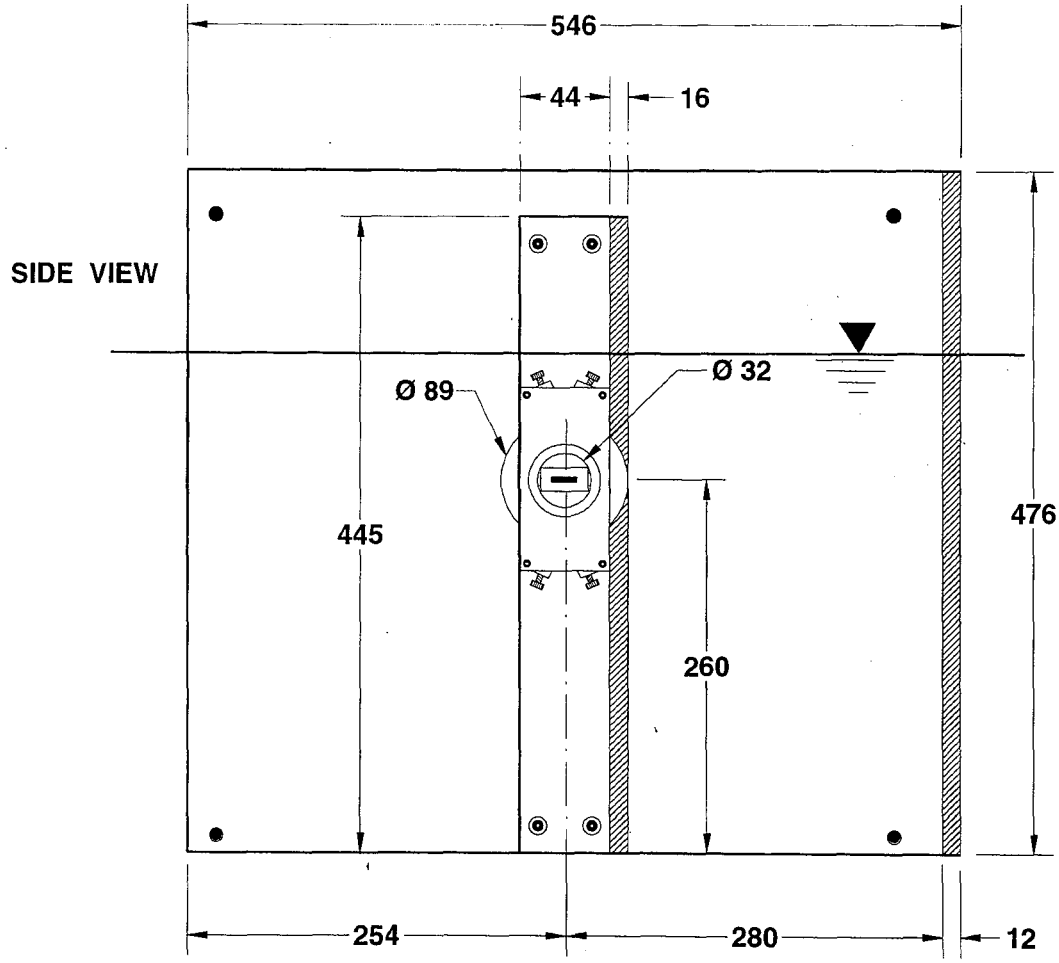

Figure 2-2: Side view of the test section of experimental system. All dimensions in millimeters.

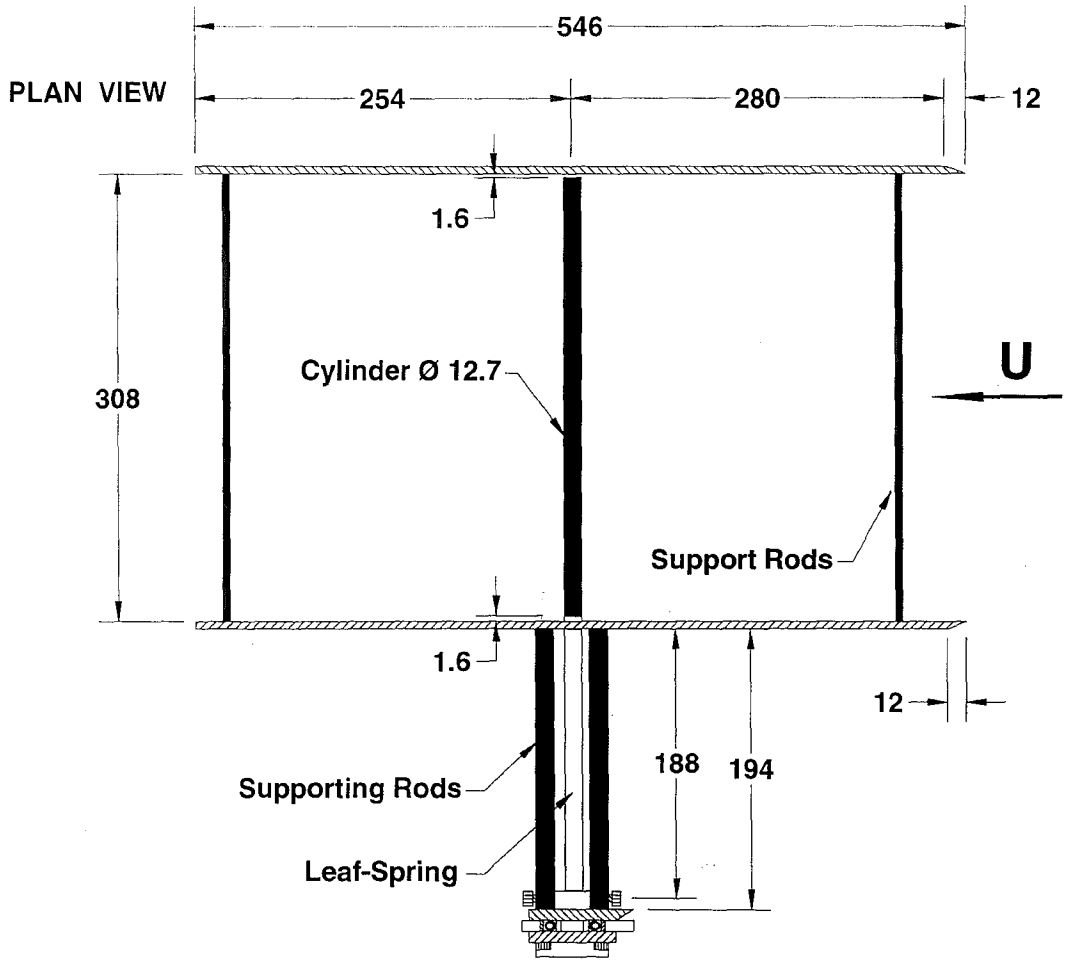

Figure 2-3: Plan view of the test section of experimental system. All dimensions in millimeters.

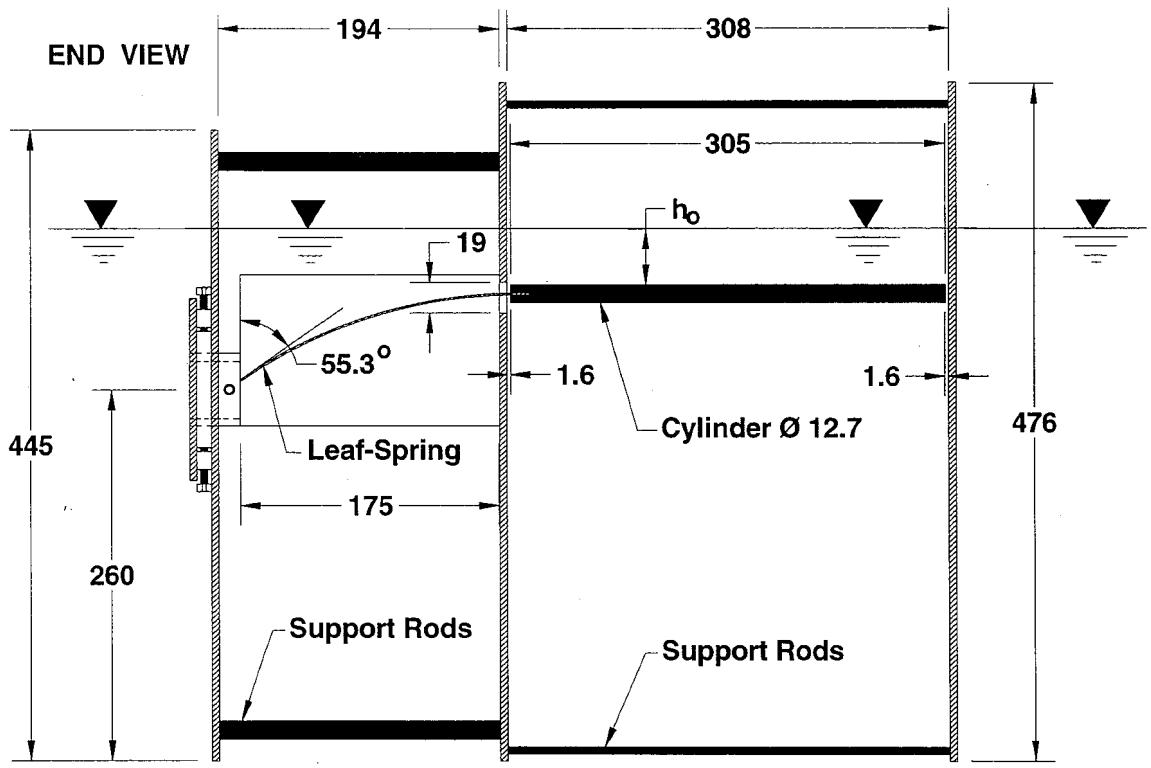

Figure 2-4: End view of the test section of the experimental system. All dimensions in millimeters.

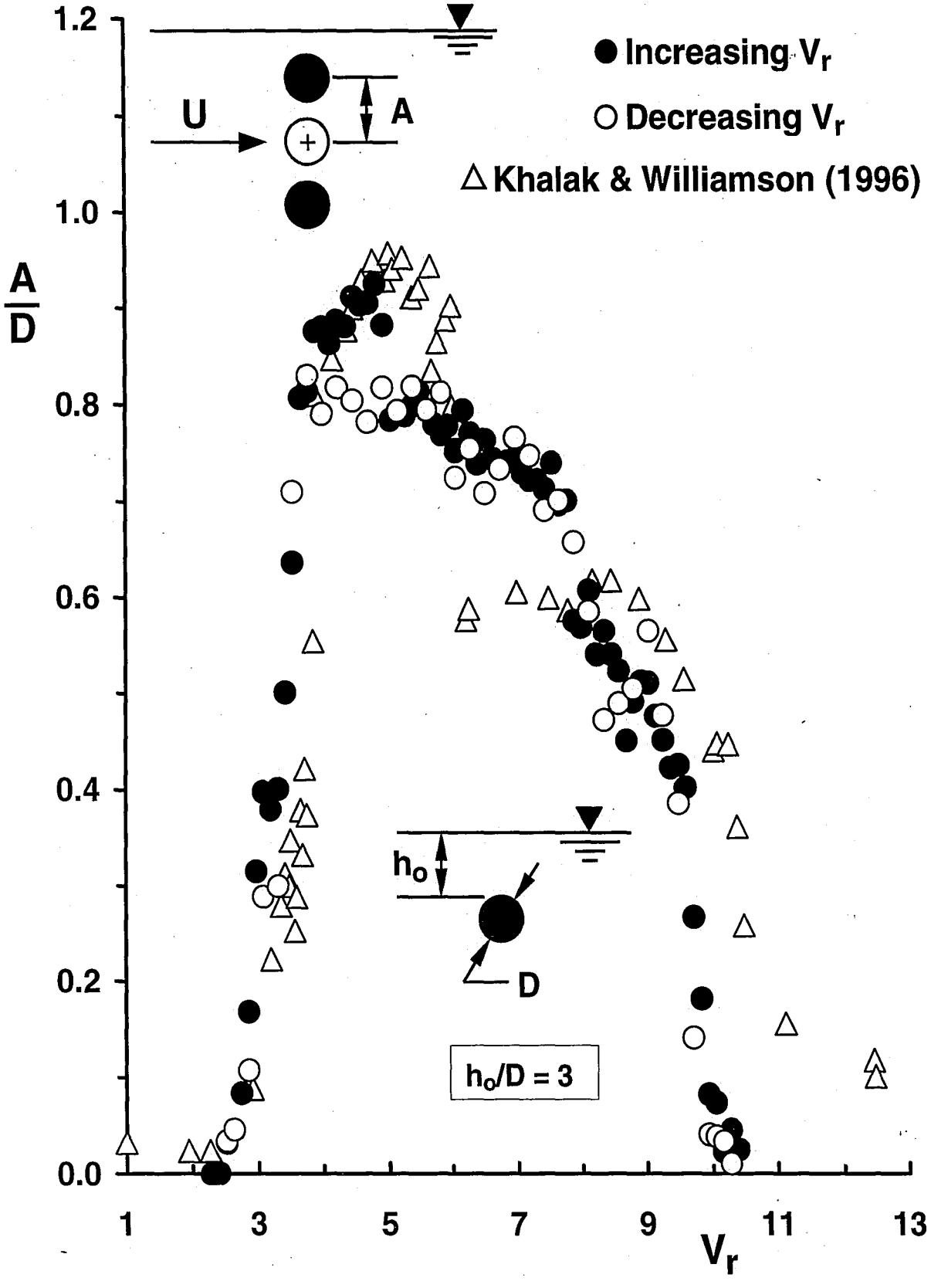

Figure 3-1: Relative response amplitude for the depth of submergence $h^* = h_o/D = 3$ of present experiments compared to those of Khalak and Williamson (1996) for a vertical, surface-piercing cylinder.

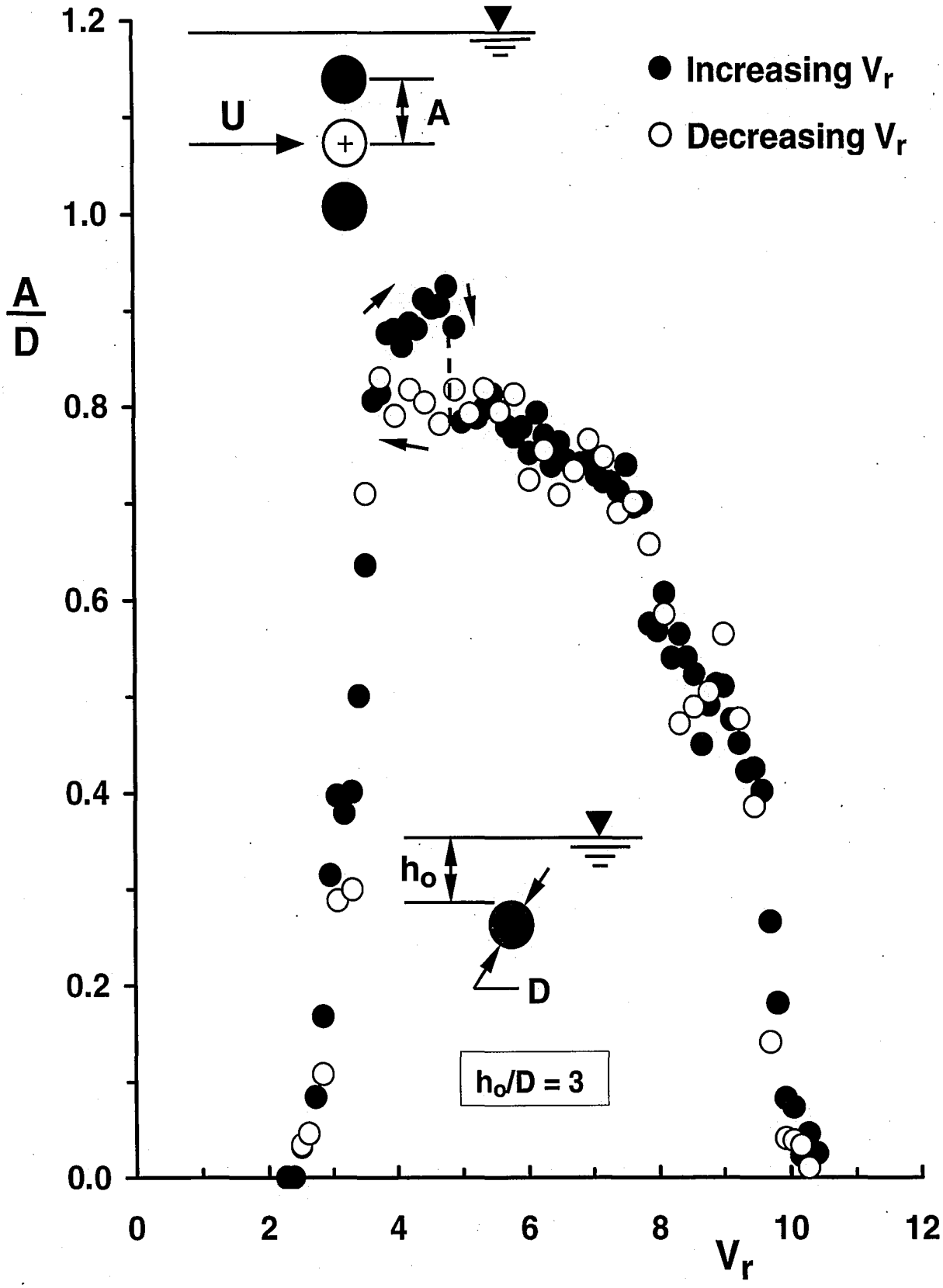

Figure 3-2: Relative response amplitude for increasing and decreasing V_r for the depth of submergence $h^* = h_o/D = 3$.

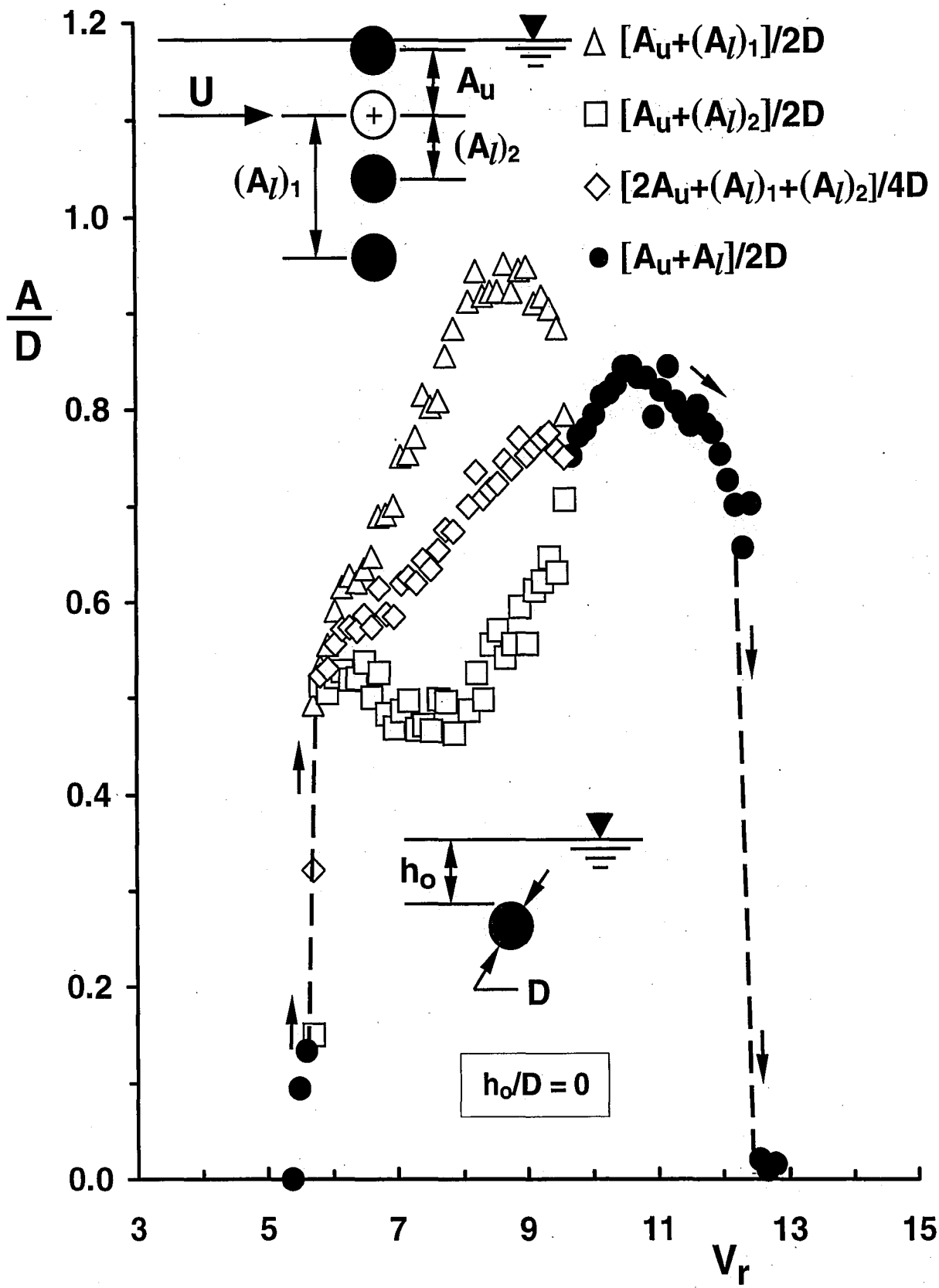

Figure 3-3: Relative response amplitude for increasing and decreasing V_r for the depth of submergence $h^* = h_o/D = 0$.

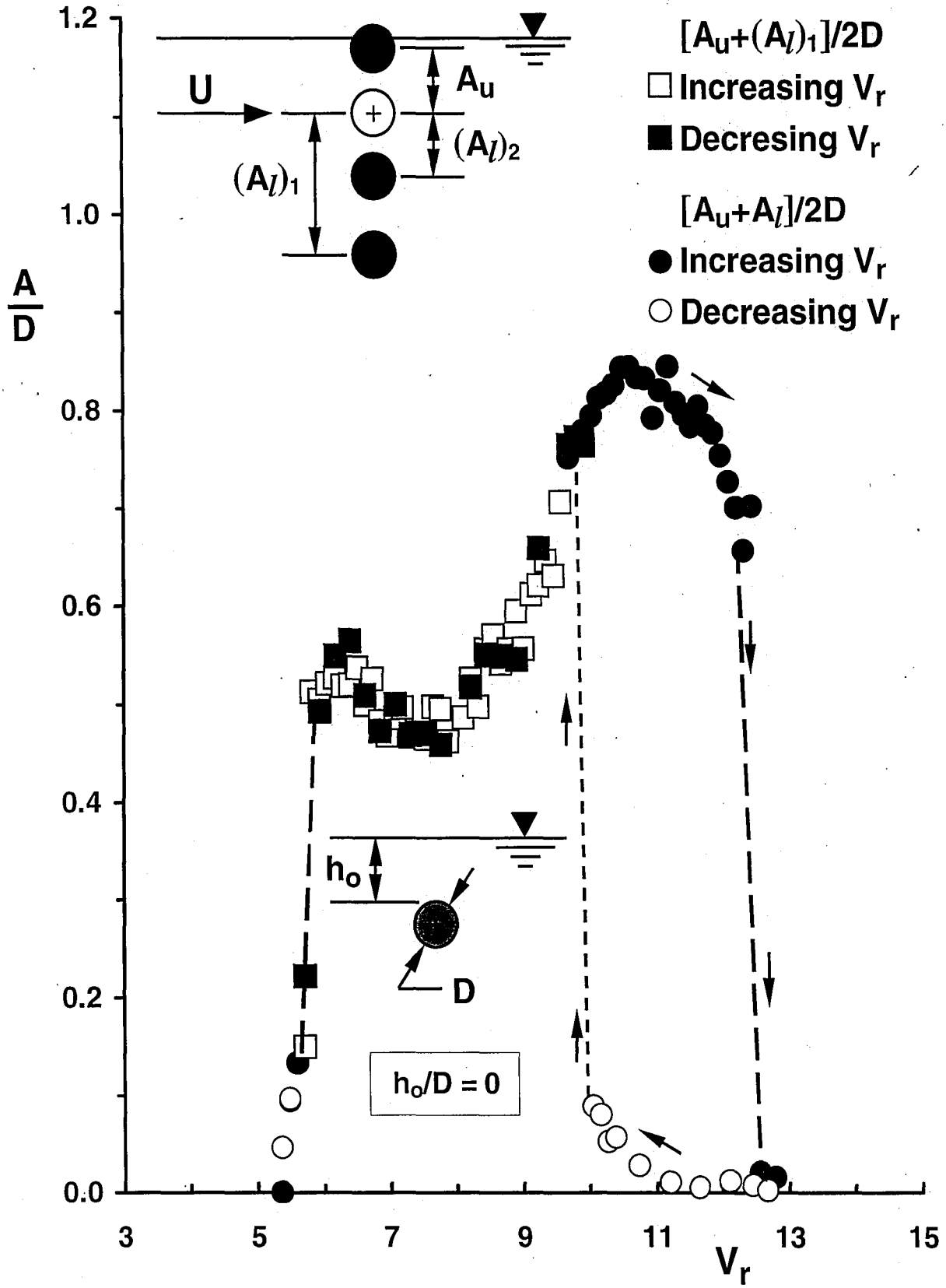

Figure 3-4: Relative response amplitude of lower-dual-amplitude branch for increasing and decreasing V_r for the depth of submergence $h^* = h_o/D = 0$.

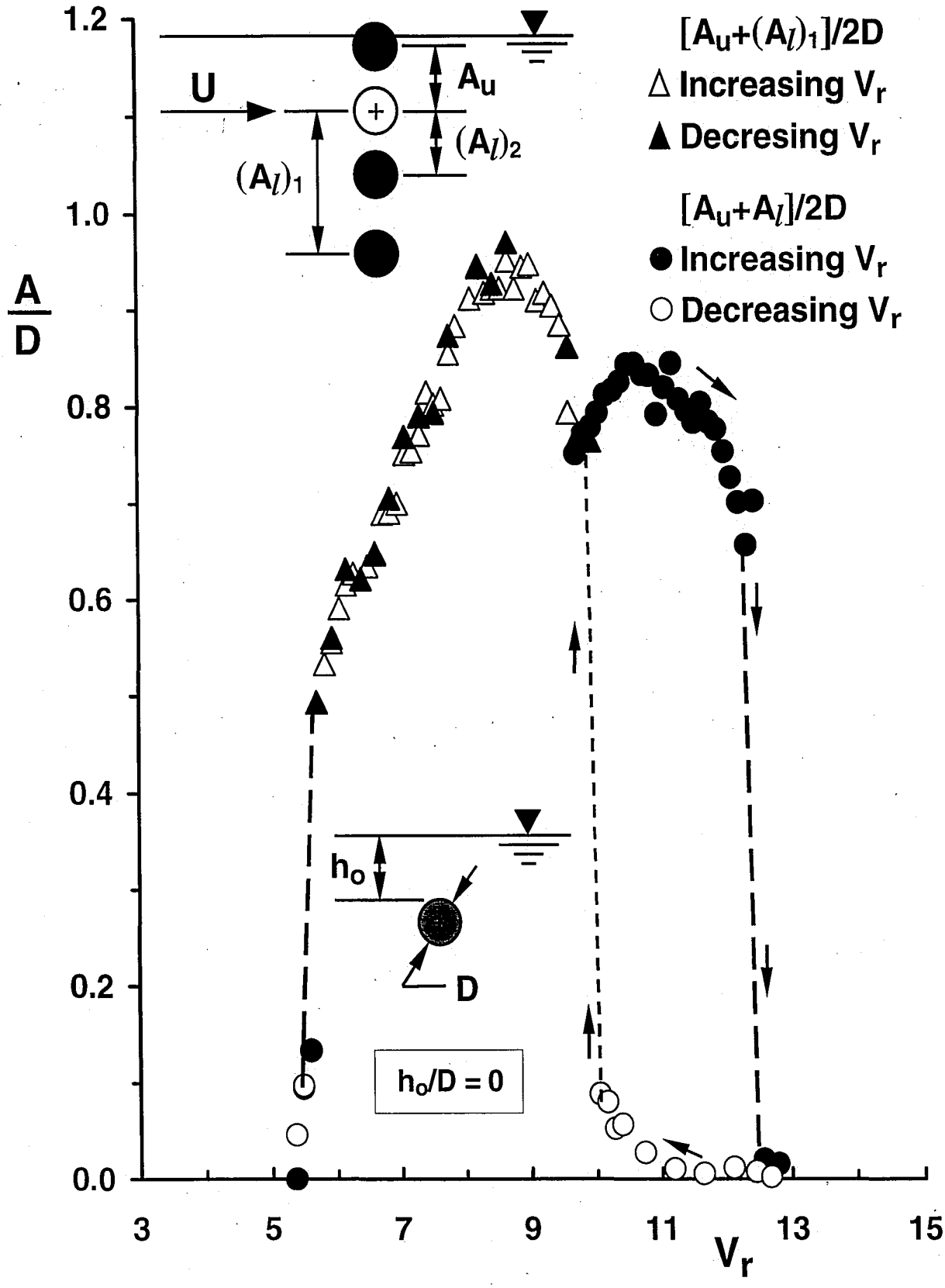

Figure 3-5: Relative response amplitude of higher-dual-amplitude branch for increasing and decreasing V_r for the depth of submergence $h^* = h_o/D = 0$.

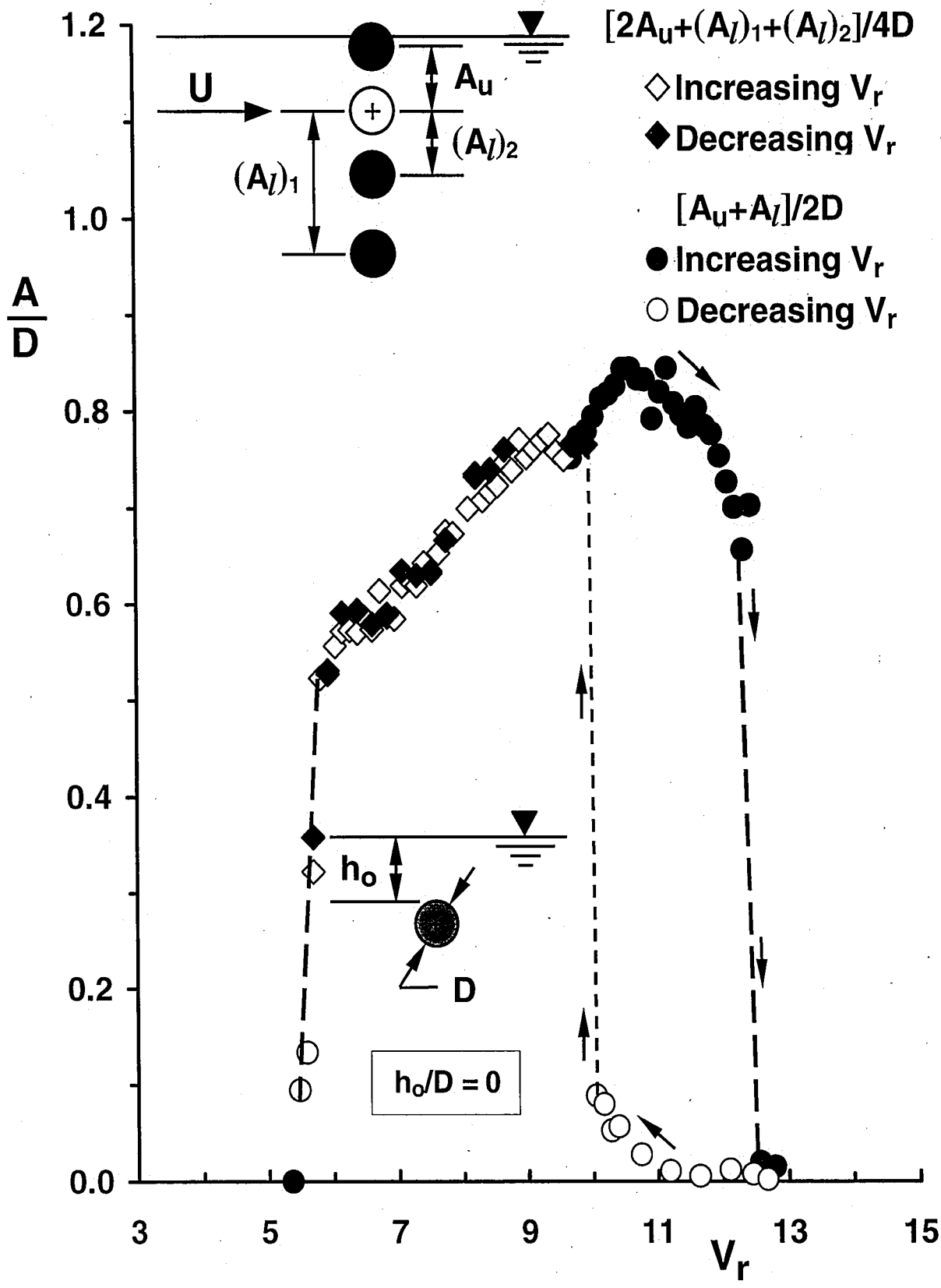

Figure 3-6: Relative response amplitude of average value between higher-dual-amplitude and lower-dual-amplitude branches for increasing and decreasing V_r for the depth of submergence $h^* = h_o/D = 0$.

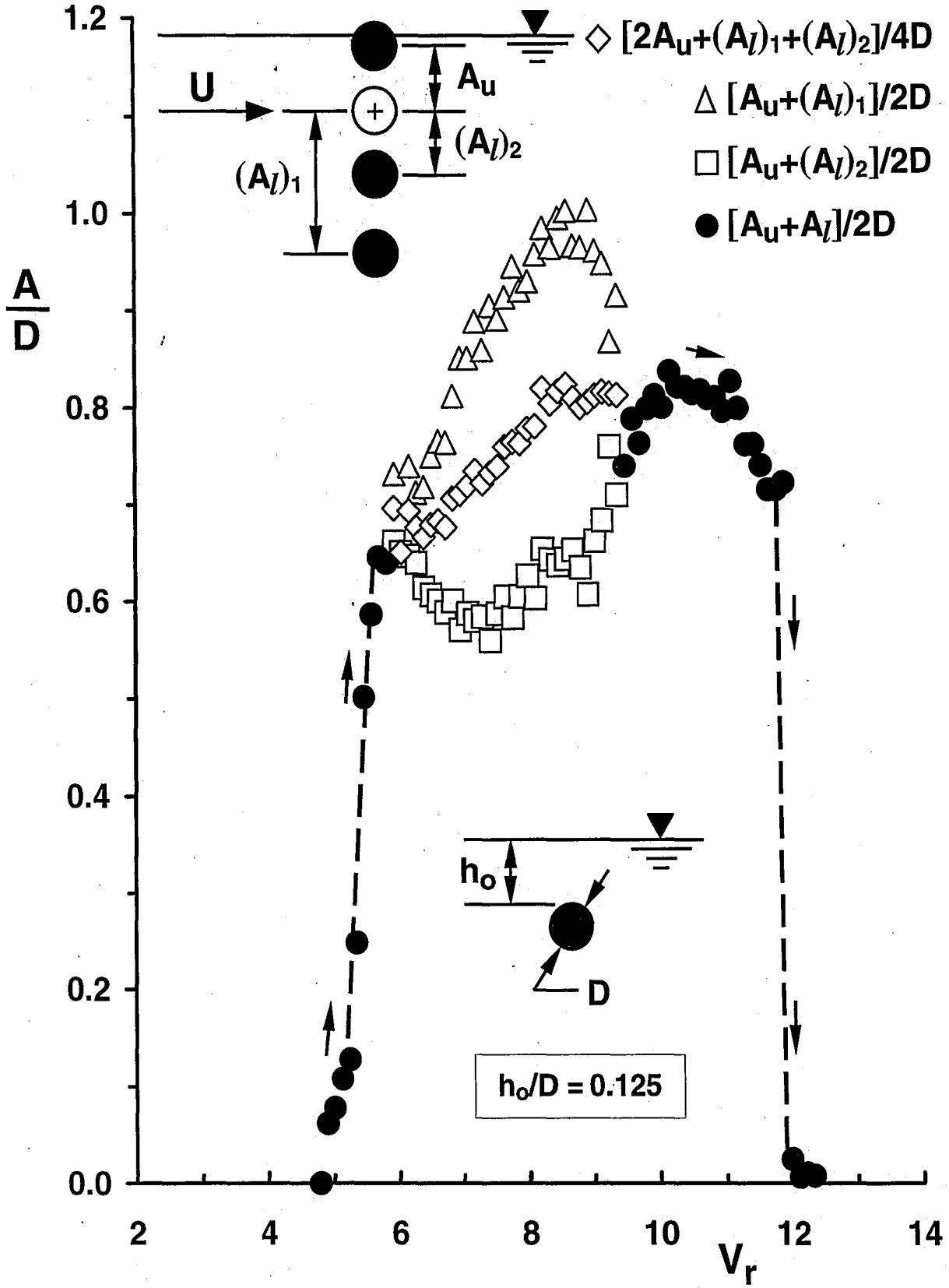

Figure 3-7: Relative response amplitude for increasing and decreasing V_r for the depth of submergence $h^* = h_o/D = 0.125$.

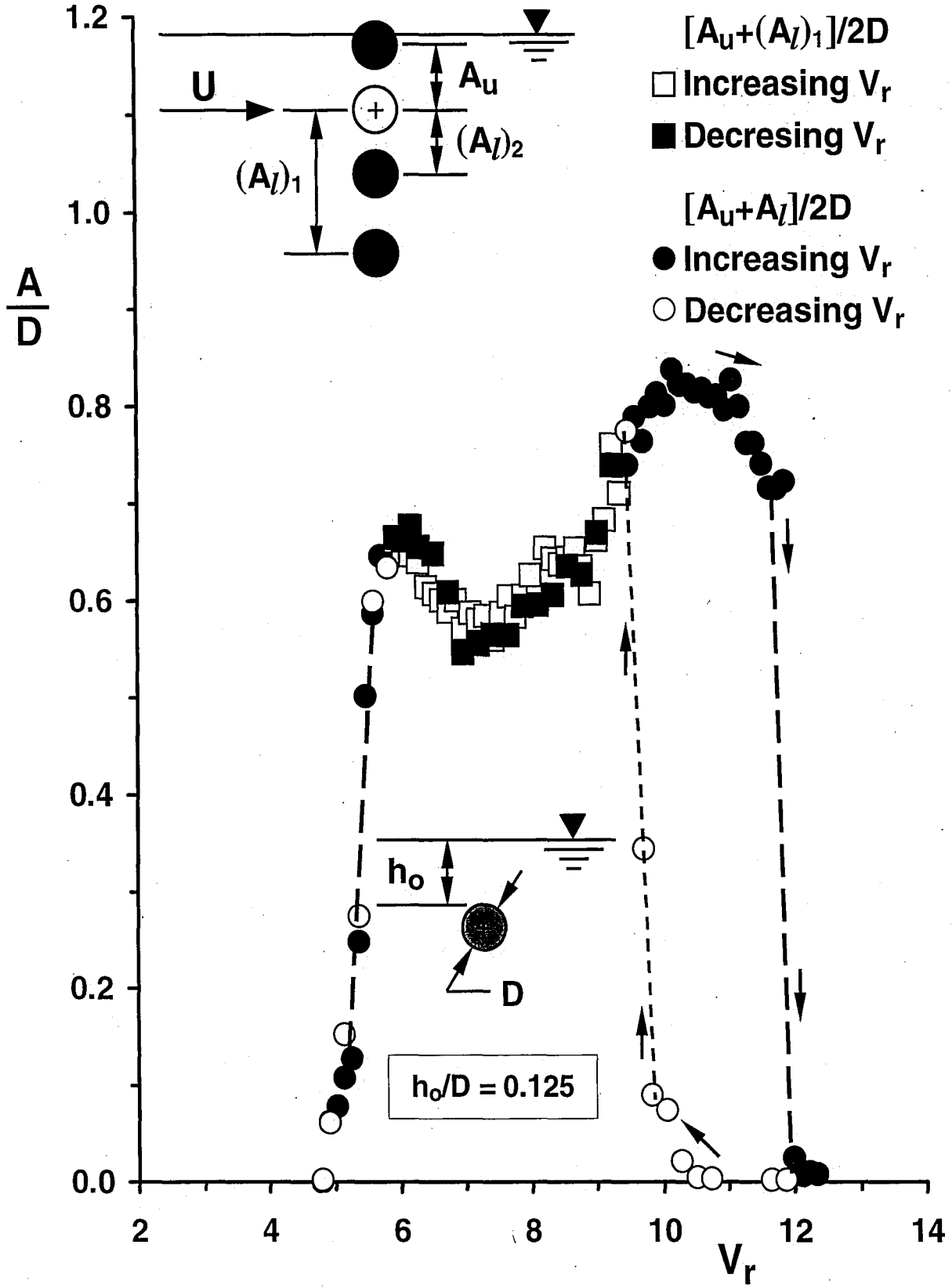

Figure 3-8: Relative response amplitude of lower-dual-amplitude branch for increasing and decreasing V_r for the depth of submergence $h^* = h_o/D = 0.125$.

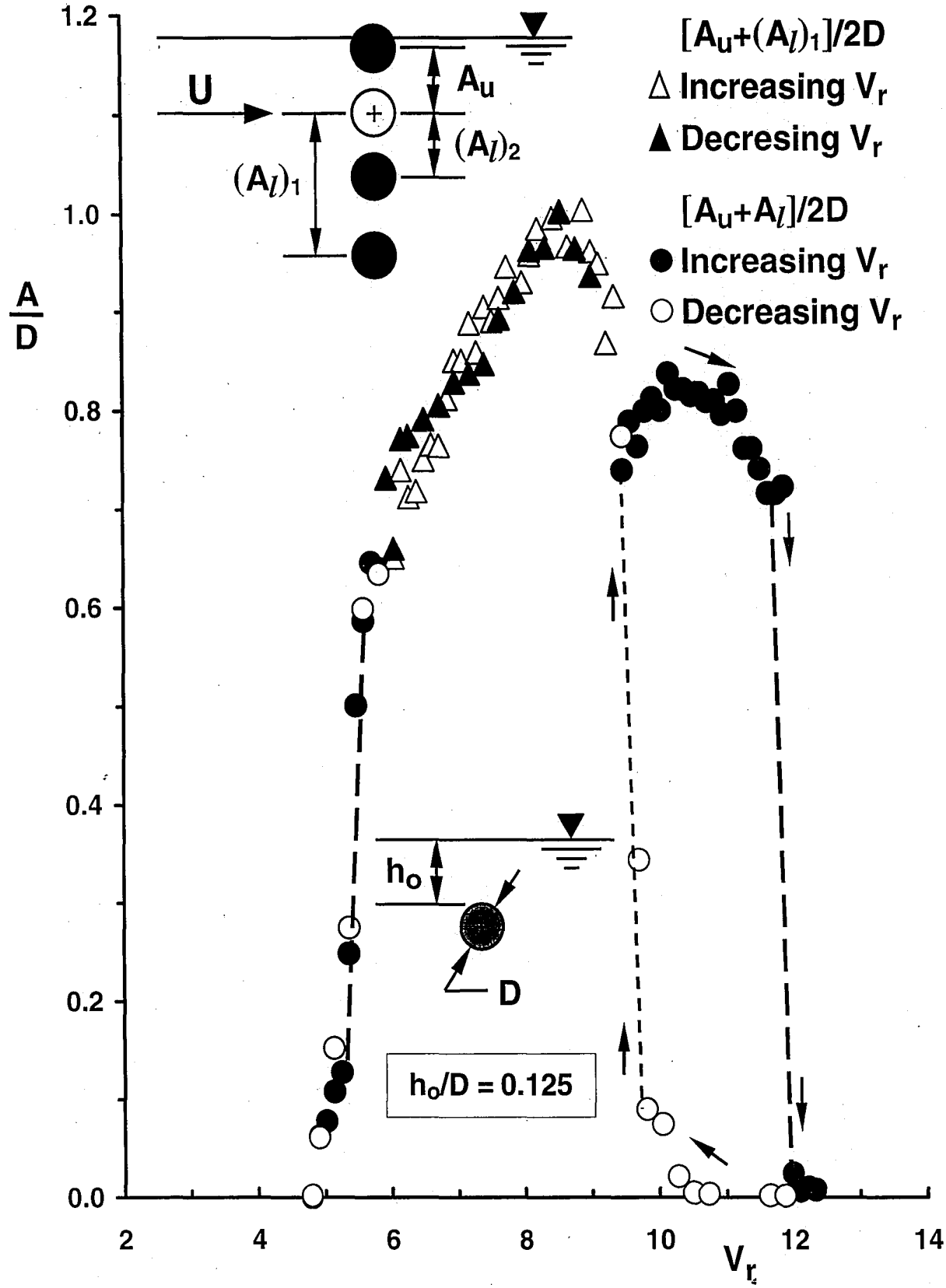

Figure 3-9: Relative response amplitude of higher-dual-amplitude branch for increasing and decreasing V_r for the depth of submergence $h^* = h_o/D = 0.125$.

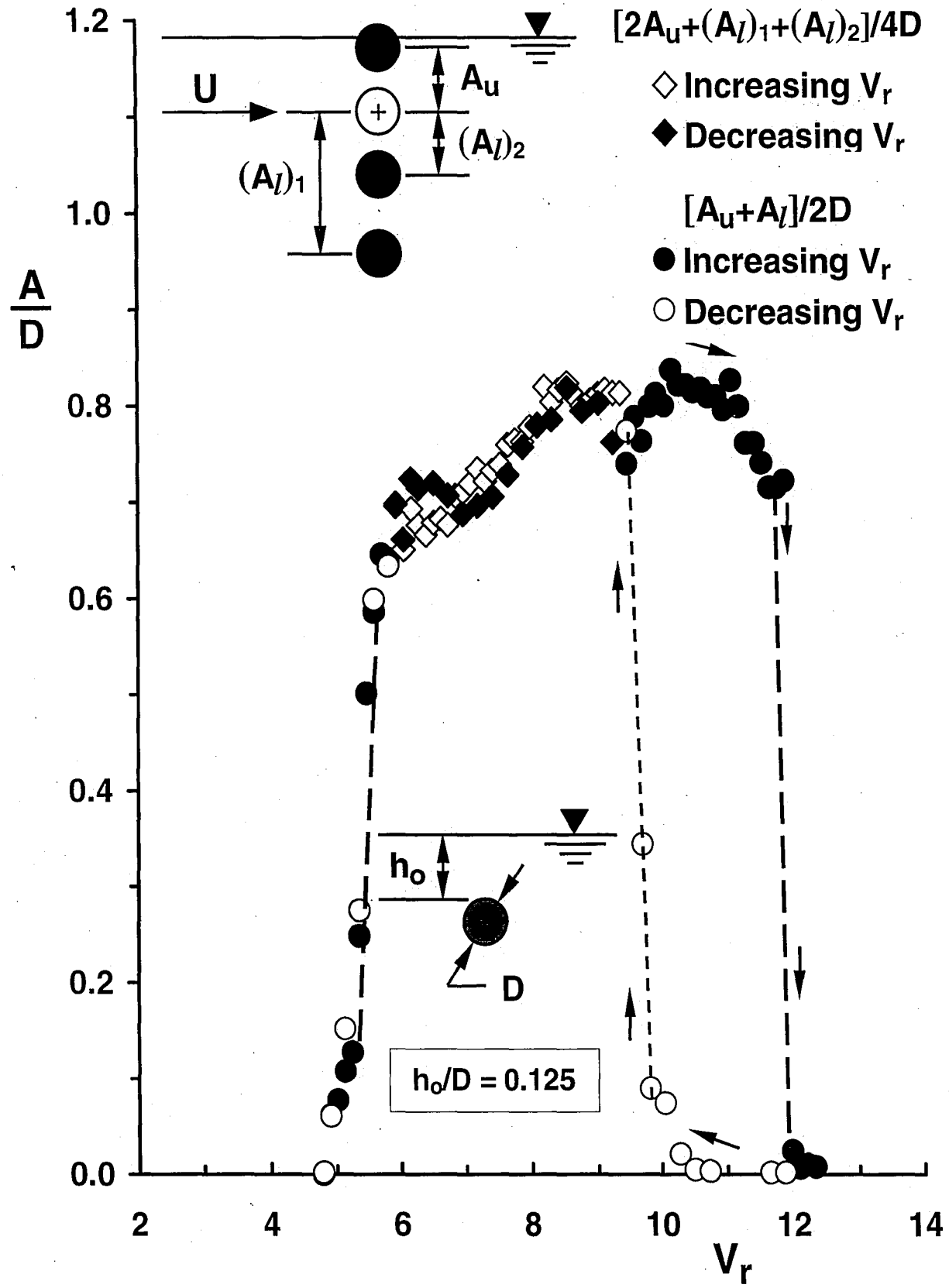

Figure 3-10: Relative response amplitude of average value between higher-dual-amplitude and lower-dual-amplitude branches for increasing and decreasing V_r for the depth of submergence $h^* = h_o/D = 0.125$.

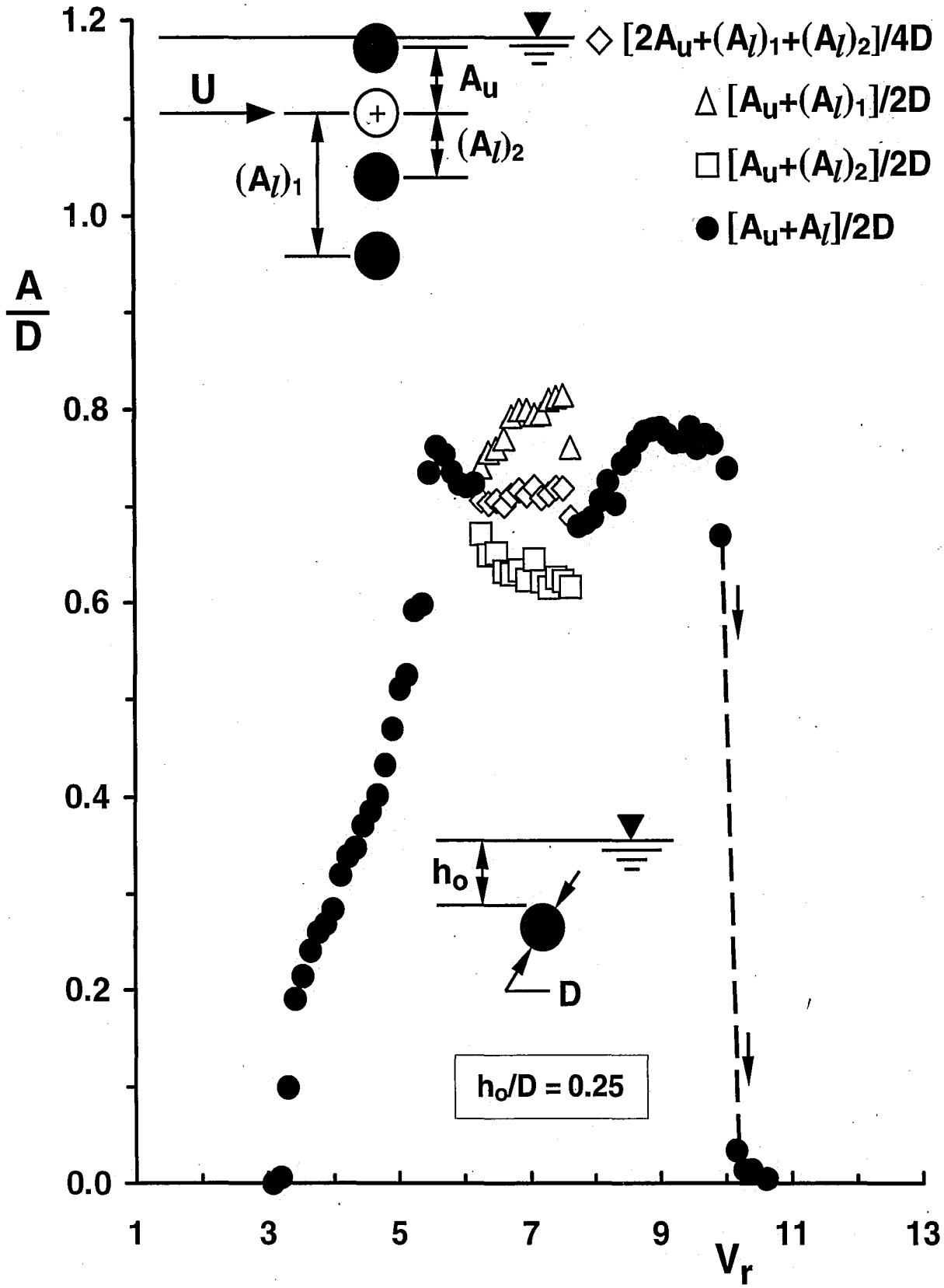

Figure 3-11: Relative response amplitude for increasing and decreasing V_r for the depth of submergence $h^* = h_o/D = 0.25$.

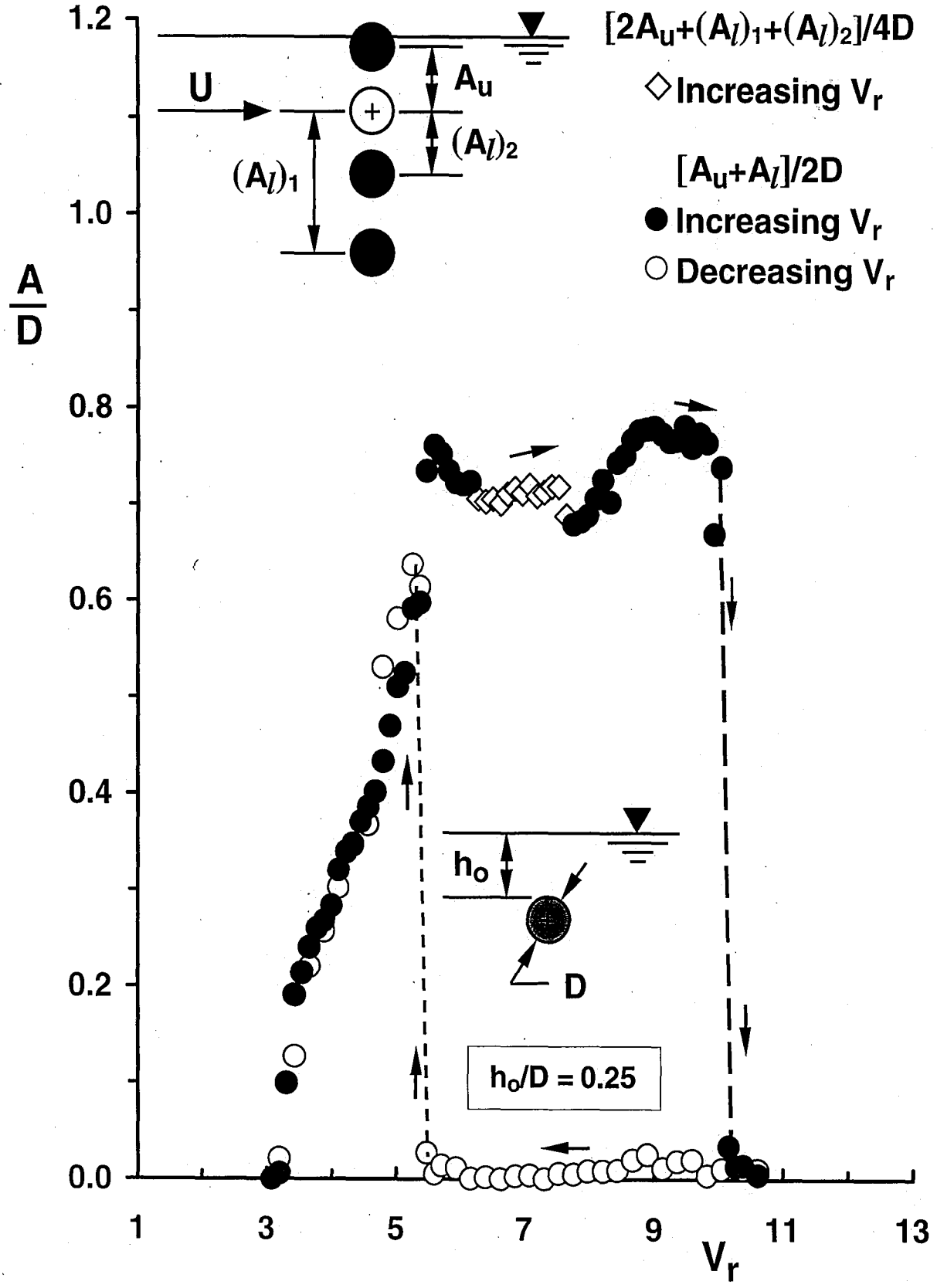

Figure 3-12: Relative response amplitude of average value between higher-dual-amplitude and lower-dual-amplitude branches for increasing and decreasing V_r for the depth of submergence $h^* = h_o/D = 0.25$.

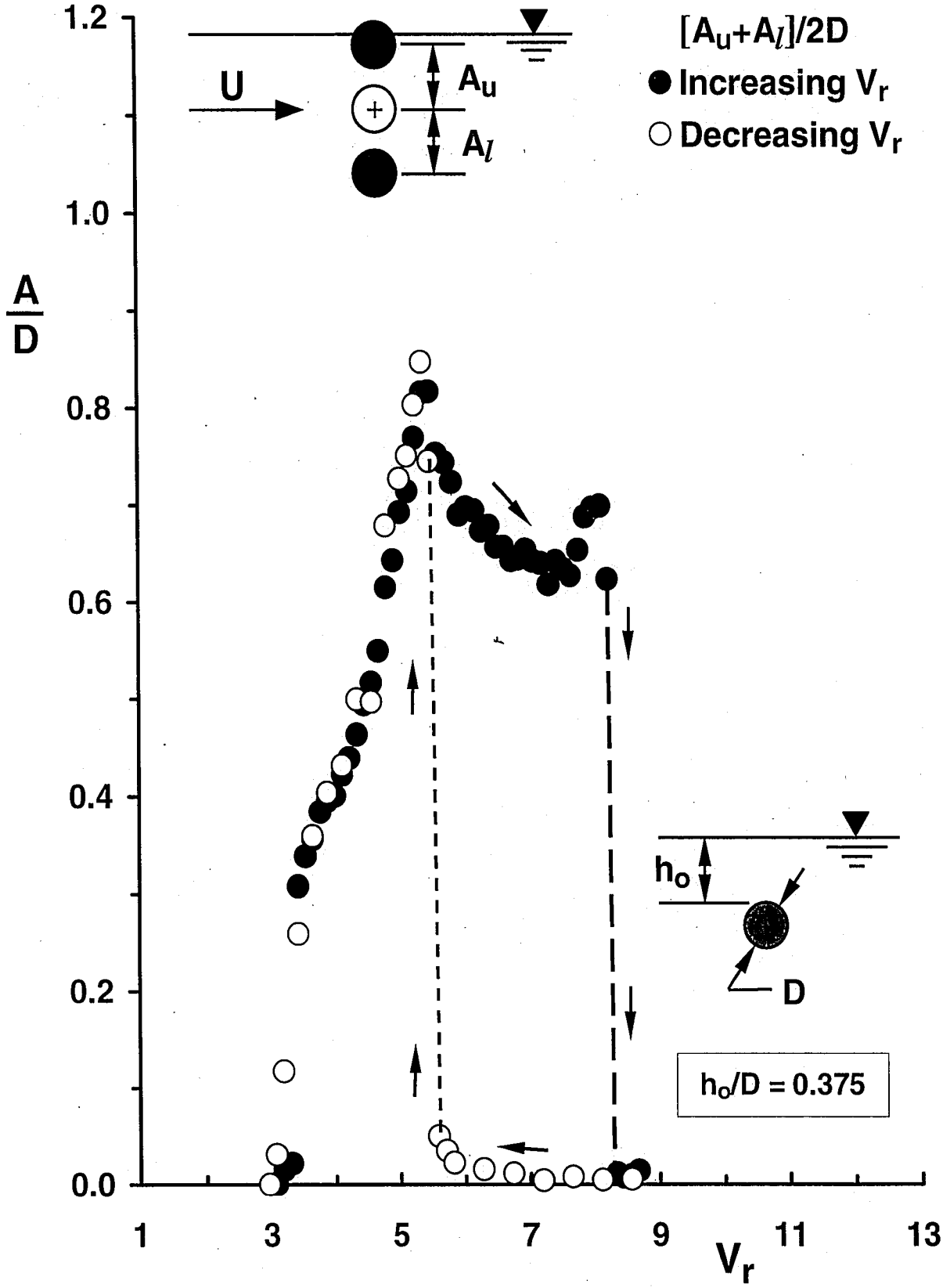

Figure 3-13: Relative response amplitude for increasing and decreasing V_r for the depth of submergence $h^* = h_o/D = 0.375$.

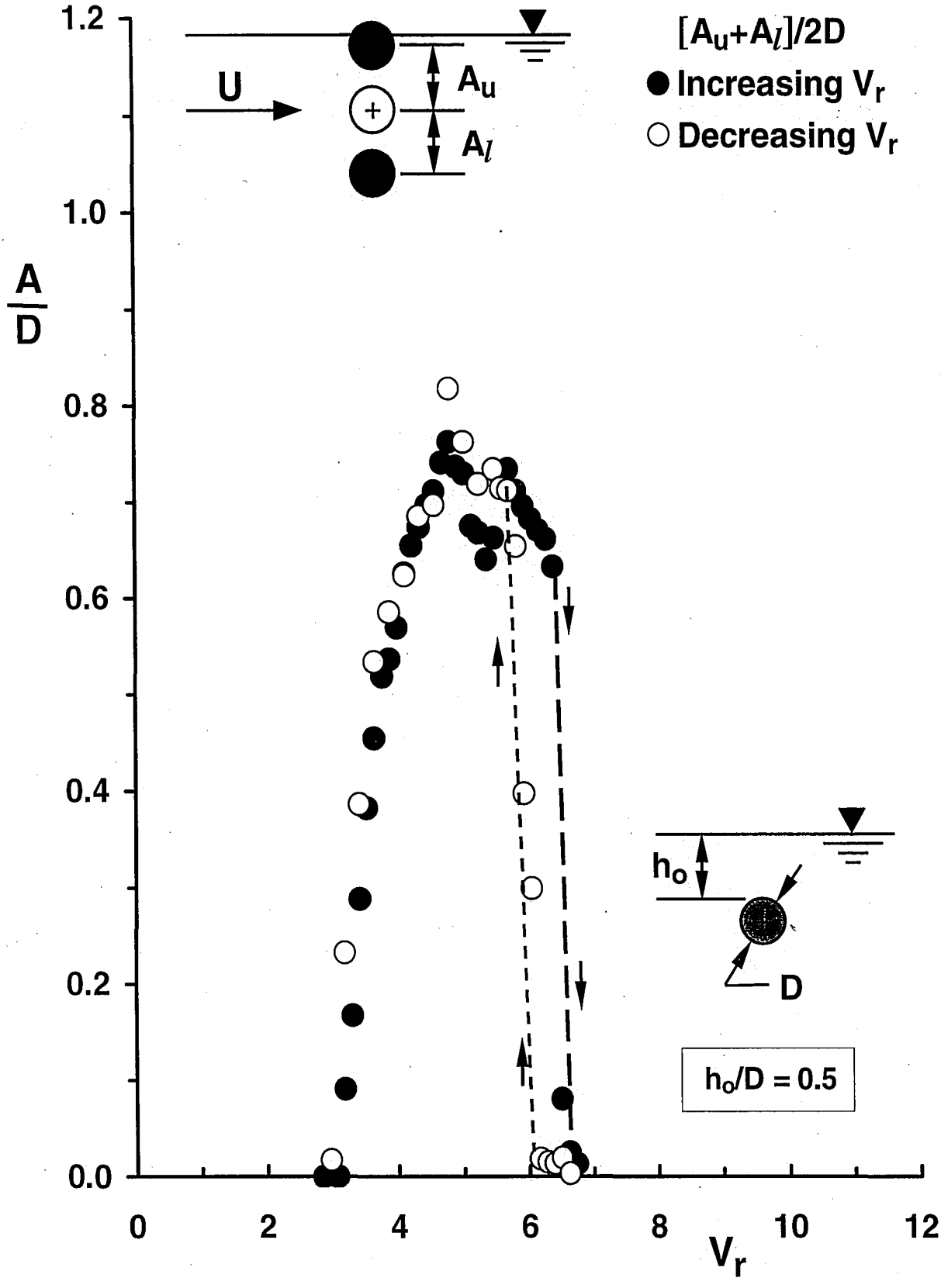

Figure 3-14: Relative response amplitude for increasing and decreasing V_r for the depth of submergence $h^* = h_o/D = 0.5$.

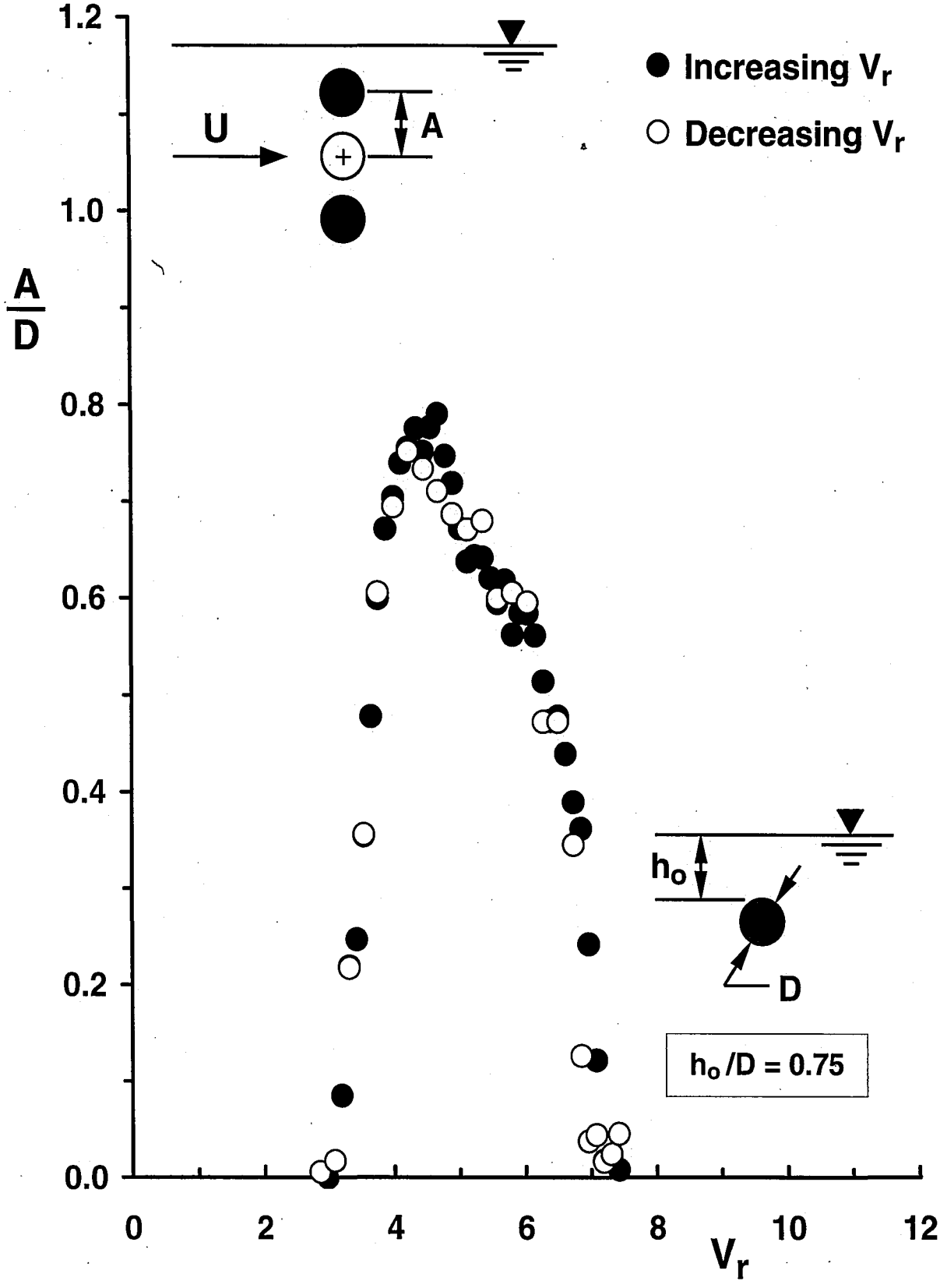

Figure 3-15: Relative response amplitude for increasing and decreasing V_r for the depth of submergence $h^* = h_o/D = 0.75$.

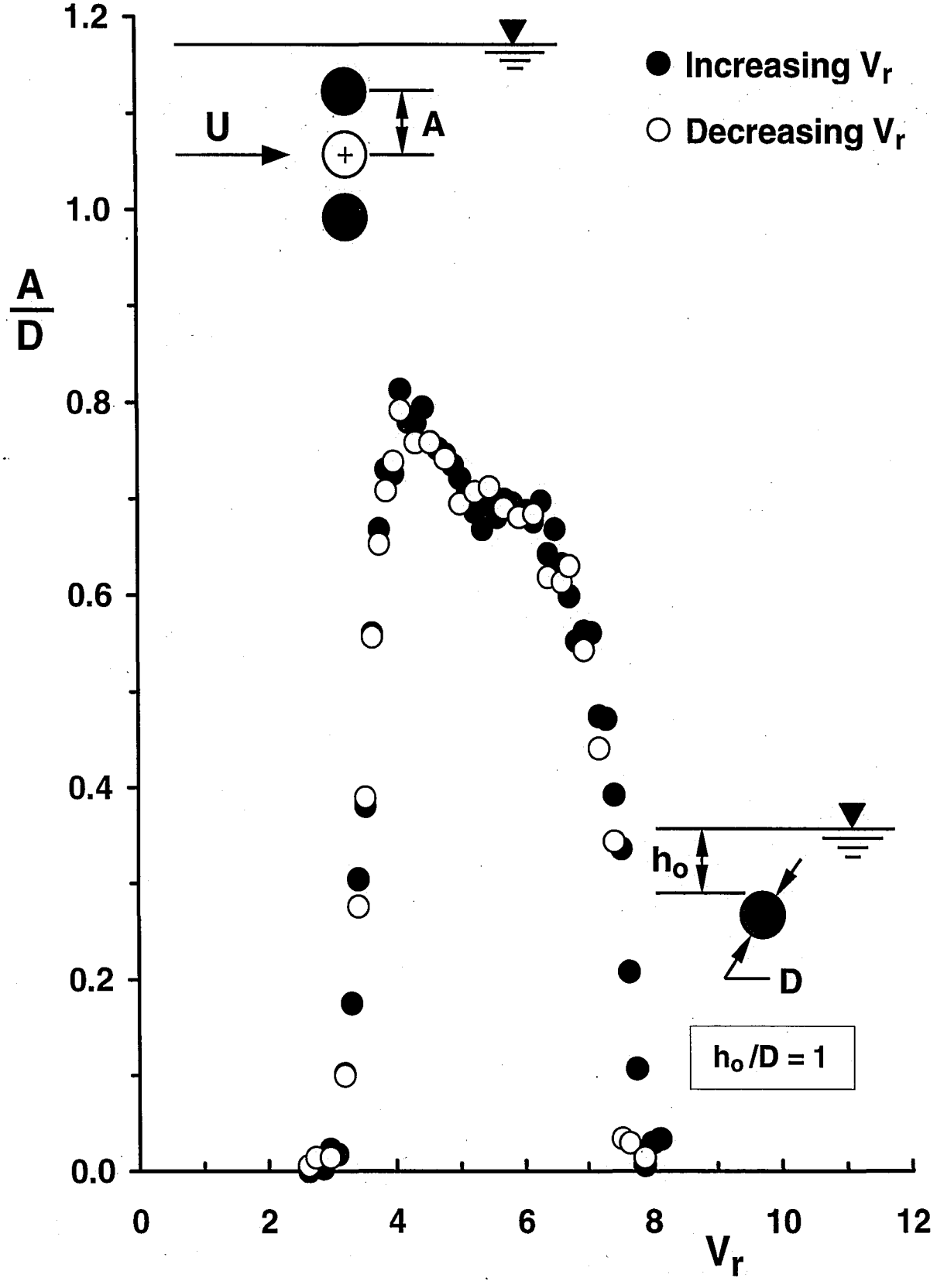

Figure 3-16: Relative response amplitude for increasing and decreasing V_r for the depth of submergence $h^* = h_o/D = 1$.

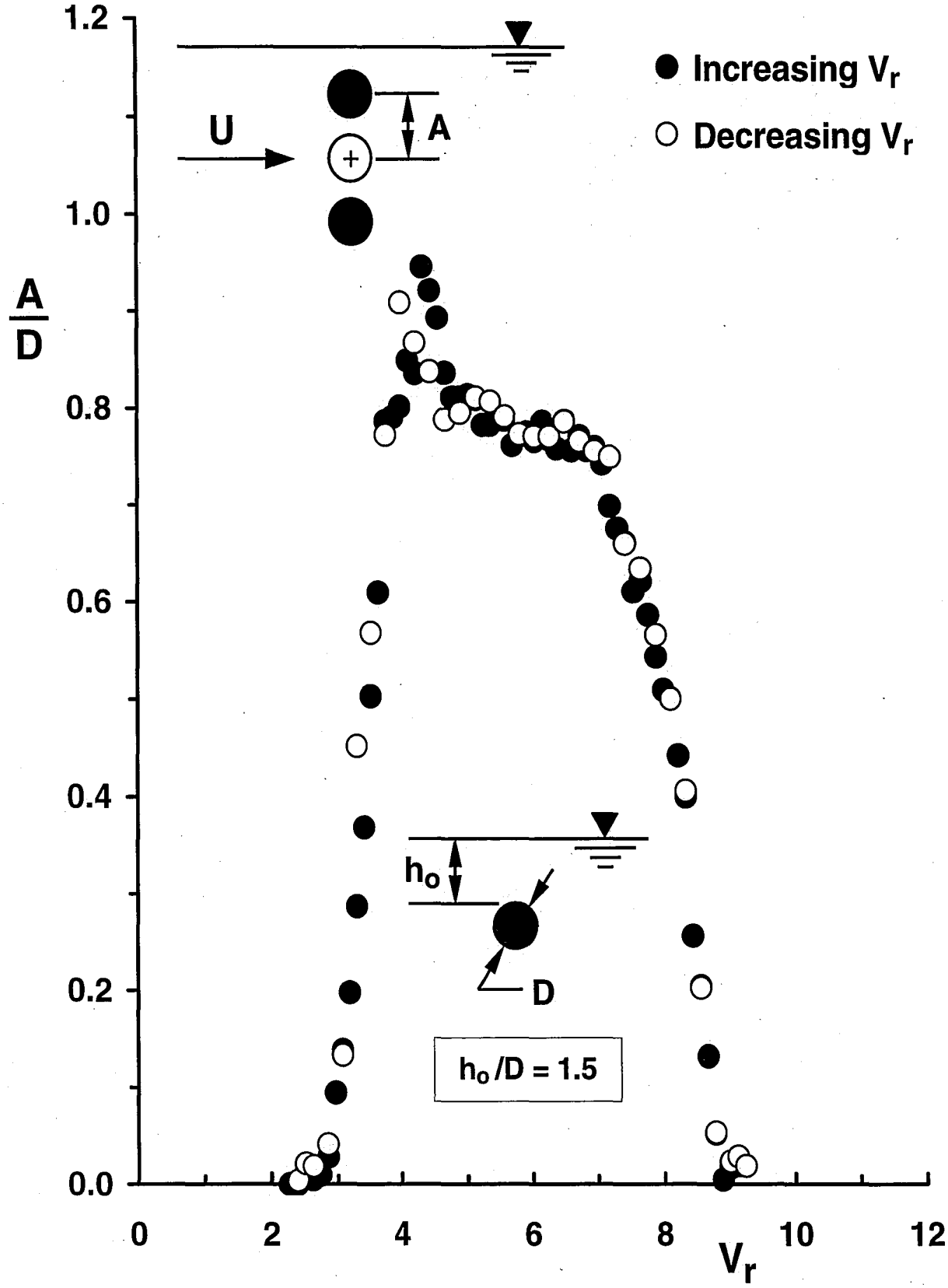

Figure 3-17: Relative response amplitude for increasing and decreasing V_r for the depth of submergence $h^* = h_o/D = 1.5$.

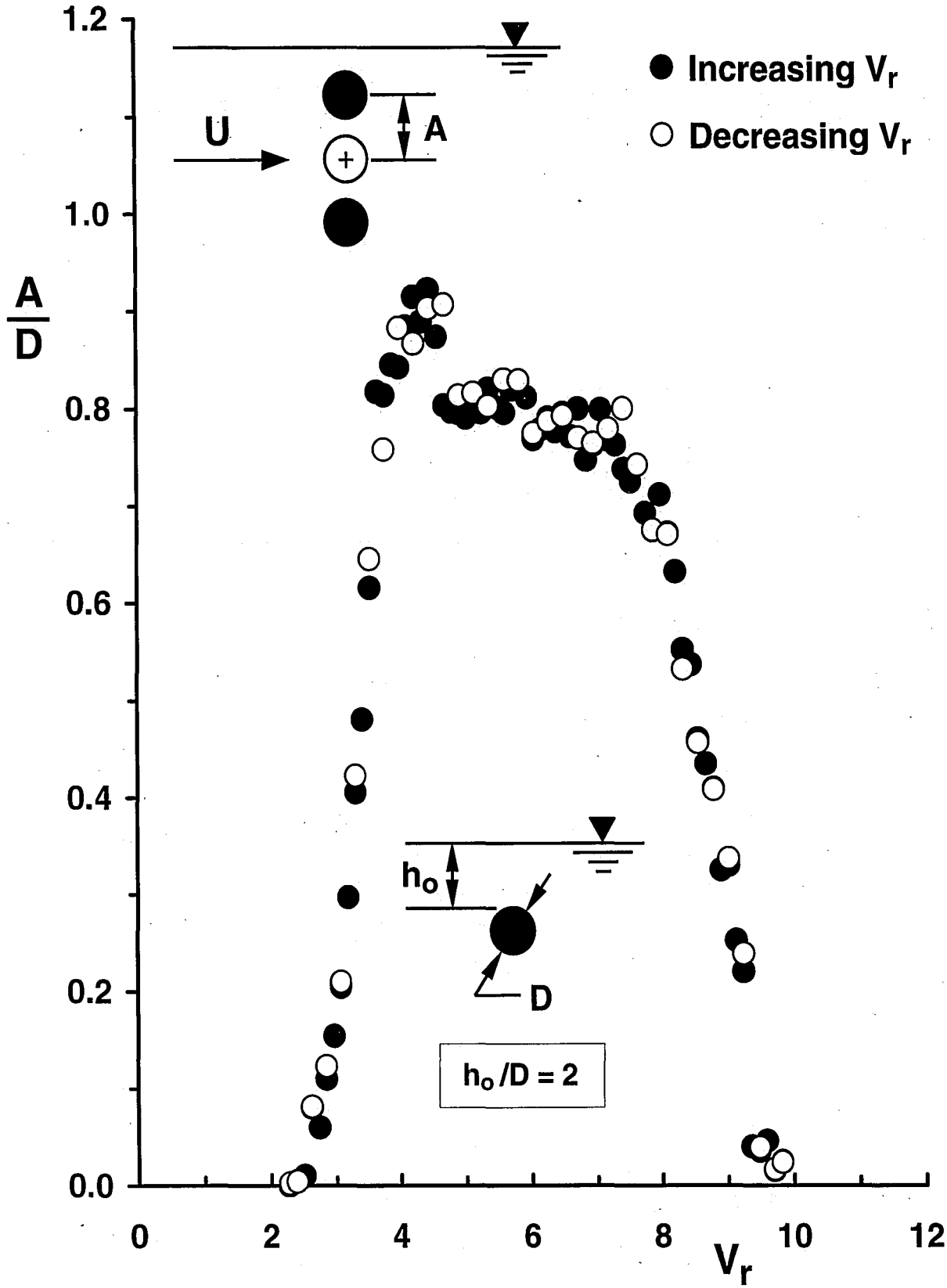

Figure 3-18: Relative response amplitude for increasing and decreasing V_r for the depth of submergence $h^* = h_o/D = 2$.

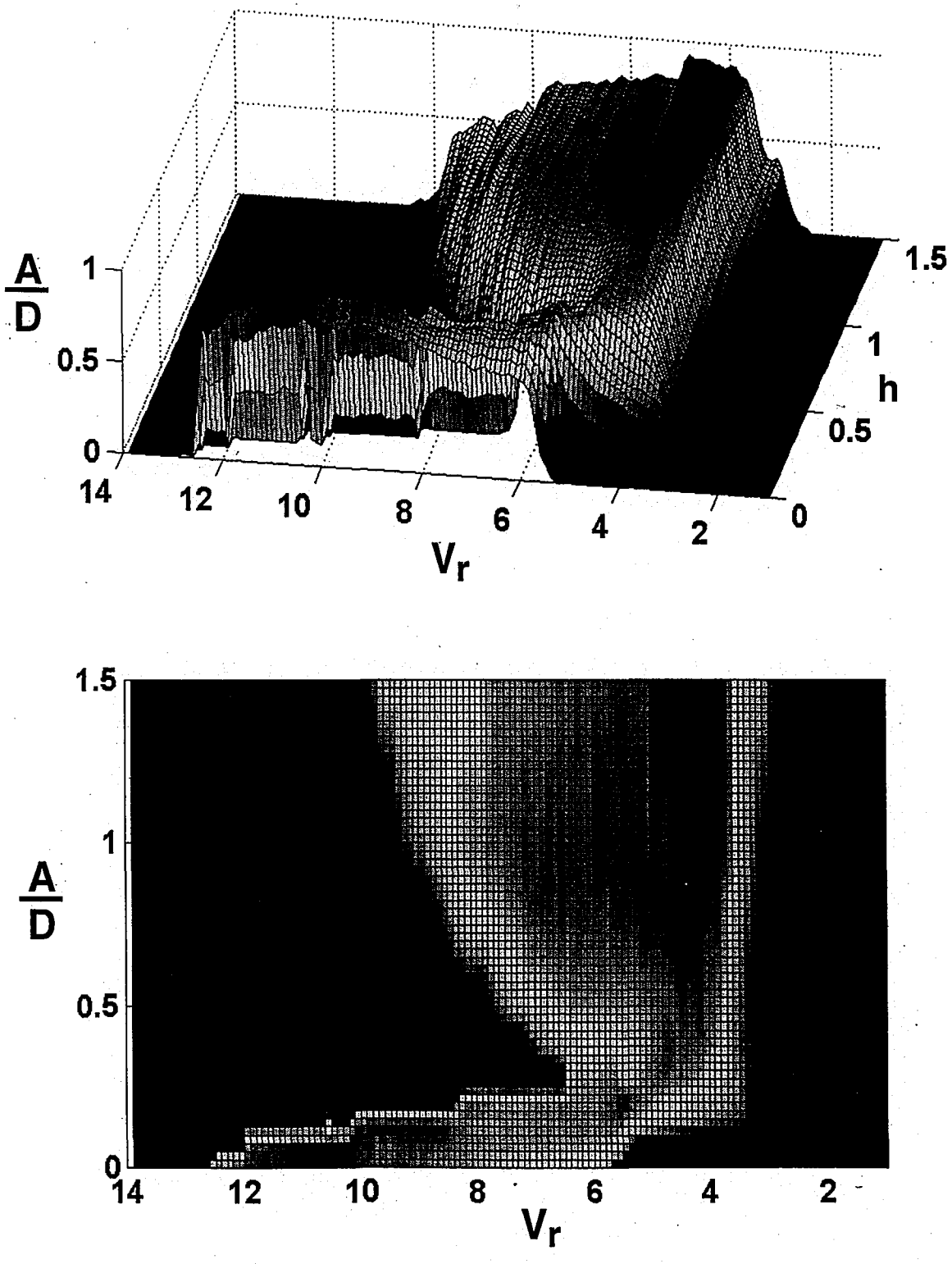

Figure 3-19: Three dimensional plot of relative response amplitude in increasing flow velocity direction for all depths of submergence $h^* = h_o/D$.

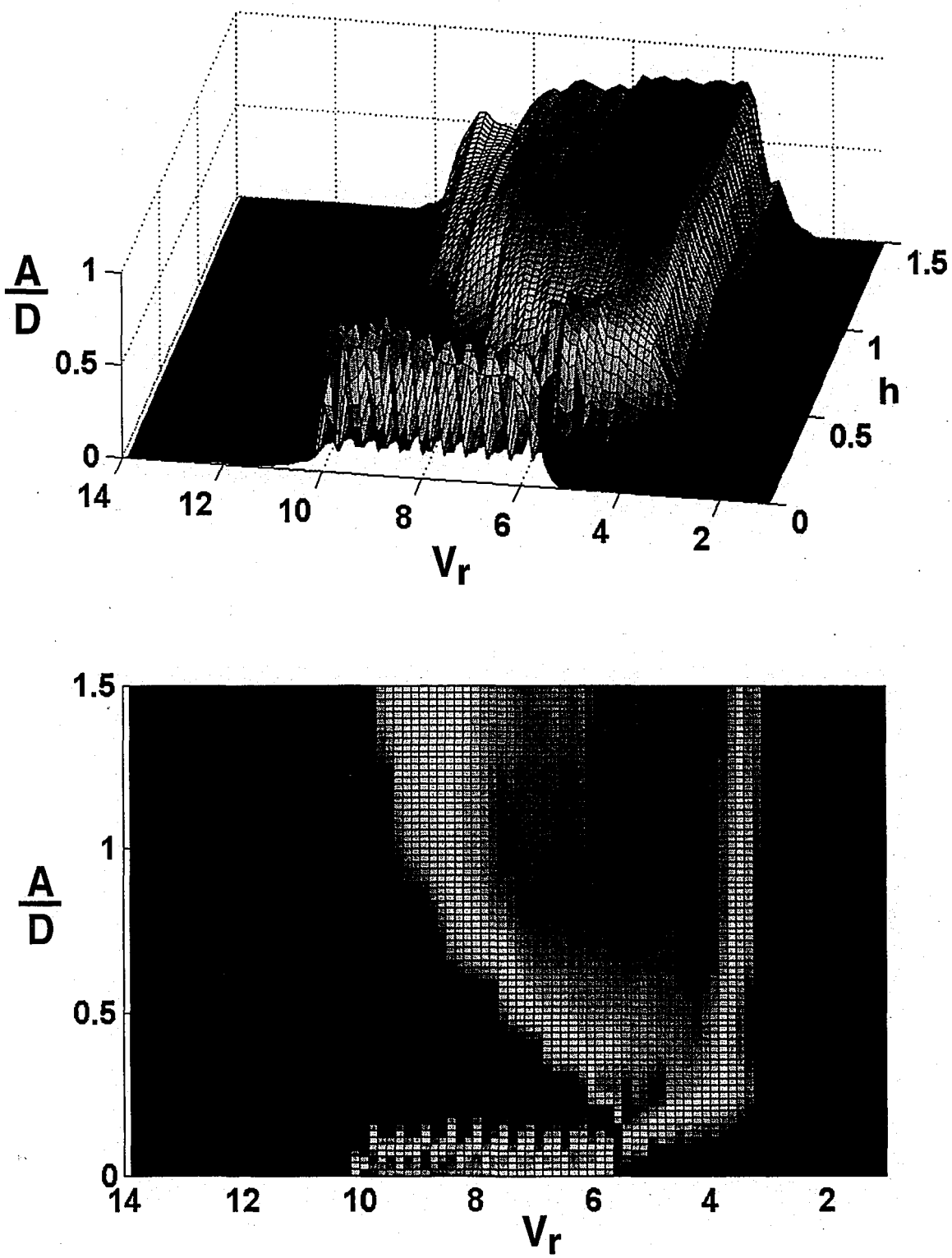

Figure 3-20: Three dimensional plot of relative response amplitude in decreasing flow velocity direction for all depths of submergence $h^* = h_o/D$.

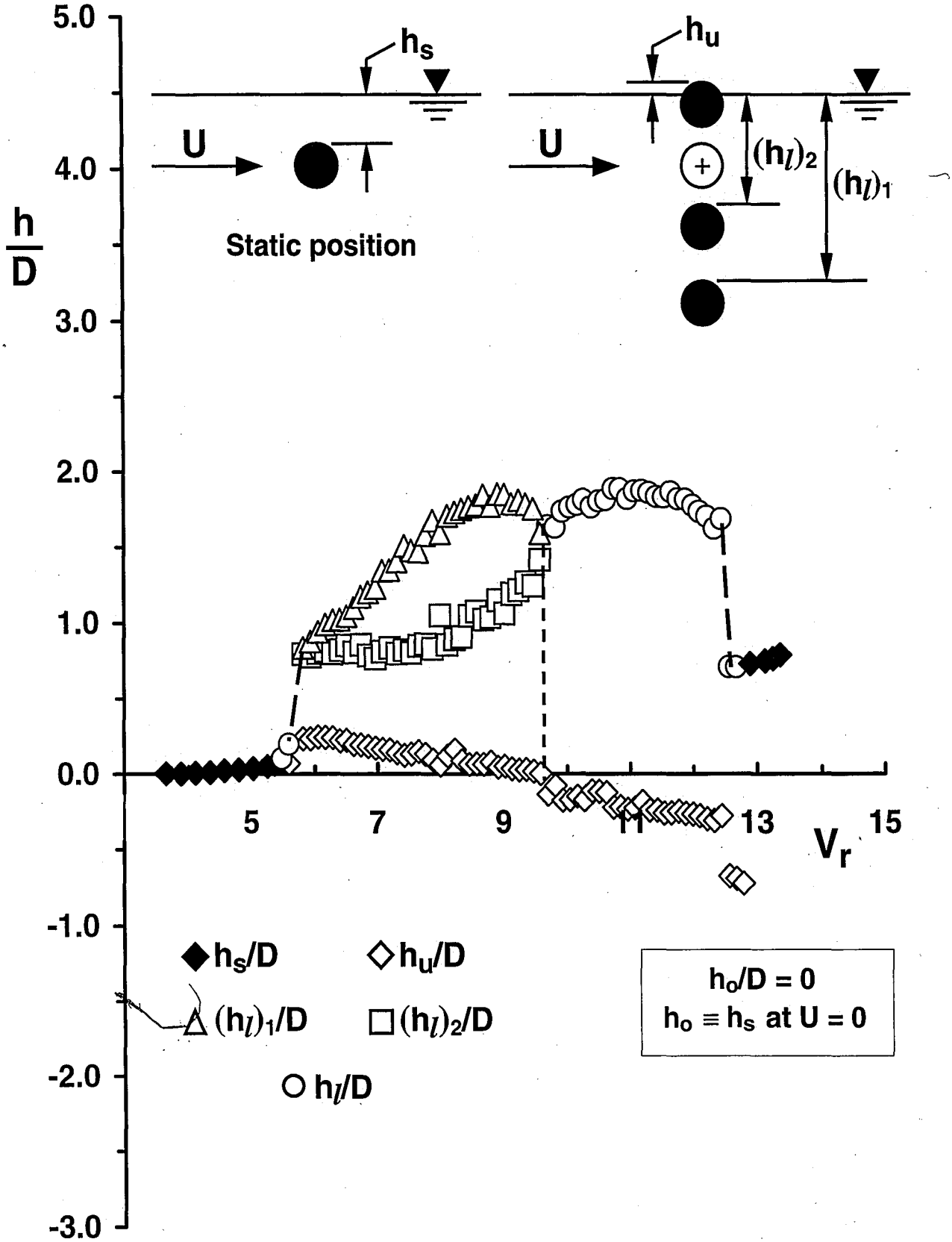

Figure 3-21: Displacement h of cylinder from the free-surface as a function of reduced velocity V_r for the depth of submergence $h^* = h_o/D = 0$.

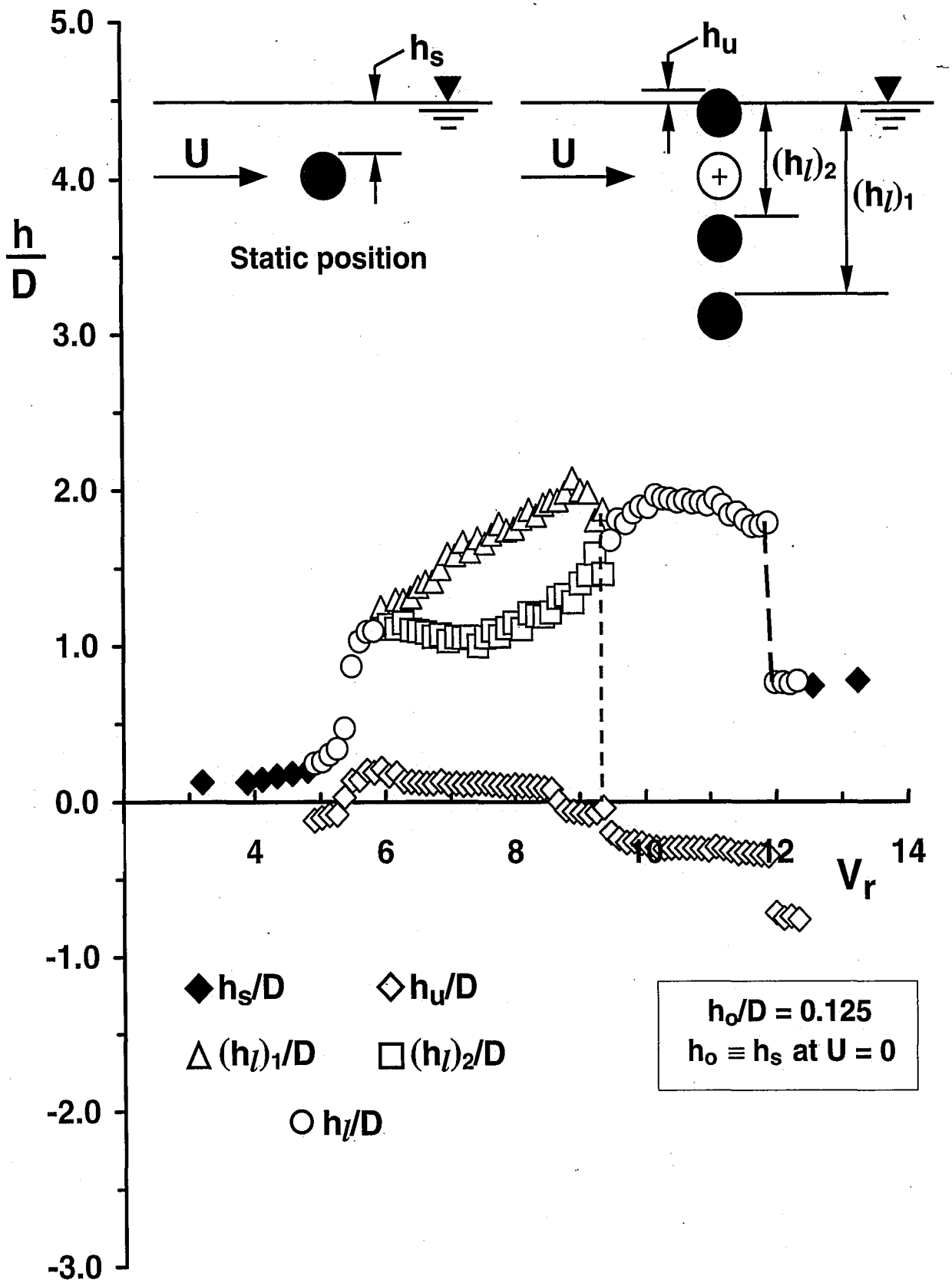

Figure 3-22: Displacement h of cylinder from the free-surface as a function of reduced velocity V_r for the depth of submergence $h^* = h_o/D = 0.125$.

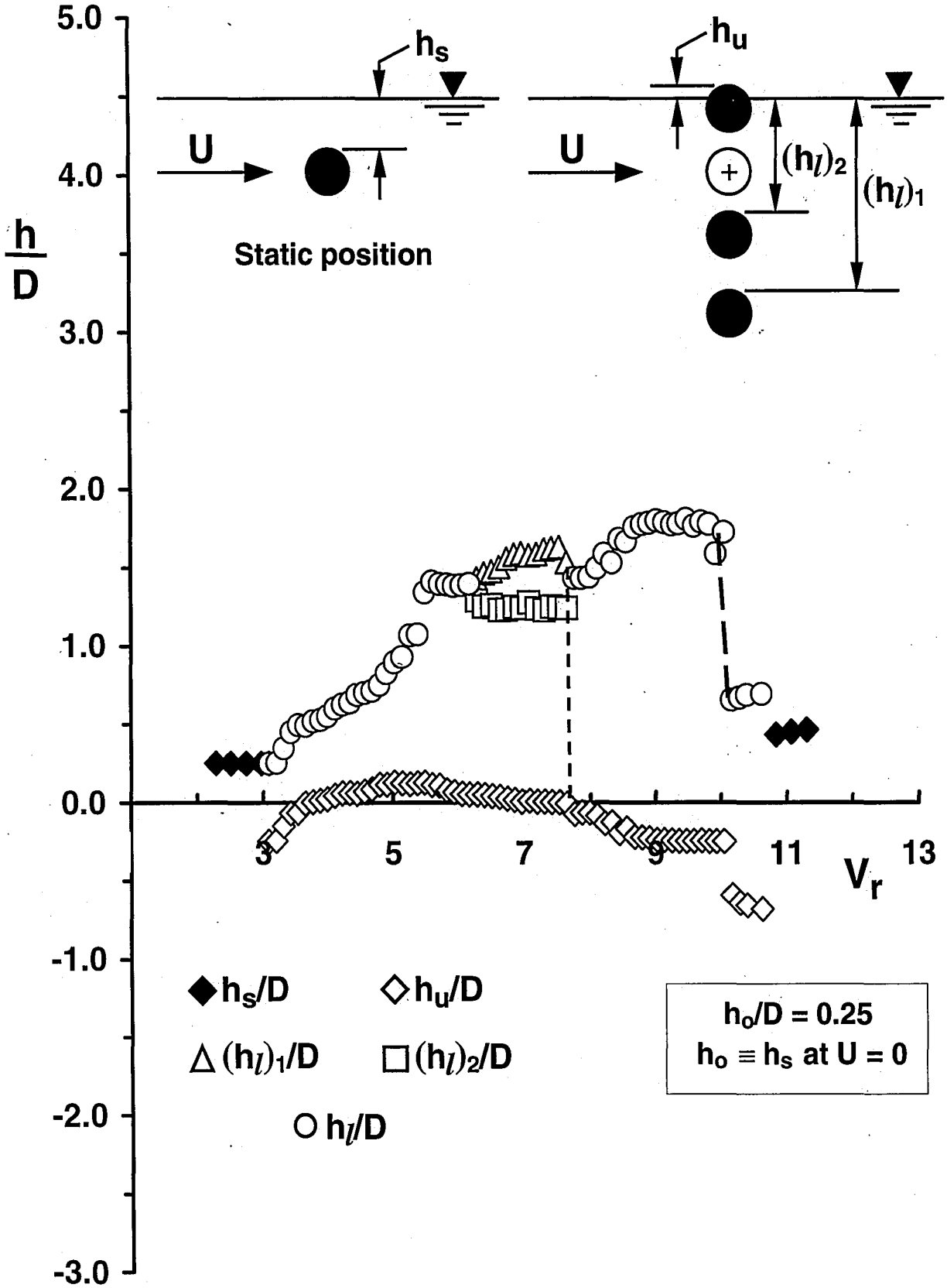

Figure 3-23: Displacement h of cylinder from the free-surface as a function of reduced velocity V_r for the depth of submergence $h^* = h_o/D = 0.25$.

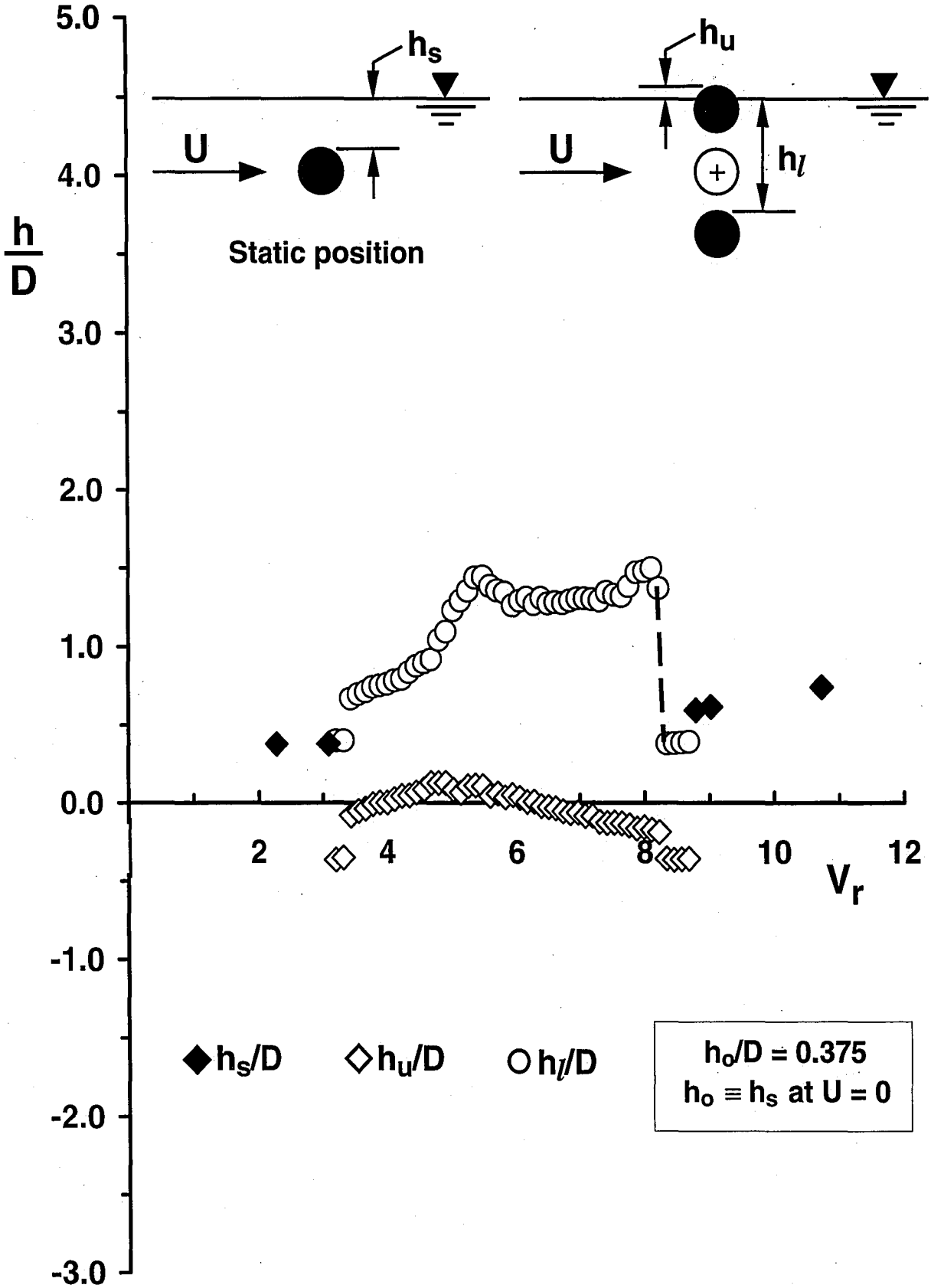

Figure 3-24: Displacement h of cylinder from the free-surface as a function of reduced velocity V_r for the depth of submergence $h^* = h_o/D = 0.375$.

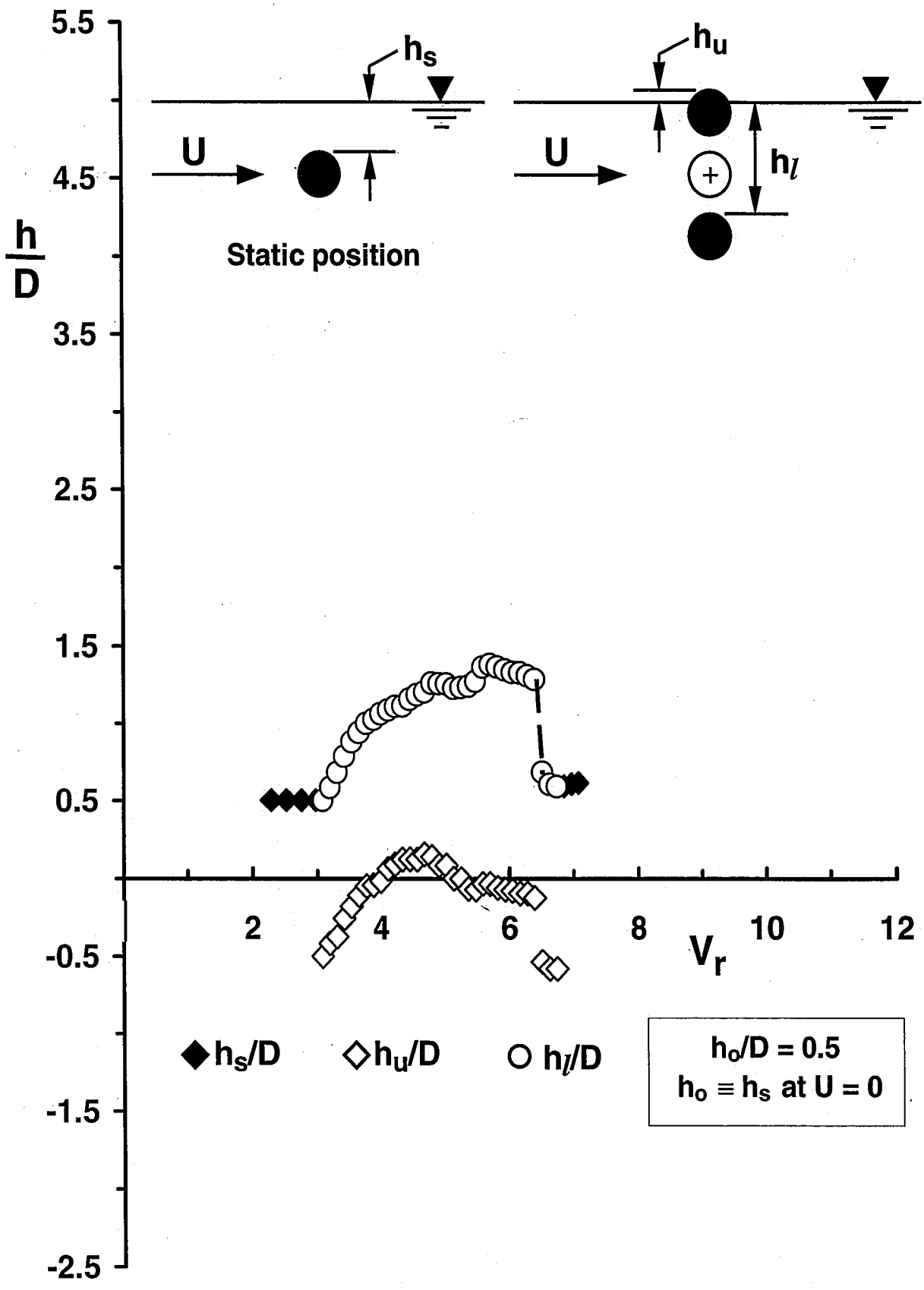

Figure 3-25: Displacement h of cylinder from the free-surface as a function of reduced velocity V_r for the depth of submergence $h^* = h_o/D = 0.5$.

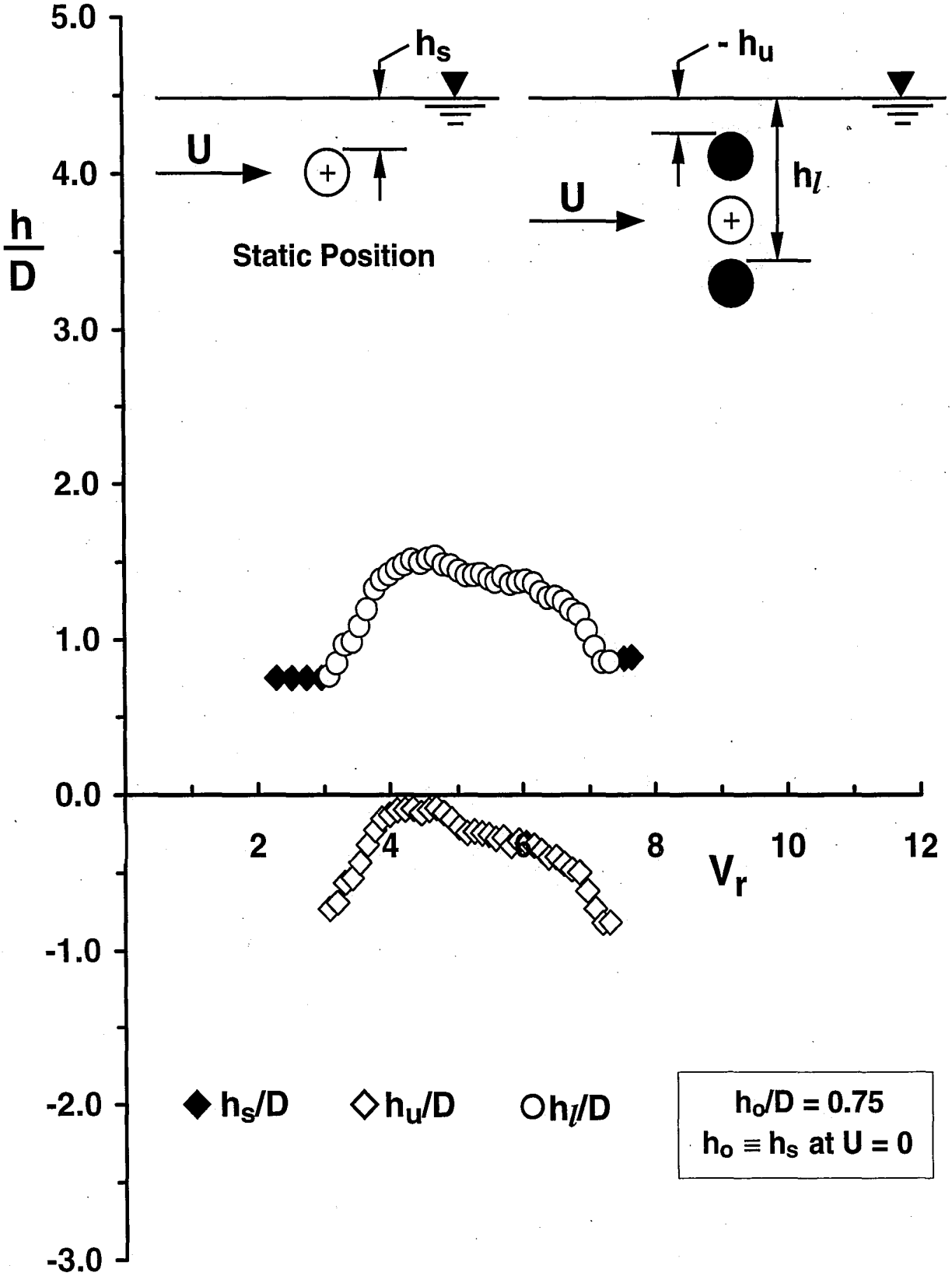

Figure 3-26: Displacement h of cylinder from the free-surface as a function of reduced velocity V_r for the depth of submergence $h^* = h_o/D = 0.75$.

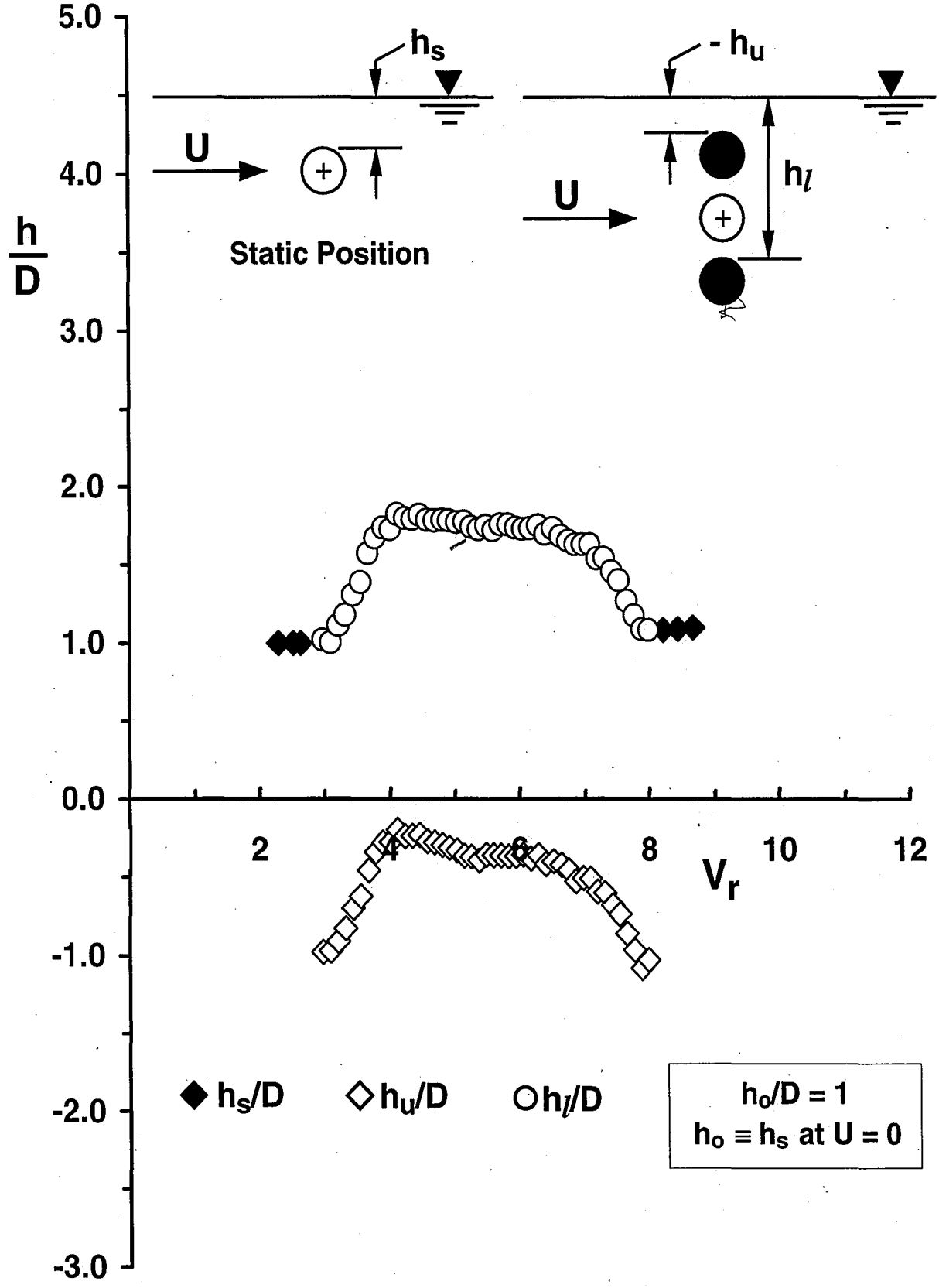

Figure 3-27: Displacement h of cylinder from the free-surface as a function of reduced velocity V_r for the depth of submergence $h^* = h_o/D = 1$.

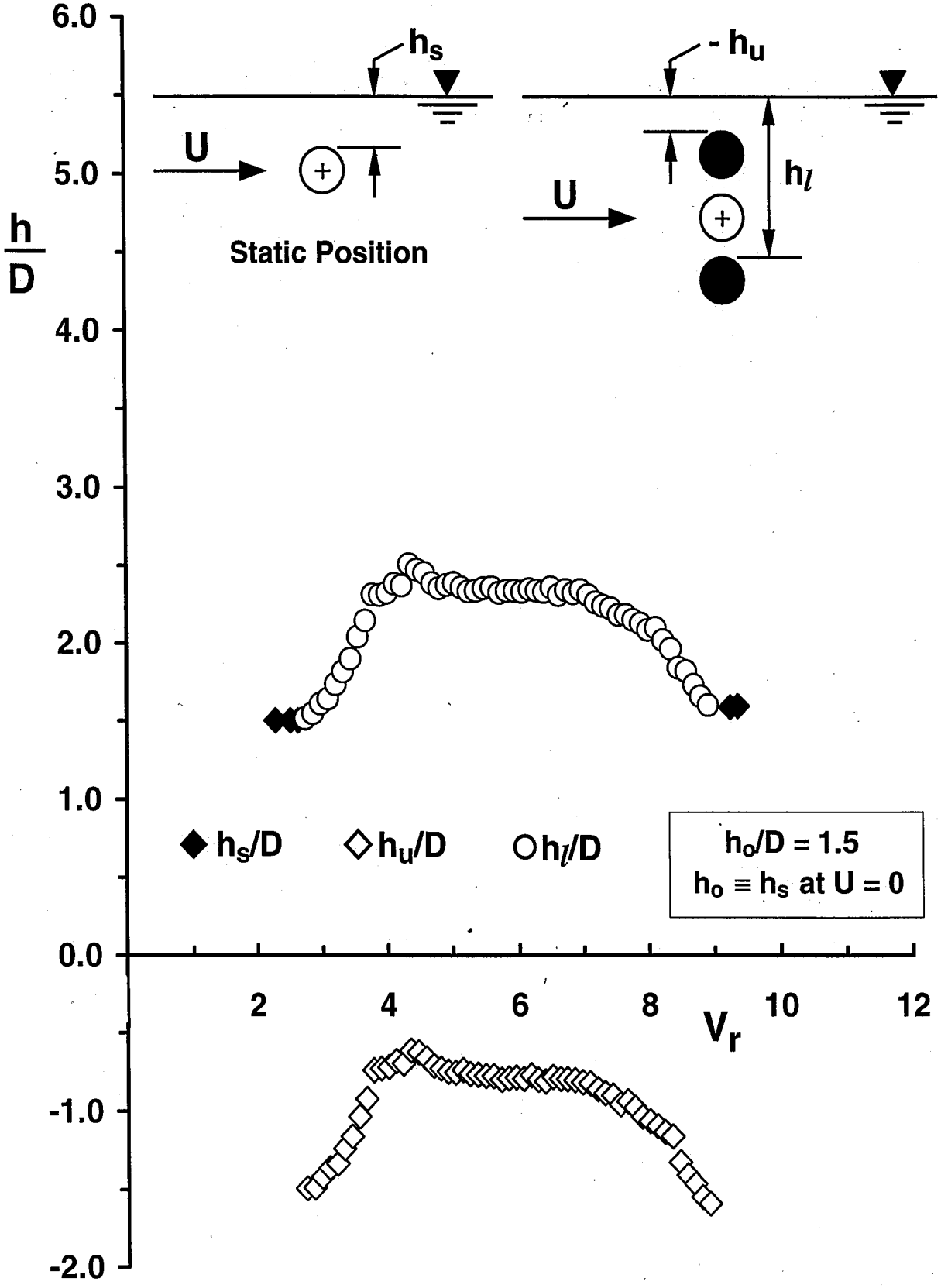

Figure 3-28: Displacement h of cylinder from the free-surface as a function of reduced velocity V_r for the depth of submergence $h^* = h_o/D = 1.5$.

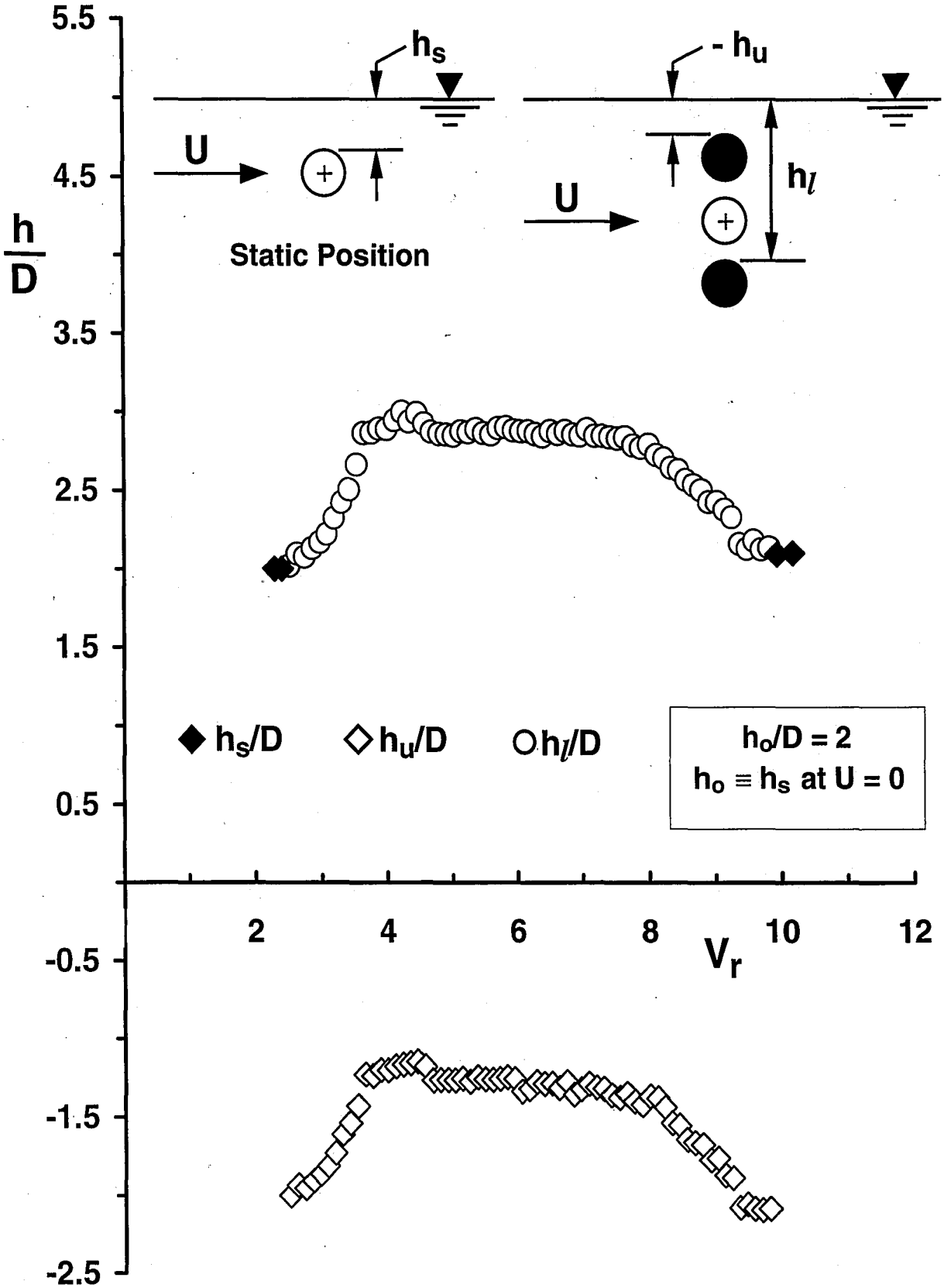

Figure 3-29: Displacement h of cylinder from the free-surface as a function of reduced velocity V_r for the depth of submergence $h^* = h_o/D = 2$.

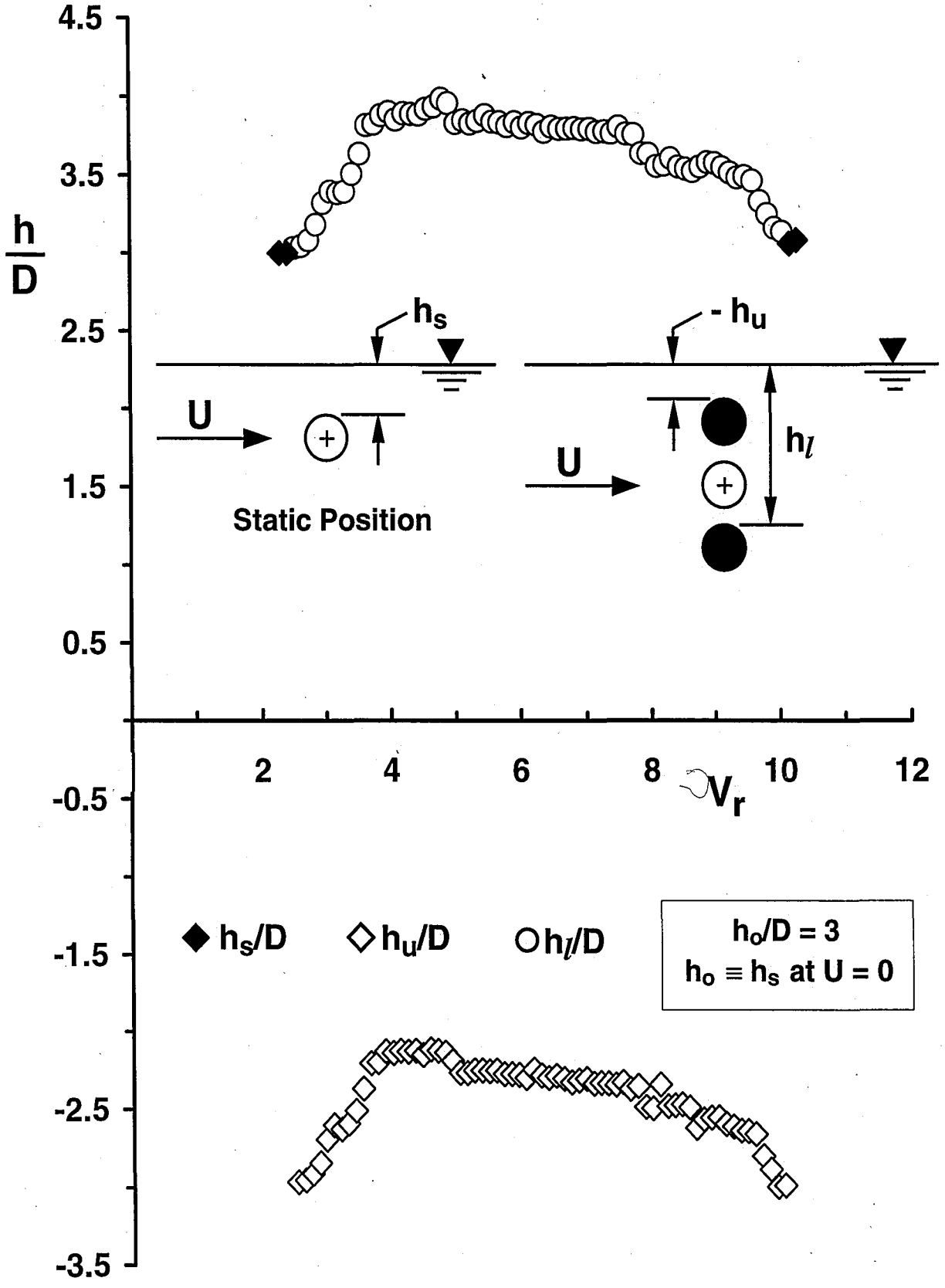

Figure 3-30: Displacement h of cylinder from the free-surface as a function of reduced velocity V_r for the depth of submergence $h^* = h_o/D = 3$.

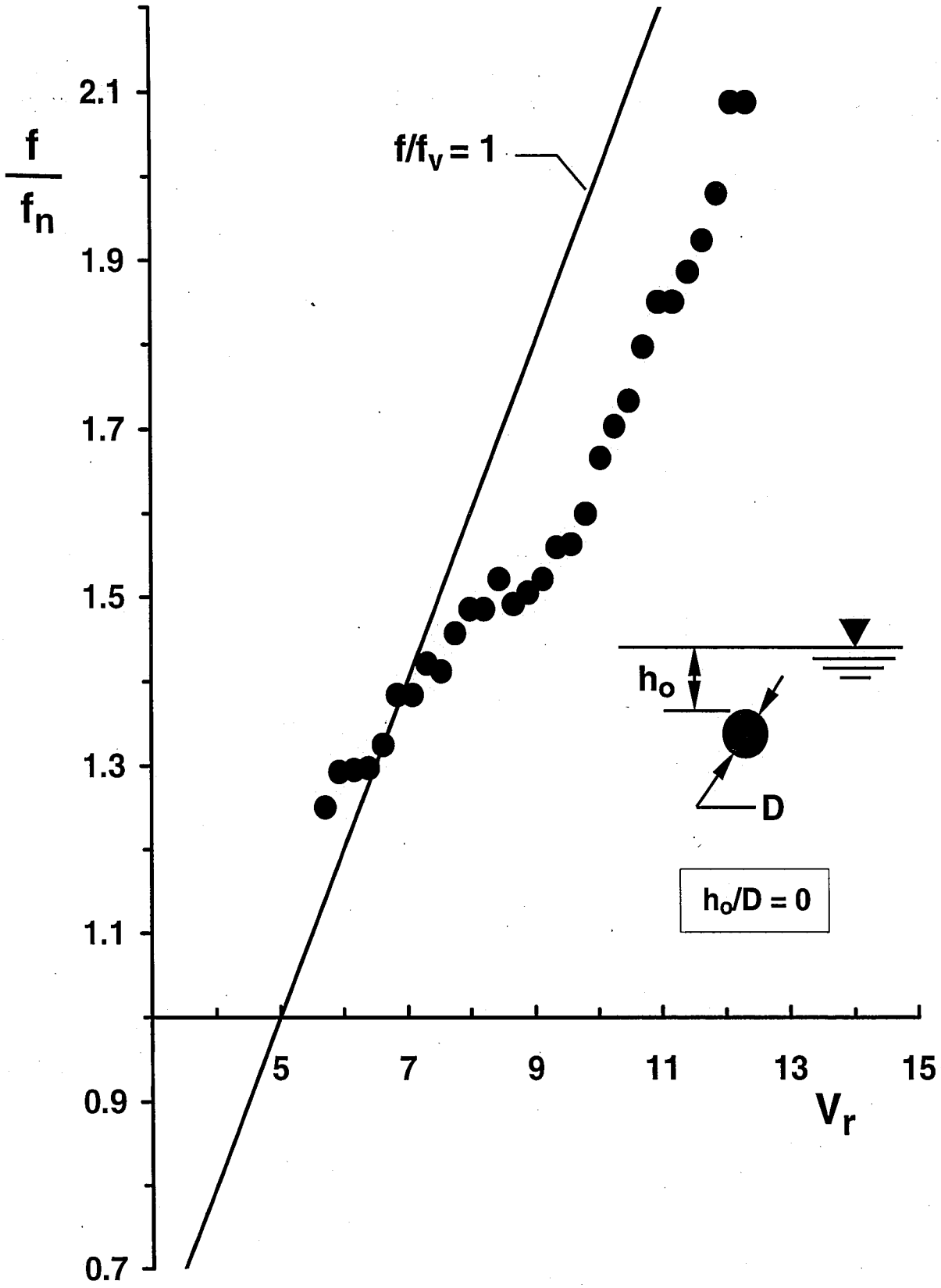

Figure 3-31: Frequency ratio $f^* = f/f_n$ (oscillating frequency/natural frequency) for the depth of submergence $h^* = h_o/D = 0$.

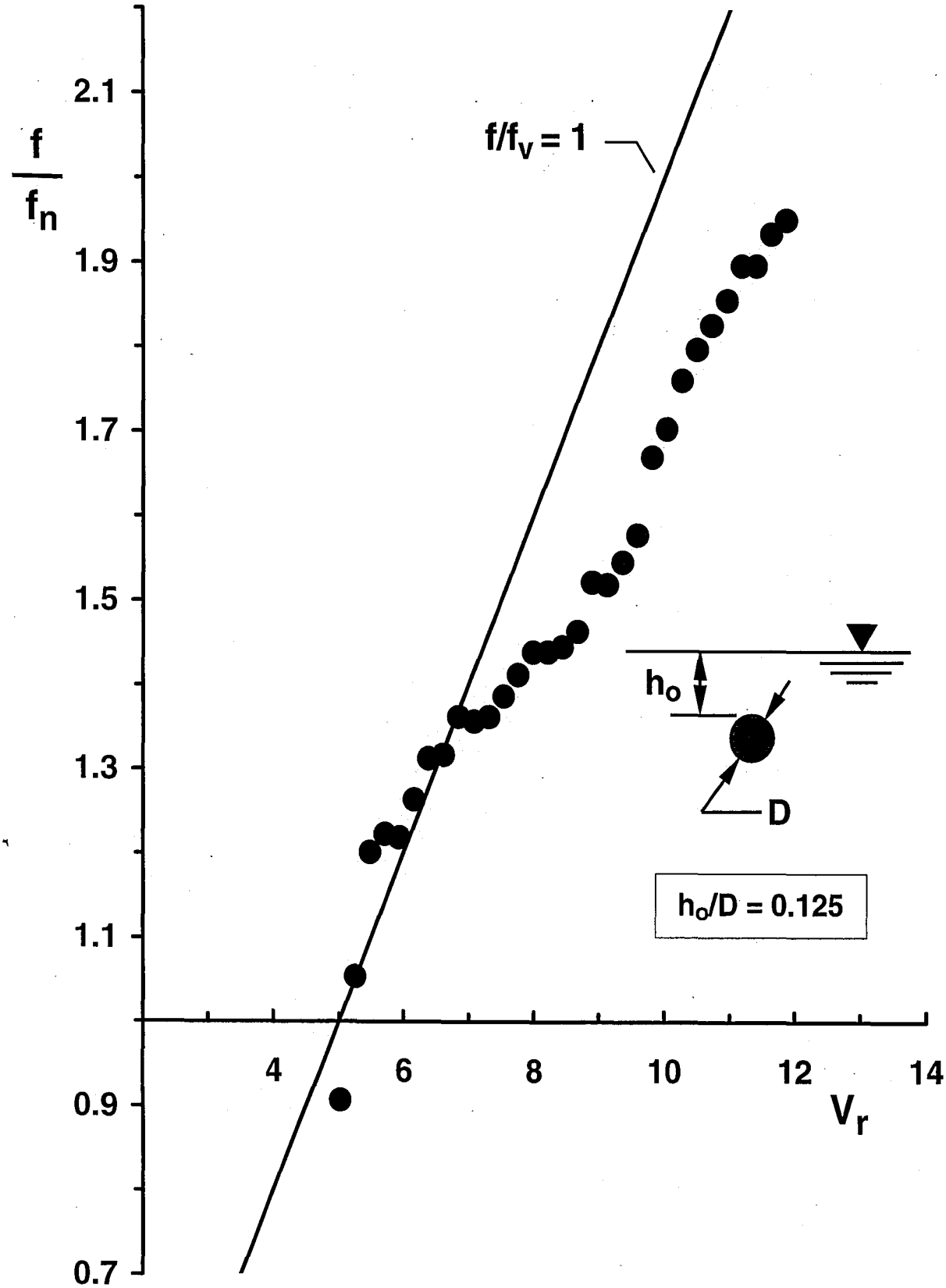

Figure 3-32: Frequency ratio $f^* = f/f_n$ (oscillating frequency/natural frequency) for the depth of submergence $h^* = h_o/D = 0.125$.

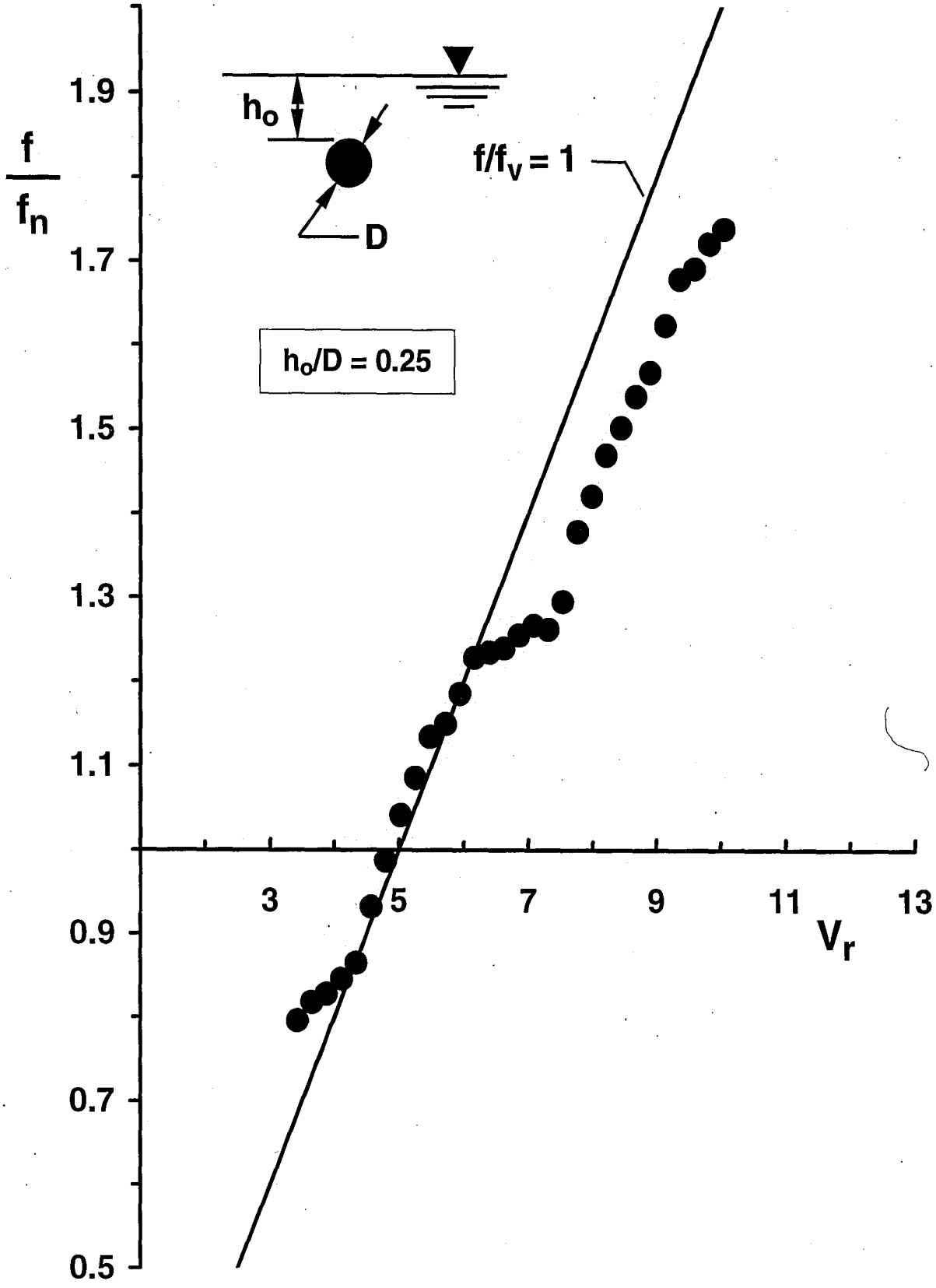

Figure 3-33: Frequency ratio $f^* = f/f_n$ (oscillating frequency/natural frequency) for the depth of submergence $h^* = h_o/D = 0.25$.

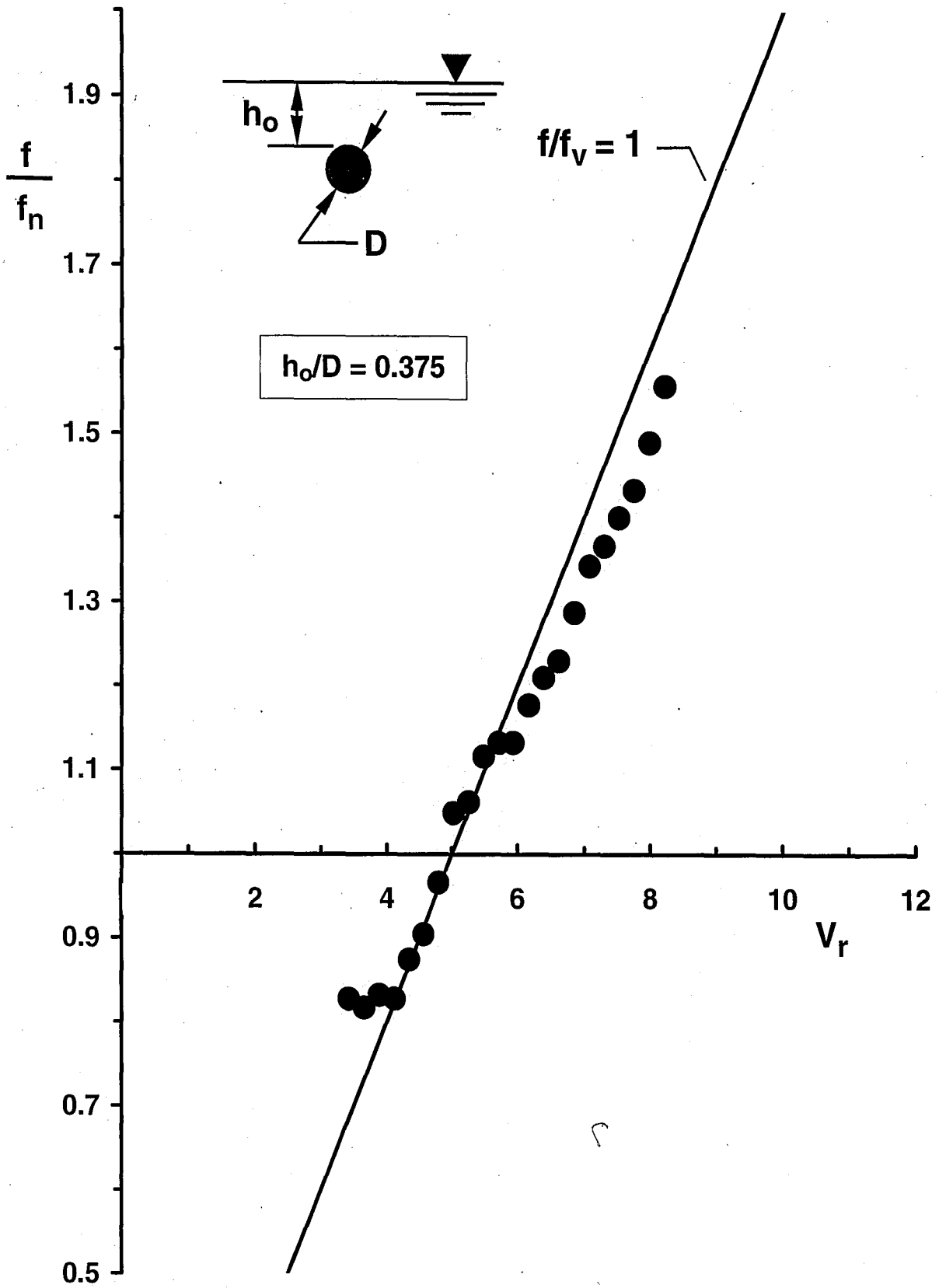

Figure 3-34: Frequency ratio $f^* = f/f_n$ (oscillating frequency/natural frequency) for the depth of submergence $h^* = h_o/D = 0.375$.

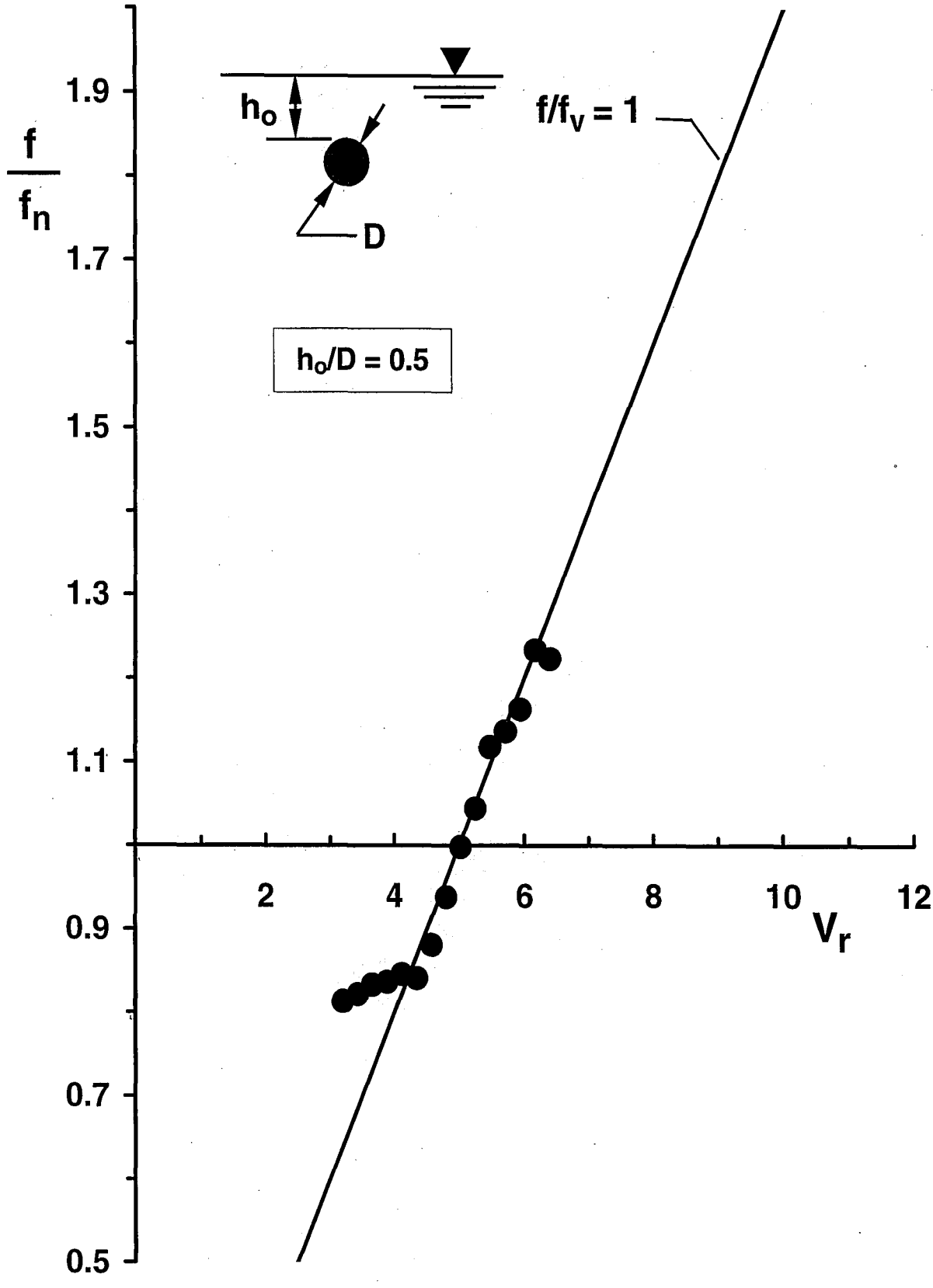

Figure 3-35: Frequency ratio $f^* = f/f_n$ (oscillating frequency/natural frequency) for the depth of submergence $h^* = h_o/D = 0.5$.

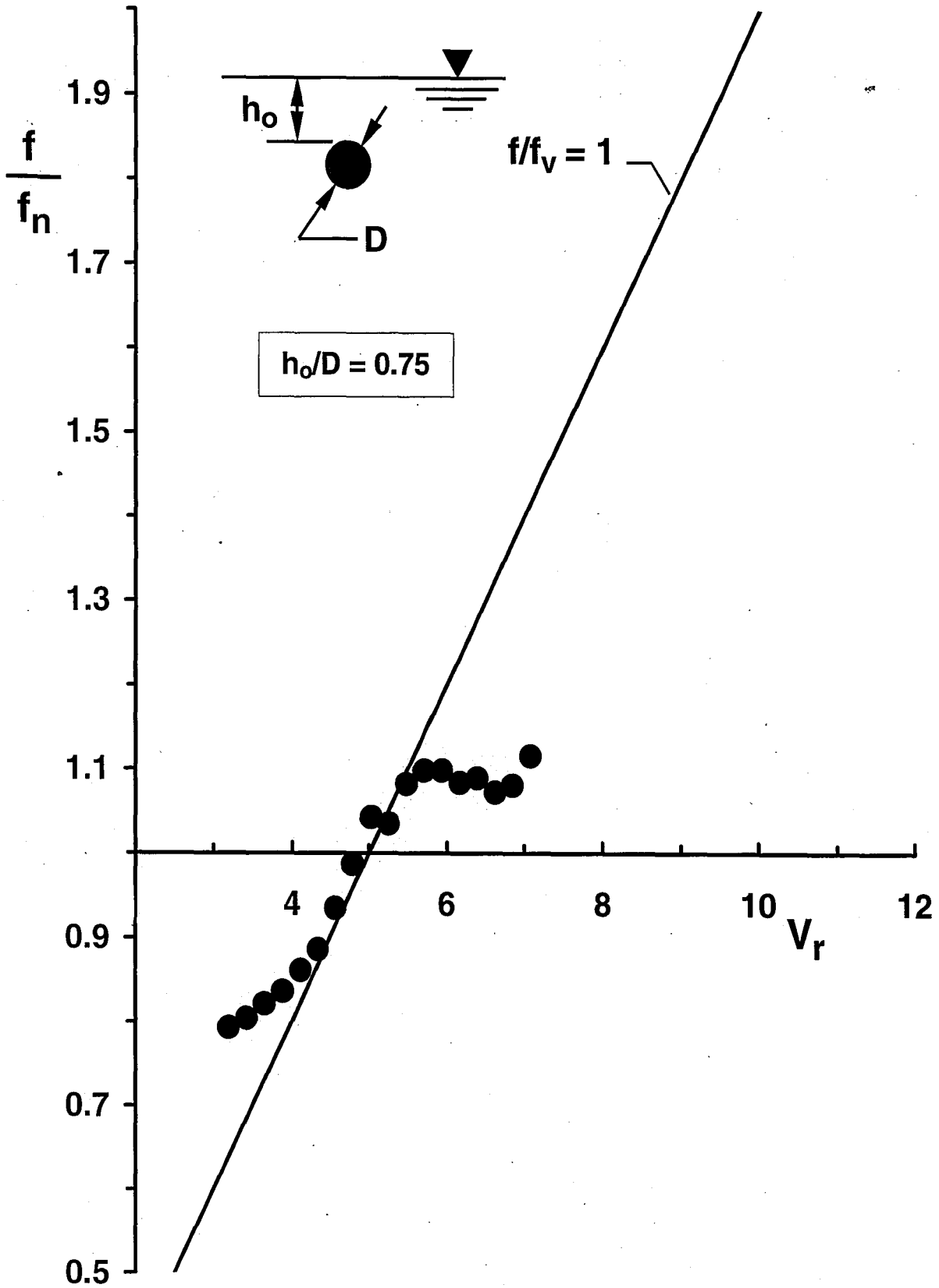

Figure 3-36: Frequency ratio $f^* = f/f_n$ (oscillating frequency/natural frequency) for the depth of submergence $h^* = h_o/D = 0.75$.

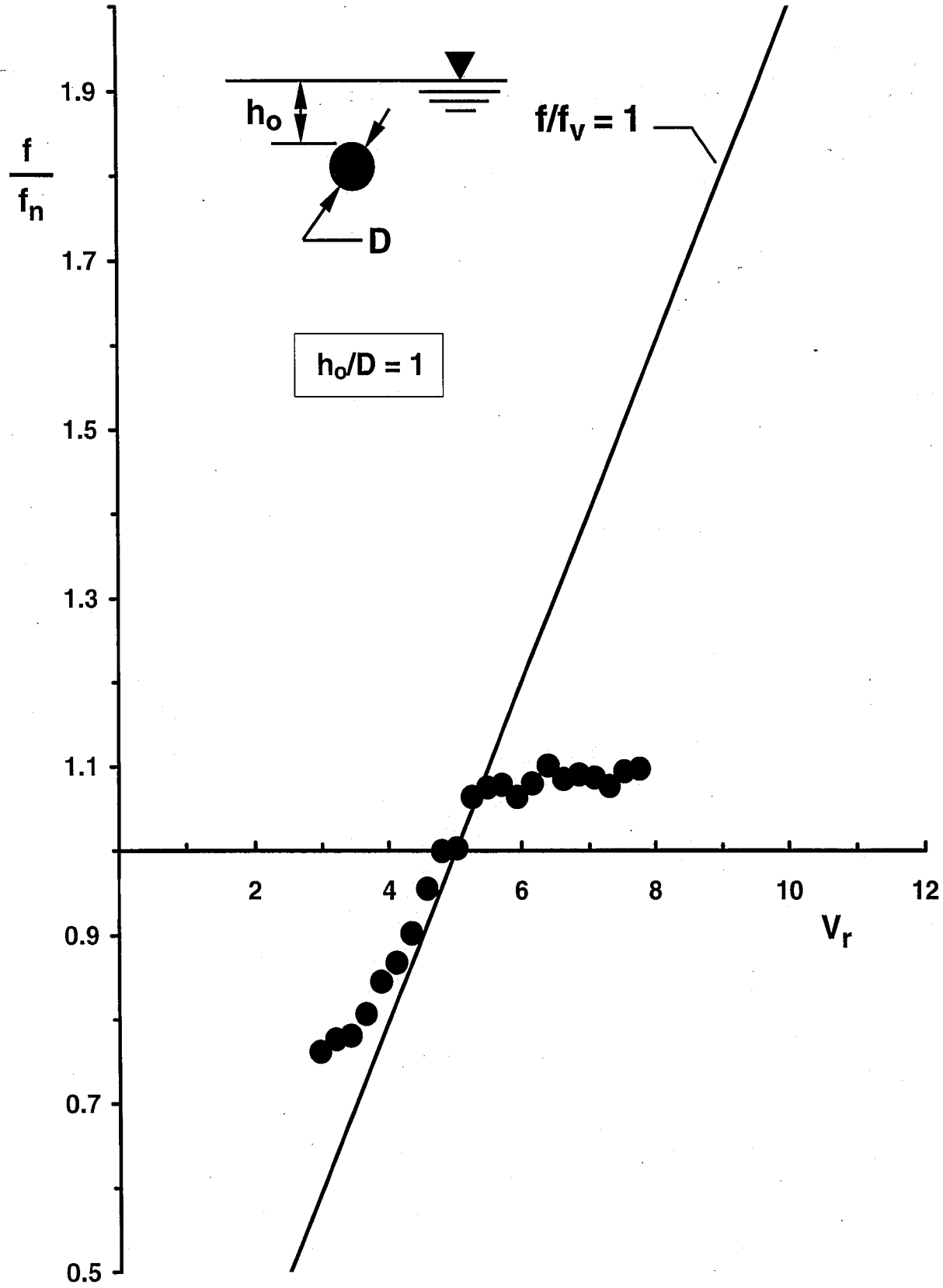

Figure 3-37: Frequency ratio $f^* = f/f_n$ (oscillating frequency/natural frequency) for the depth of submergence $h^* = h_o/D = 1$.

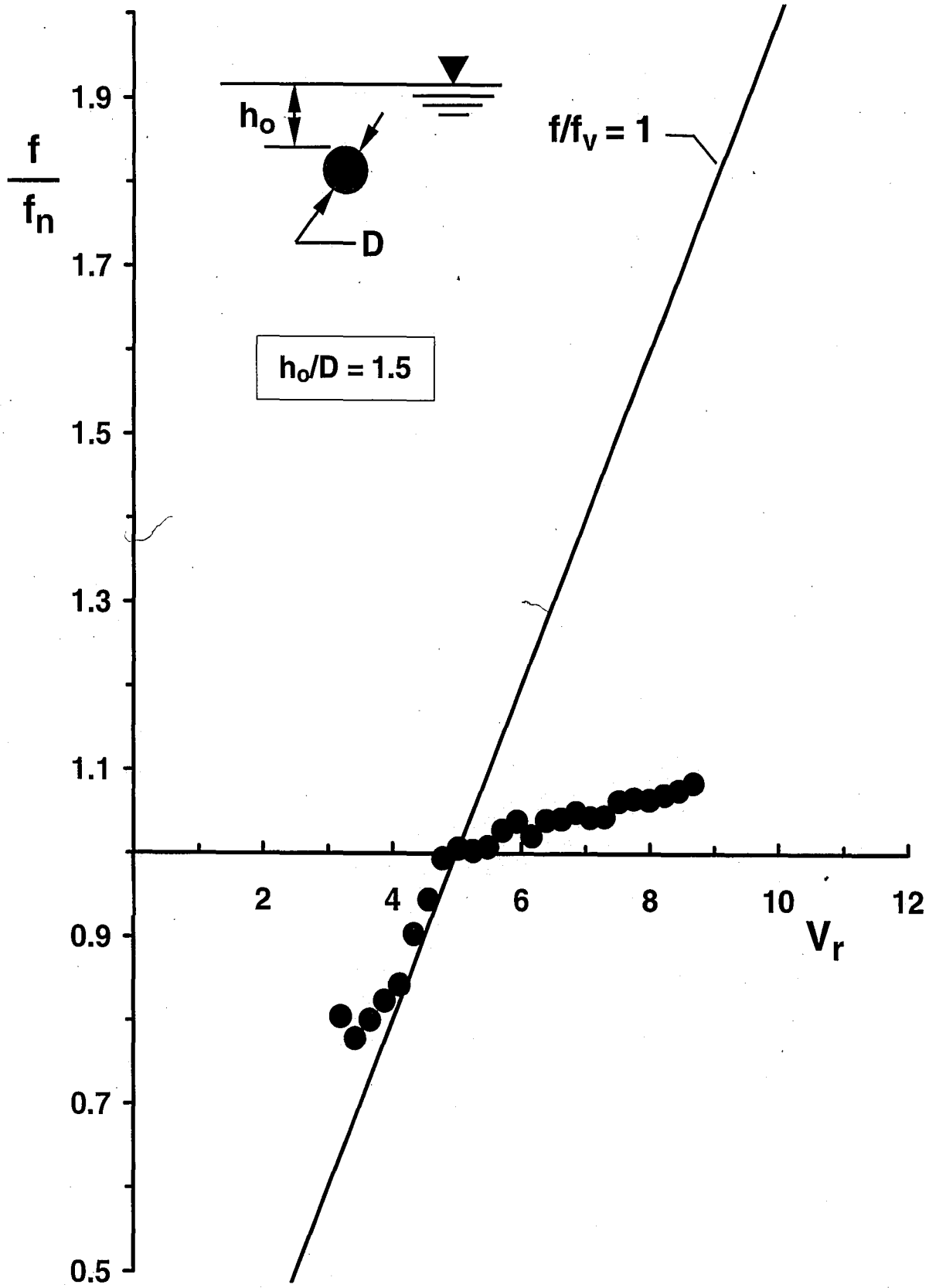

Figure 3-38: Frequency ratio $f^* = f/f_n$ (oscillating frequency/natural frequency) for the depth of submergence $h^* = h_o/D = 1.5$.

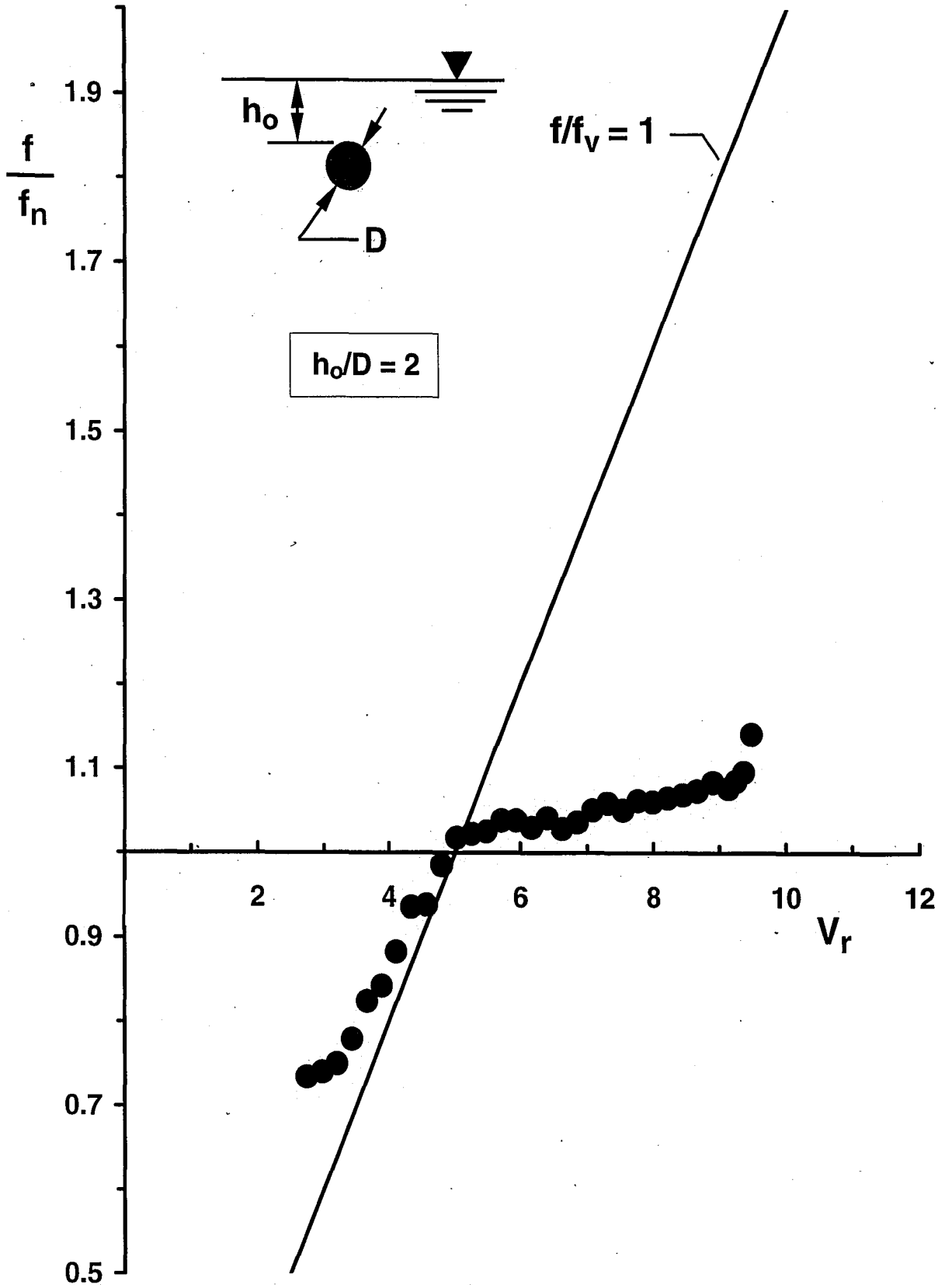

Figure 3-39: Frequency ratio $f^* = f/f_n$ (oscillating frequency/natural frequency) for the depth of submergence $h^* = h_o/D = 2$.

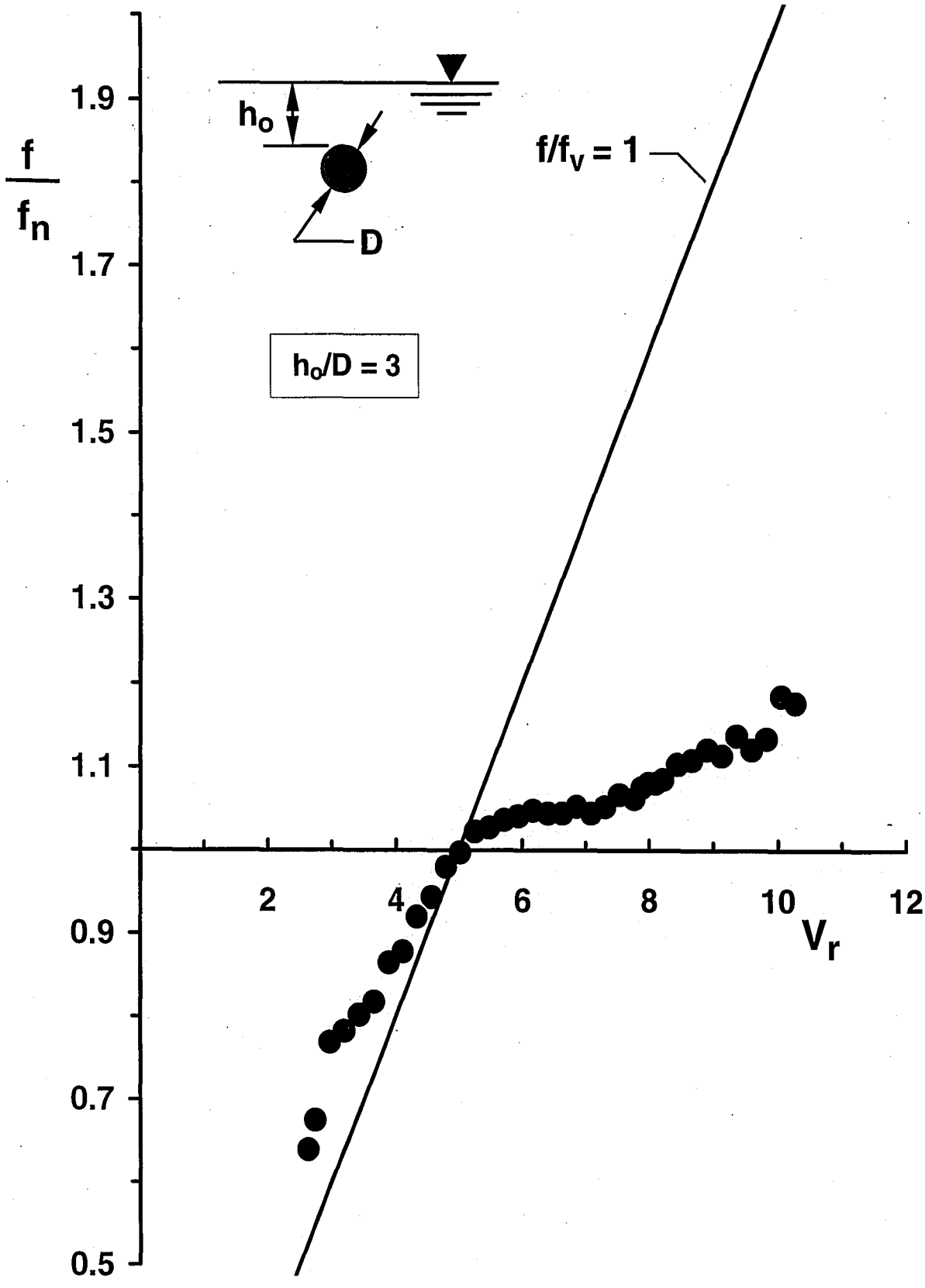

Figure 3-40: Frequency ratio $f^* = f/f_n$ (oscillating frequency/natural frequency) for the depth of submergence $h^* = h_o/D = 3$.

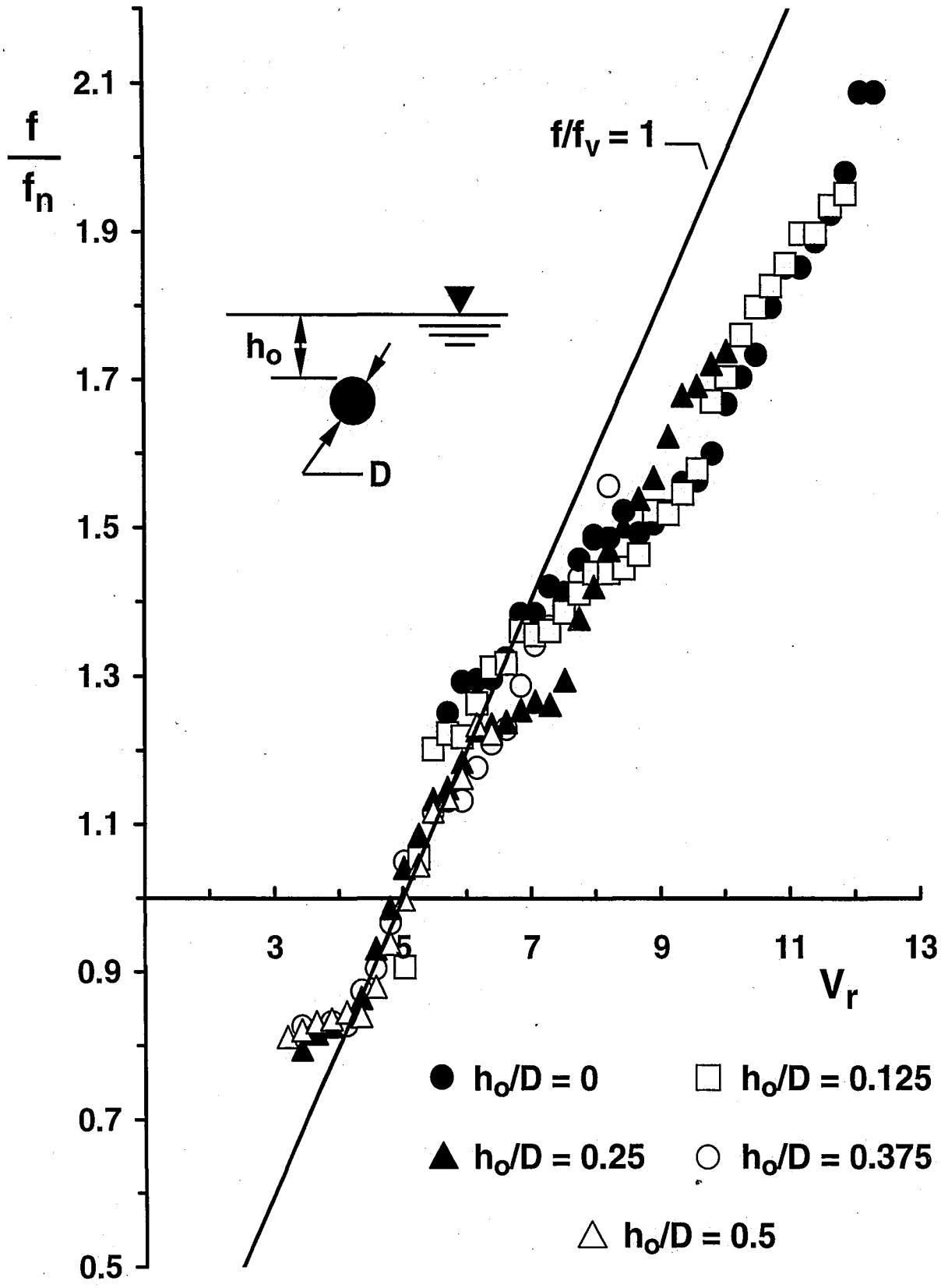

Figure 3-41: Frequency ratio $f^* = f/f_n$ (oscillating frequency/natural frequency) for the depth of submergence $h^* = h_o/D = 0, 0.125, 0.25, 0.375$, and 0.5.

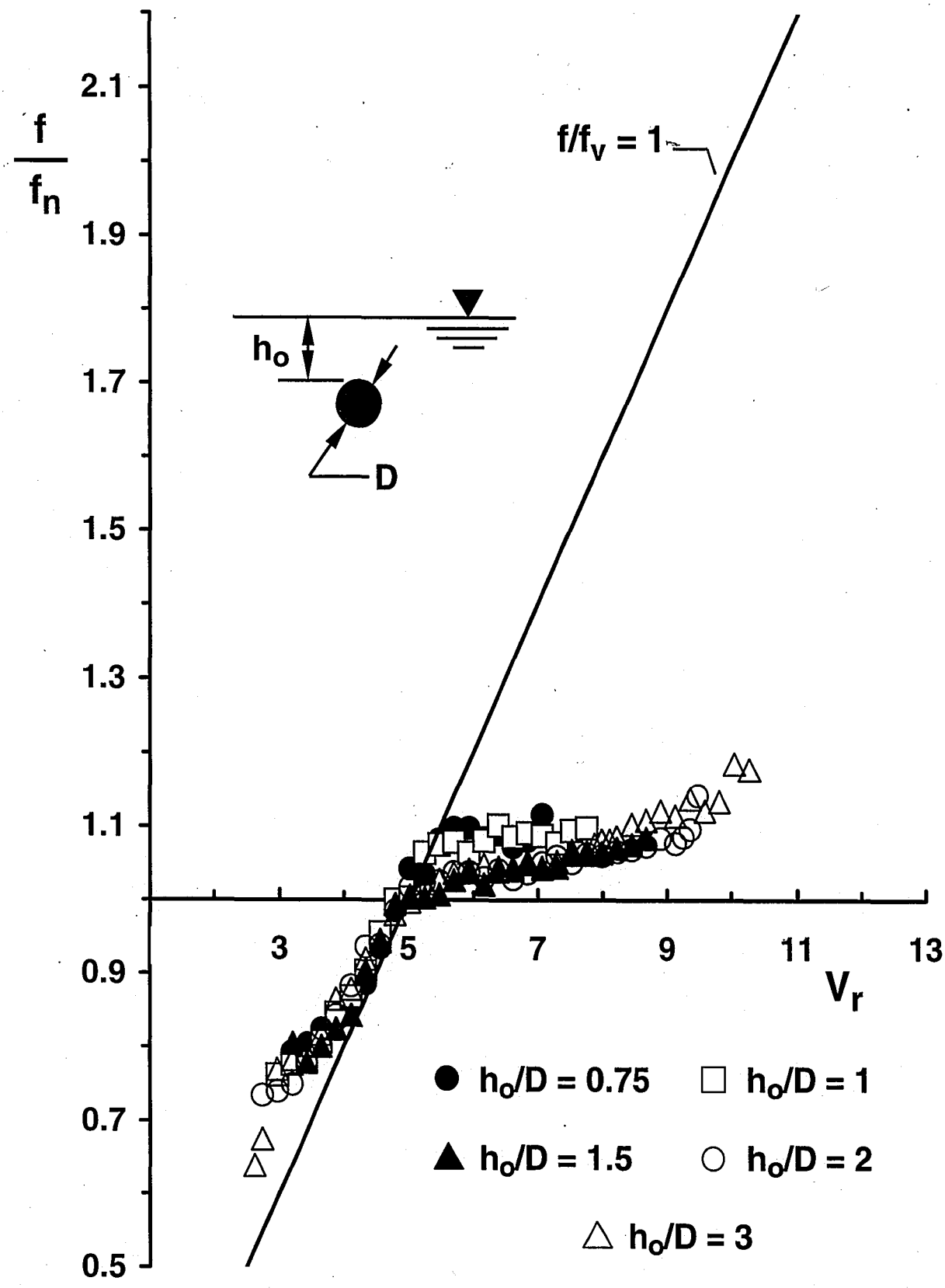

Figure 3-42: Frequency ratio $f^* = f/f_n$ (oscillating frequency/natural frequency) for the depth of submergence $h^* = h_o/D = 0.75$, 1, 1.5, 2, and 3.

APPENDIX A: DETERMINATION OF DAMPING RATIO (ζ)

Since the mass-damping ratio is the central parameter for the elastically mounted horizontally set up cylinder system in the present investigation, and the mass-damping ratio achieved here is an order of magnitude smaller than those of Khalak and Williamson (1996). In this appendix, some widely used techniques for evaluating the damping ratio (ζ) will be mentioned.

Damping Ratio (ζ)

Generally, the resistance provided by surrounding medium (except in an absolute vacuum) can cause the diminution of free vibration amplitude, and such vibrations are called damped free vibration. In term of the energy dissipation, damping ratio or damping factor can be represented by the energy dissipated as the system vibrates. In the other word, the damping ratio is proportional to the ratio of the energy dissipated in one cycle to the total energy of the structure (Blevins 1990).

There are the certain techniques for determining damping ratio available, for example, logarithmic decrement or free decay method, bandwidth method, and magnification factor or quality factor method. These techniques have been discussed extensively in Blevins (1990), and in Shabana (1991).

Logarithmic Decrement or Free Decay Method

For the logarithmic decrement or sometimes-called free decay method, the system is set to an initial displacement and then release to vibrate freely. The consecutive amplitudes of vibration are recorded in order to calculate the logarithmic decrement and eventually the damping ratio.

Considering a simple mass-spring-damper system with linear spring and damping, the equation of motion that governs the system takes the form

$$m\ddot{y} + c\dot{y} + ky = F(t) \tag{A-1}$$

where F(t) is a resultant external force which, in this case, is zero. Basically, the solution of the second order differential equation above can be described as

$$y(t) = A\exp(n_1 t) + B\exp(n_2 t) \tag{A-2}$$

where A and B are arbitrary constants. The parameter n_1 and n_2, the roots of the characteristic equation, are given by

$$n_1 = -\frac{c}{2m} + \frac{1}{2m}\sqrt{c^2 - 4mk} \tag{A-3}$$

$$n_2 = -\frac{c}{2m} - \frac{1}{2m}\sqrt{c^2 - 4mk} \tag{A-4}$$

Since, however, damping ratio ζ can be expressed as

$$\zeta = \frac{c}{c_{cr}} = \frac{c}{2\sqrt{mk}} \tag{A-5}$$

therefore, n_1 and n_2 becomes

$$n_1 = -\zeta\omega + \omega\sqrt{\zeta^2 - 1} \tag{A-6}$$

$$n_2 = -\zeta\omega - \omega\sqrt{\zeta^2 - 1} \tag{A-7}$$

For underdamped systems, $\zeta < 1$, we have

$$n_1 = -\zeta\omega + i\omega_d \tag{A-8}$$

$$n_2 = -\zeta\omega - i\omega_d \tag{A-9}$$

where $\omega_d = \omega_n\sqrt{1-\zeta^2}$ is defined as damped natural frequency and $\omega = \sqrt{\frac{k}{m}}$ is called the natural frequency. Applying the equations (A-8) and (A-9) leads us to the solution $y(t)$ of the system as shown

$$y(t) = Y\exp(-\zeta\omega_n t)\sin(\omega_d t + \phi) \tag{A-10}$$

here the amplitude Y and the phase angle ϕ are constant and can be evaluated from the initial conditions. By differentiating equation (A-10) with respect to time, the velocity $\dot{y}(t)$ is obtained.

$$\dot{y}(t) = Y\exp(-\zeta\omega_n t)\{-\zeta\omega_n \sin(\omega_d t + \phi) + \omega_d \cos(\omega_d t + \phi)\} \tag{A-11}$$

In order to find the time corresponding to the relative maximum amplitudes, we set $\dot{y}(t)$ equal to zero and then yield the following equation

$$\tan(\omega_d t_i + \phi) = \frac{\omega_d}{\omega_n\zeta} = \frac{\sqrt{1-\zeta^2}}{\zeta} \tag{A-12}$$

or

$$\sin(\omega_d t_i + \phi) = \sqrt{1-\zeta^2} \tag{A-13}$$

Substitution of equation (A-13) into equation (A-10) leads us to the peak amplitude i^{th} as

$$y_i = y(t_i) = Y\exp(-\zeta\omega_n t_i)\sqrt{1-\zeta^2} \tag{A-14}$$

To develop an experimental procedure for determining the damping ratio, the system would be given an initial displacement and then released to vibrate freely. By comparing the amplitude of any two successive cycles, the damping ratio can be found.

According to equation (A-14), the amplitude of the $(i+1)^{th}$ cycle is given by

$$y_{i+1} = y(t_i + \tau_d) = Y\exp(-\zeta\omega_n(t_i + \tau_d))\sqrt{1-\zeta^2} \tag{A-15}$$

where $\tau_d = \frac{2\pi}{\omega_d}$ is called the damped periodic time. Whence,

$$\frac{y_i}{y_{i+1}} = \frac{Y\exp(-\zeta\omega_n t_i)\sqrt{1-\zeta^2}}{Y\exp(-\zeta\omega_n (t_i+\tau_d))\sqrt{1-\zeta^2}} = \exp(\zeta\omega_n \tau_d) \tag{A-16}$$

Taking the natural logarithm of the equation (A-16) leads to

$$\ln\left(\frac{y_i}{y_{i+1}}\right) = \zeta\omega_n\tau_d = \delta \tag{A-17}$$

(see Figure A-1 for definition terms and Figure A-2 for the free decay amplitude in still air of the system used in this research) where δ is a constant named the logarithmic decrement which after applying the fact that $\omega_d = \omega_n\sqrt{1-\zeta^2}$, the logarithmic decrement can be written in the form

$$\delta = \frac{2\pi\zeta}{\sqrt{1-\zeta^2}} \tag{A-18}$$

Furthermore, for lightly damped system or specifically speaking $\zeta << 1$, the previous equation implies

$$\delta \cong 2\pi\zeta \tag{A-19}$$

Alternatively, in case of this lightly damped system, the ratio of non-successive amplitudes can be employed to evaluate the damping ratio as well. After N cycles from i^{th} cycle, from equation (A-17), we obtain

$$\ln\left(\frac{y_i}{y_{i+N}}\right) = N\zeta\omega_n\tau_d = N\delta \tag{A-20}$$

Practically, in this method a transducer such as an accelerometer might be helpful.

Bandwidth Method

Considering a single degree of freedom system, which is subjected to a harmonic forcing function $F(t)$. Regarding to Newton's second law of motion, we come up with the second order differential equation which is written in the same form as in equation (A-1).

For a sake of simplicity of evaluation of damping factor, $F(t)$ can be selected as a harmonic function, says,

$$F(t) = F\sin\omega t \tag{A-21}$$

where ω is the excitation frequency. Substituting $F(t) = F\sin\omega t$ into the equation of motion yields

$$m\ddot{y} + c\dot{y} + ky = F\sin\omega t \tag{A-22}$$

The steady state solution y_p of the governing equation can be expressed in the form

$$y_p = A\sin\omega t + B\cos\omega t \tag{A-23}$$

By differentiating with respect to time, the velocity and the acceleration can be achieved

$$\dot{y}_p = A\omega\cos\omega t - B\omega\sin\omega t \tag{A-24}$$

$$\ddot{y}_p = -A\omega^2\sin\omega t - B\omega^2\cos\omega t = -\omega^2 y_p \tag{A-25}$$

Substituting $\dot{y}_p$ and $\ddot{y}_p$ into the equation of motion and after rearranging terms yields

$$\left(\left(k - m\omega^2\right)A - c\omega B\right)\sin\omega t + \left(c\omega A + \left(k - m\omega^2\right)B\right)\cos\omega t = F\sin\omega t \tag{A-26}$$

At this point, by comparing coefficient and divided the equation by k the algebraic equations in A and B are yielded

$$\left(1-\left(\frac{\omega}{\omega_n}\right)^2\right)A-2\zeta\left(\frac{\omega}{\omega_n}\right)B=\frac{F}{k}=Y \tag{A-27}$$

$$2\zeta\left(\frac{\omega}{\omega_n}\right)A+\left(1-\left(\frac{\omega}{\omega_n}\right)^2\right)B=0 \tag{A-28}$$

These two algebraic equations can be solved by Cramer's rule, that is,

$$A=\frac{\begin{vmatrix}\frac{F}{k} & -2\zeta\left(\frac{\omega}{\omega_n}\right)\\ 0 & 1-\left(\frac{\omega}{\omega_n}\right)^2\end{vmatrix}}{\Delta}=\frac{\left(1-\left(\frac{\omega}{\omega_n}\right)^2\right)\frac{F}{k}}{\Delta} \tag{A-29}$$

$$B=\frac{\begin{vmatrix}1-\left(\frac{\omega}{\omega_n}\right)^2 & \frac{F}{k}\\ 2\zeta\left(\frac{\omega}{\omega_n}\right) & 0\end{vmatrix}}{\Delta}=\frac{-2\zeta\left(\frac{\omega}{\omega_n}\right)\frac{F}{k}}{\Delta} \tag{A-30}$$

where $\Delta=\left(1-\left(\frac{\omega}{\omega_n}\right)^2\right)^2+\left(2\zeta\left(\frac{\omega}{\omega_n}\right)\right)^2$

Consequently,

$$y_p=\frac{\frac{F}{k}}{\sqrt{\left(1-\left(\frac{\omega}{\omega_n}\right)^2\right)^2+4\zeta^2\left(\frac{\omega}{\omega_n}\right)^2}}\sin(\omega t-\phi)=Y\sin(\omega t-\phi) \tag{A-31}$$

where Y is the amplitude of the response function and ϕ is the phase angle defined by

$$\phi = \tan^{-1}\left(\frac{2\zeta\left(\frac{\omega}{\omega_n}\right)}{1-\left(\frac{\omega}{\omega_n}\right)^2}\right) \tag{A-32}$$

In case of lightly damped system $(\zeta < 0.05)$, the value of the amplitude ratio $\left(\frac{Y}{F/k}\right)$ when the oscillator approaches resonance $(\omega \cong \omega_n)$ becoming maximum

$$\left(\frac{Y}{\delta_{st}}\right)_{\max} \cong \left(\frac{Y}{\delta_{st}}\right)_{\omega=\omega_n} = \frac{1}{2\zeta} = Q \tag{A-33}$$

where $\delta_{st} = \frac{F}{k}$ is static deflection under the force F and Q is called quality factor of the system or Q factor (see definition terms in Figure A-3).

Sometimes when δ_{st} can not be determined, the half power point method could be used to find Q factor. The half power point method requires very accurate data of the vibration amplitude for excitation frequencies in the proximity of resonance. Consider the response curve as shown in figure A-2, the points P_1 and P_2 are called half power points corresponding to the amplitude $\frac{1}{\sqrt{2}}\left(\frac{Y}{F/k}\right)$. Since the energy dissipated in one cycle of vibration is proportional to Y^2, the energy dissipation is decreased by 50% when the amplitude is reduced by a factor of $\frac{1}{\sqrt{2}}$.

From equation (A-33), thus

$$\left(\frac{Y}{F/k}\right)_{\max} = \frac{1}{\sqrt{2}} \tag{A-34}$$

and

$$\frac{1}{\sqrt{2}}\left(\frac{Y}{F/k}\right)_{\max}=\frac{1}{\sqrt{8}\zeta}=\frac{1}{\sqrt{\left(1-\left(\frac{\omega}{\omega_n}\right)^2\right)^2+4\zeta^2\left(\frac{\omega}{\omega_n}\right)^2}} \tag{A-35}$$

Whence,

$$\left(1-\left(\frac{\omega}{\omega_n}\right)^2\right)^2+4\zeta^2\left(\frac{\omega}{\omega_n}\right)^2=8\zeta^2 \tag{A-36}$$

and

$$\left(\frac{\omega}{\omega_n}\right)^2=\left(1-2\zeta^2\right)\pm 2\zeta\sqrt{1-\zeta^2} \tag{A-37}$$

That is,

$$\frac{\omega_2^2-\omega_1^2}{\omega_n^2}=\left(\frac{\omega_2-\omega_1}{\omega_n}\right)\left(\frac{\omega_2+\omega_1}{\omega_n}\right)=2\left(\frac{\omega_2-\omega_1}{\omega_n}\right) \tag{A-38}$$

Since $\omega=\left(\frac{\omega_1+\omega_2}{2}\right)$ is corresponding to assumed a symmetrical response curve for small damping. Therefore,

$$Q=\frac{1}{2\zeta}\cong\frac{\omega_n}{\omega_2-\omega_1}=\frac{\omega_n}{\Delta\omega} \tag{A-39}$$

where $\Delta\omega$ is the frequency bandwidth at the half power points. The equation mentioned above is often used as a convenient way of determining the damping ratio.

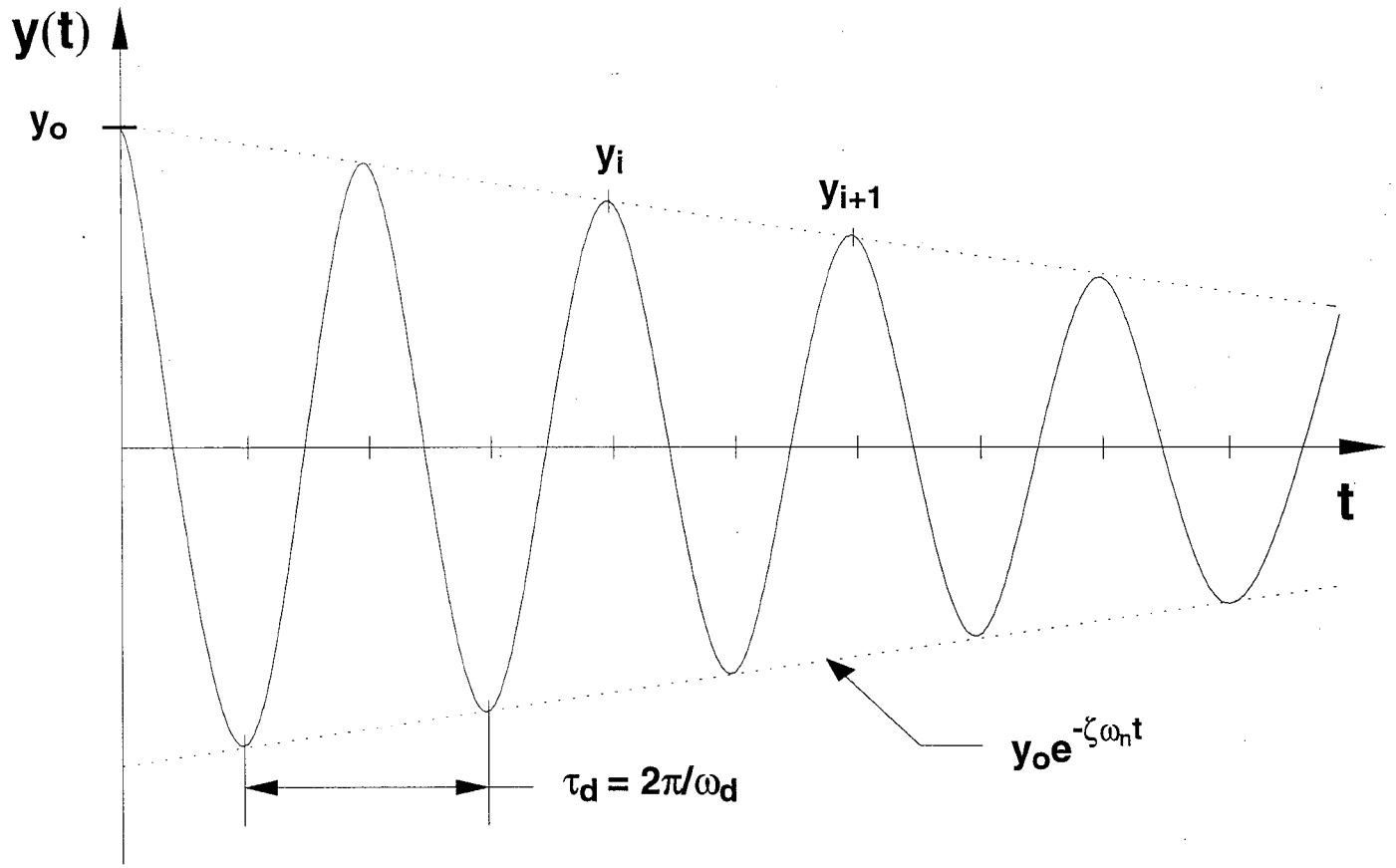

Figure A-1: Displacement of an underdamped system as a function of time; two consecutive displacement amplitudes used to determine the damping ratio of the system; referred as a logarithmic decrement method.

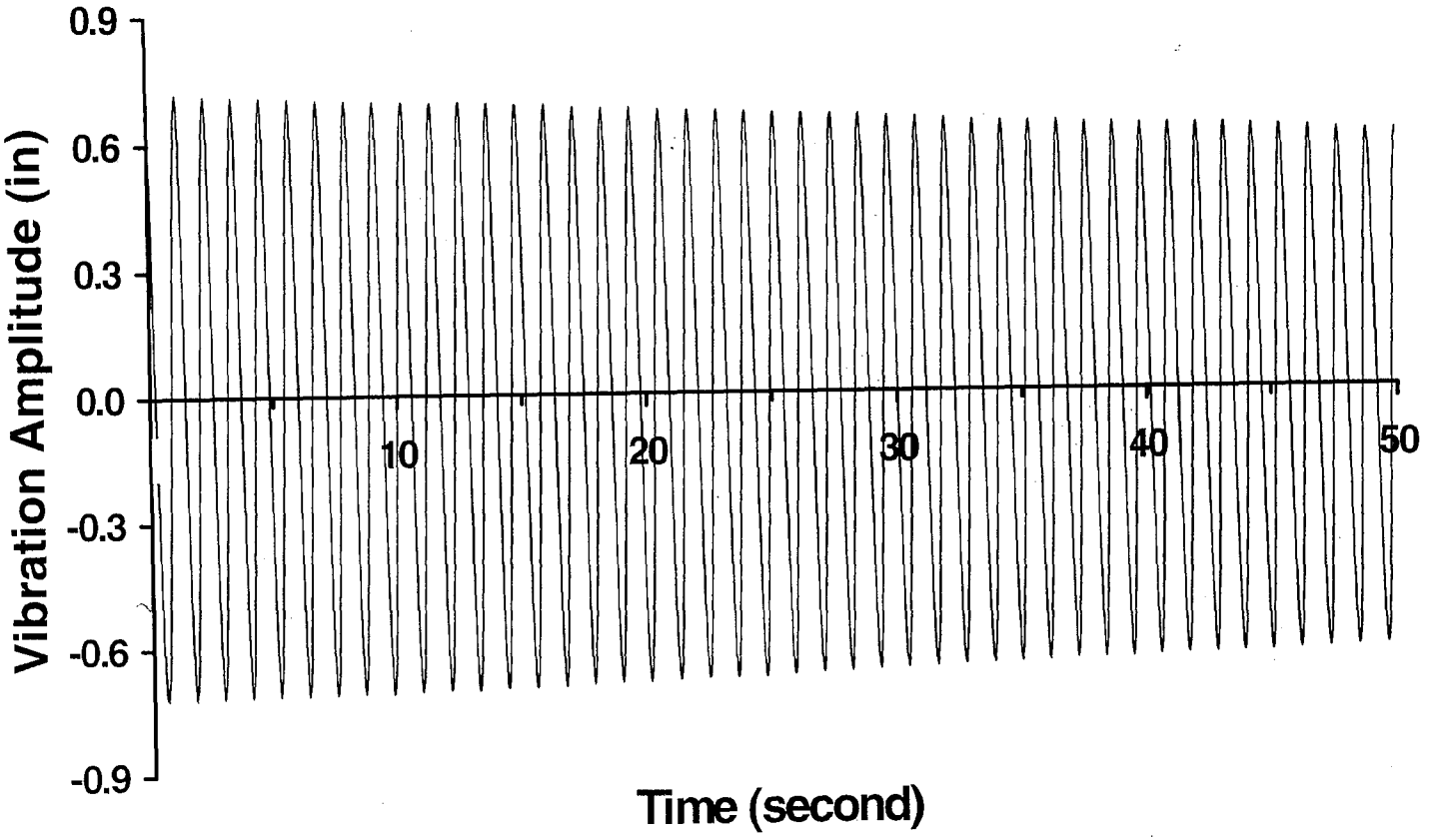

Figure A-2: Free decay of vibration amplitude of the cylinder in still air in determining of damping ratio and natural frequency of the system.

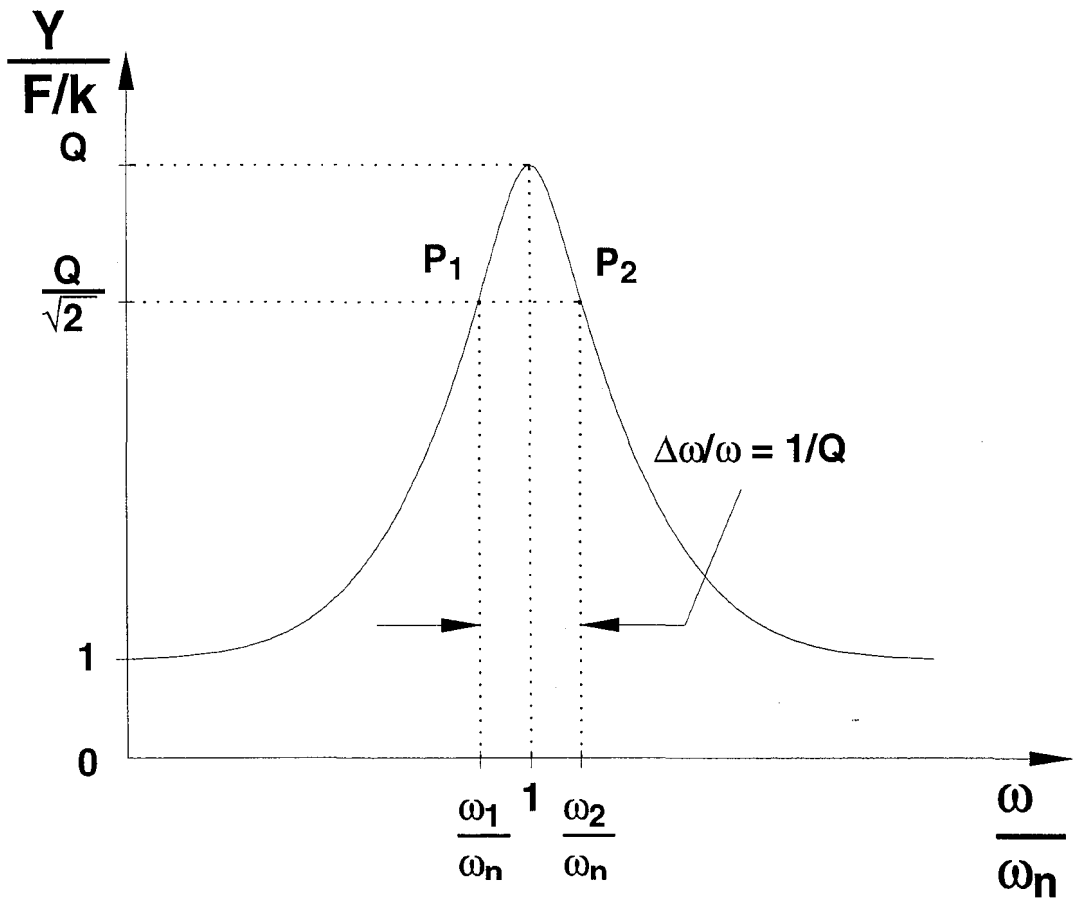

Figure A-3: Bandwidth method of determining damping.

VITA

Nattapong Saelim was born to Thienchai Saelim and Maneerat Tunsirisakunthum on July 6, in Bangkok, Thailand. He obtained his high school diploma from Debsirin High School in Bangkok 1991. Nattapong Saelim graduated from Srinakharinwirot University, in Thailand, with a B.S. degree (1^{st} honors) in Mechanical Engineering in 1996. He continued his education at Lehigh University until December 1999, studying to achieve his M.S. degree in Mechanical Engineering.

The author will attend Lehigh for his Ph.D. in Mechanical Engineering.

END OF TITLE